High Power Analysis of Filters and Diplexers

by

Desireh Shojaei-Asanjan

A thesis
presented to the University of Waterloo
in fulfillment of the
thesis requirement for the degree of
Master of Applied Science
in
Electrical and Computer Engineering

Waterloo, Ontario, Canada, 2012

AUTHOR'S DECLARATION

I hereby declare that I am the sole author of this thesis. This is a true copy of the thesis, including any required final revisions, as accepted by my examiners.

I understand that my thesis may be made electronically available to the public.

Abstract

The ever-increasing popularity and usage of communication devices has resulted in power density becoming more demanding due to crowding of frequency spectrums and narrowing of bandwidths. Consequently, the power-handling capability of filters has emerged as an important research area. With the size and mass of filters shrinking to accommodate the needs of the latest technology, designing narrowband filters necessitates the operation of filters close to their maximum power capacities. Hence, there is an urgent need to properly measure and estimate power-handling capability in filter-based products such as satellite multiplexers and wireless diplexers.

In this research, the design of filters and diplexers capable of handling higher power was investigated using modifications of available methods to predict the maximum input power that a filter can handle before breakdown. This method was utilized to improve the power-handling capability and quality factor of the conventional coaxial resonator while avoiding time-consuming EM simulations.

A novel coaxial resonator configuration was proposed using this method and the performance of suggested configuration was validated by designing 2-pole filters using both conventional and novel configurations. A 4-pole chebyshev filter was also designed and realized using the proposed configuration, and a power-handling analysis utilizing HFSS was compared with that of the estimated value.

A novel approach in the design procedure of coaxial diplexers was proposed that provided a faster design method using step-by-step group delay matching of EM simulation results with a diplexer equivalent circuit. A method for predicting air breakdown was also applied to the diplexers to determine maximum power-handling capability.

Acknowledgements

First and foremost, I like to thank my supervisor, Professor Raafat Mansour for his great guidance and kind support throughout my graduate studies. His approach and teaching has inspired me to continue my graduate studies.

My deepest gratitude goes to all the members of my family, for the wonderful support they all provided; specially my husband, Mohammad Saleh Moonesan, my mother, Dr. Parisa Derakhshan Moghaddam, my father, Behrouz Shojaei-Asanjan, my brother, Khashayar Shojaei-Asanjan, my aunt , Paria Derakhshan-Moghaddam, my mother in law, Shamsi Maahve-Bidokhti, and my father in law, Mohammad-Taghi Moonesan. Special thanks to my grandparents Tourandokht Sarfarazan and Farajollah Derakhshan-Moghaddam for their endless love and support.

I would like to thank Dr. Ali Safavi-Naieni and Dr. Shehakamal Jayaram for reviewing my thesis.

I would also like to thank my friends in CIRFE laboratory at the University of Waterloo: Payam, Sormeh, Sara, Raisa, Fengxi, Alborz, Bahaeddine, Saman, Scott, Geoffrey, Oliver, Ahmed and all other members of our group, you all contributed to my learning experience.

My thanks go to all my dear friends who have enriched my life.

Dedication

To my dear husband and parents.

Table of Contents

List of Figures

List of Tables

Chapter 1
Introduction

1.1 Motivation

Filters are used in most RF and microwave systems, operating in a wide range of frequencies that are used for both low-power and high-power applications. Filters are also commonly used as building blocks of diplexers in order to combine or separate transmit and receive signals in multiple-frequency bands. While there are many commercial tools available to determine the performance of filters at low power, no commercial tool is yet available to predict their performance at high power. Thus, it is desirable to have a tool to estimate the power-handling capability of the filter structure.

Power handling can be estimated at the prototype stage of simple structures such as rectangular waveguides; however, for all other types, an EM simulator has to be used. Based on the application of the filter, a special kind of resonator is usually used to consider the relationship between the insertion loss and the size of the resonator for different types of filters. Although waveguides have very good performance in terms of insertion loss, coaxial resonators are more desirable in the 1 or 2 GHz frequency range due to their smaller size. The filter has to be designed and tuned perfectly to reflect the power-handling capability in EM simulation, which is a very time-consuming process even with fast computers and efficient software. Moreover, they are extremely sensitive to changes in dimension, especially in cases where the filter is narrowband.

In addition, in order to determine the exact dimensions of a filter structure, fine tuning needs to be performed. There are different methods available for tuning, all of which are time-consuming. Hence, using a method to avoid this drawback would be desirable; even more so would be to utilize a method capable of estimating the voltage/power distribution of a narrowband filter before designing the complete filter. Indeed, with such a method, it would be possible to examine various resonator configurations in a single cavity as building blocks of a filter or diplexers to find the best geometry to yield maximum power-handling capacity. The ultimate aim here would be to design a filter or diplexer with a higher power rating.

1.2 Objectives

The main objectives of the proposed research are:

- Development of an efficient method for estimating the power-handling capability of microwave filters.
- Devising of novel combline resonator configurations capable of handling higher power levels compared to conventional combline resonators.
- Analysis and characterization of diplexers for high power applications.

1.3 Thesis Outline

The first chapter provides an introduction and Chapter 2 reviews research-related literature, including filter design, simplified methods to predict power handling, and design methods for diplexers. The third chapter studies the power handling of filters, focusing on a method to predict air breakdown in the resonators. This method is applied to determine the power handling of various filters and to find a new structure with higher power-handling capability. Chapter 4 investigates diplexer power handling and proposes a systematic method for diplexer design, and the fifth and final chapter draws conclusions from the research.

Chapter 2
Literature Survey

In this chapter, a literature survey on the power handling of high-power microwave filters and the design of diplexers is presented.

The power handling of band pass filters has been studied for many years. In 1959, Cohn [1] presented a formula for finding the cavity electric field strengths at the center of the pass band direct-coupled cavity filter. In 1960 [2], Young derived formulas for calculating the peak field inside each cavity of the direct-coupled cavity filter. The internal fields were reported to be minimum in the center frequency and maximum just outside the pass band. He also established a relation between group delay and internal field amplitudes, which was verified later by [3] and [4]. In 1987 [5], Nishikawa et al. calculated the stored energy and electric field intensity of each dielectric quarter cut dielectric resonator in TE01 mode used to build an eight-pole elliptic function type filter. In 1999, Ernest and Postoyalko [3] showed that the relation between stored energy and group delay does not depend on the method used for realizing the filter but rather relies on the filter transfer function. In the same year T. Olsen et al. [6] compared the theoretical results of finding the breakdown threshold in air-filled microwave components with those of experimental results.

In 2000, Harish et al. [7] proposed a method to find the voltages in filter. A circuit model was used to determine the stored energy in resonators, which is related to maximum voltage by a factor that can be found using a single cavity in an EM simulator. In the same year, Sivadas et al. [8] also found a method for computing the maximum voltage inside a band pass filter. They used a cross-coupled lumped element prototype of the filter network for this means. In 2001, Wang et al. [9] presented an analysis method on band pass filter power handling using a normalized general two-port network. The stored energy was compared to the maximum electric field in order to determine the maximum power handling.

In 2003, Ernest et al. [10] offered formulas for calculating the maximum electric field within the cavities of a direct-coupled waveguide chebyshev filter. They used the relation between electric field strength and stored energy to predict the peak electric field within each

resonator. In 2007, Ming Yu [11] studied power handling of high-power filters in terms of multipaction and ionization, while using earlier-mentioned stored energy methods to predict the maximum electric field in a resonator. Yu also suggested some design considerations according his findings. In 2012, Hagensen [12] used a simplified prediction of power handling in a single resonator to determine maximum power handling in a filter. They compared the predicted value with that obtained by simulating a complete filter in HFSS.

In the following section, the most important methods used in the literature to predict the power handling of filters are described in detail.

2.1 Simplified Analysis for High-Power Microwave Band Pass Filters

The literature contains several studies on the simplified analysis of high-power band pass filters. Three of the most important methods are described below.

2.1.1 Method 1

In [8], the peak cavity voltage is determined by computing resonator voltages using their circuit model and considering a scale factor to relate circuit peak voltage to cavity peak voltage. Figure 2.1 shows the low pass filter configuration used in their work, which consists of N resonators coupled through admittance invertors.

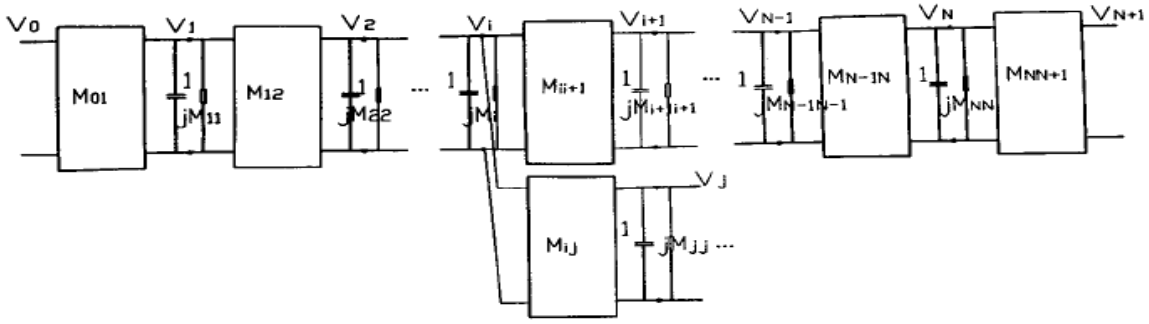

Figure 2.1. General admittance inverter low pass filter prototype [8].

A band pass filter model was obtained using the following transformation:

$$\frac{f_0}{BW}\left(\frac{S}{W_0}+\frac{W_0}{S}\right)\rightarrow S \tag{2.1}$$

The network is solved by writing down the nodal system of equations in the form of $Yv = i$

Then, the unit capacitances in low pass prototypes are scaled by a factor of T to make a lumped element prototype analysis equivalent to that of a distributed transmission line prototype.

$$T = n\frac{\pi}{2}\left(\frac{BW}{f_0}\right)\left(\frac{\lambda_{g0}}{\lambda_0}\right)^2 \tag{2.2}$$

This was done by multiplying all of the rows and columns in the Y matrix (except the first and last) by $\sqrt{T}$, which resulted in the internal voltages, V_1 to V_N, to be scaled by $\frac{1}{\sqrt{T}}$.

Hence, the resonator voltages in a cavity can be found by first solving the lumped prototype problem for suitable excitations and then scaling the lumped voltages, V1 to VN, by $\frac{1}{\sqrt{T}}$.

In this method, the voltage at the kth resonator is given by:

$$V_k = Z_{k,0} - \frac{Z_{k,N+1}\,Z_{N+1,0}}{(Z_L + Z_{N+1,N+1})} \qquad k = 0, \dots, N \tag{2.3}$$

Finally, the voltage ratio for an actual T.L cavity filter normalized to the incident voltage is given by:

$$\frac{V_k}{V_0}(1 + S_{11})\frac{1}{\sqrt{T}} \tag{2.4}$$

This method is general in scope and easy to implement. Overall, it serves as a quick way to find the maximum resonator voltages. However, despite its speed and simplicity, it does not deal with the real structure of the filter and therefore is not the best method available.

2.1.2 Method 2

Harish and Cameron [7] proposed a procedure for finding the peak voltage levels in each resonator. By using the optimized circuit model of the filter or multiplexer and knowing the input power of the device, the TASE (time averaged stored energy) of each resonator is calculated. They considered that the TASE is related to group delay of the filter transfer function regardless of the technology used in the realization of the resonators [13]. In addition, they related the TASE of each cavity with a predetermined factor to the peak voltage. The factor was determined according the EM analysis of the single resonator used in the actual filter. In their method a band pass-equivalent circuit of a band pass filter consisting of N admittances (Y_i), with frequency invariant self-admittances (jB_i), coupled with

admittance inverters (M_{ij}) was used. This circuit was used to find the admittance at the frequency$f$.

$$\lambda = \frac{f_0}{BW}\left(\frac{f}{f_0} - \frac{f_0}{f}\right), s = j\lambda \tag{2.6}$$

Applying nodal analysis$[Y][V] = I$, values of V were found. Then, using the following equation, the nodal voltages can be normalized to 1 Watt, where P_{in} is the input power:

$$V_{i,norm} = \frac{V_i}{\sqrt{P_{in}}} \tag{2.7}$$

The time-averaged stored energy in the i[th] resonator of the filter with 1W input power can be found using the following equation. Note that the voltage and energy are found from the filter prototype.

$$E_{f,i} = \frac{v_{i,norm}v_{i,norm}^*}{2\pi BW} \tag{2.8}$$

The actual voltage of the filter depends on the geometry of the filter and the mode of operation. Using the EM analysis of a single cavity, the eigen value (resonant frequency) and eigenvector (field distribution) can be found.

With E_c as the TASE and V_c as the corresponding voltage in the cavity, the voltage developed in the i[th] cavity of the filter is given by:

$$V_{f,i} = V_c\sqrt{\frac{E_{f,i}}{E_c}} \tag{2.9}$$

2.1.3 Method 3

A general method for finding the power handling of band pass filters is proposed by Wang and Zaki [9]. They considered the general two-port band pass filter network with N series resonators and assumed the line impedance of each resonator to be normalized to unity using:

$$Z_0 = \sqrt{\frac{L_i}{C_i}} = 1, L_i = C_i = \frac{1}{\omega_i}, \omega_i^2 = \frac{1}{L_iC_i} \tag{2.10}$$

The loop equations can be expressed as $ZI = V$

$$[R + S + jM][i_1, i_2, \dots, i_N]^t = [e_1, 0, 0, \dots, 0]^t \tag{2.11}$$

where:

$$S = \frac{j}{\omega'}\left(\frac{\omega}{\omega_0} - \frac{\omega_0}{\omega}\right), \omega' = \frac{BW}{f_0}, M_{ii} = -\boldsymbol{\lambda_i} \tag{2.12}$$

The total energy stored in each resonator can be found from:

$$W_i = \frac{1}{4}L_i i_i^2 + \frac{1}{4}C_i V_{ci}^2 = \frac{1}{2}L_i i_i^2 = \frac{i_i^2}{2\omega_0} \tag{2.13}$$

The output power of practical filter is calculated as:

$$P_0 = \frac{1}{2}R_2 \omega' i_N^2 \tag{2.14}$$

The peak internal electric field in the resonator can be found from the relationship between field distribution and stored energy in the type of resonator used. Here, the proportional relation between the stored energy and the peak electric field square was used to find the maximum power-handling capacity of the filter by setting the maximum field intensity in the resonator equal to the air breakdown field and computing the maximum input power. This method is easy to implement and also considers the filter's structure. As well, the method is very quick due to use of a proportional relationship to predict maximum power. Hence, this method, with some modifications, is selected as the preferred approach to predict power-handling capacity.

2.1.4 Air Breakdown Mechanism

Although several parameters determine maximum power handling, such as ionization, multipaction, temperature and passive intermodulation [11], the focus of this research is to improve power handling by improving the air breakdown strength of the resonator. Hence, the mechanism of the breakdown in air in a uniform field is presented as follows.

The availability of energetic electrons due to a high electric field can begin ionization by colliding and releasing new electrons. Ionization then results in making a conducting path, allowing a sharp increase in the current.

There are two theories that explain breakdown in gases. The streamer theory explains breakdown in a highly non-uniform field, and the Townsend mechanism explains breakdown in a uniform field.

The gas breakdown in a uniform or weakly non-uniform field studied by Townsend is known as the Townsend mechanism. As shown in Figure 2.2., the breakdown process can be divided into three regions (or fields) of low, intermediate, and high current.

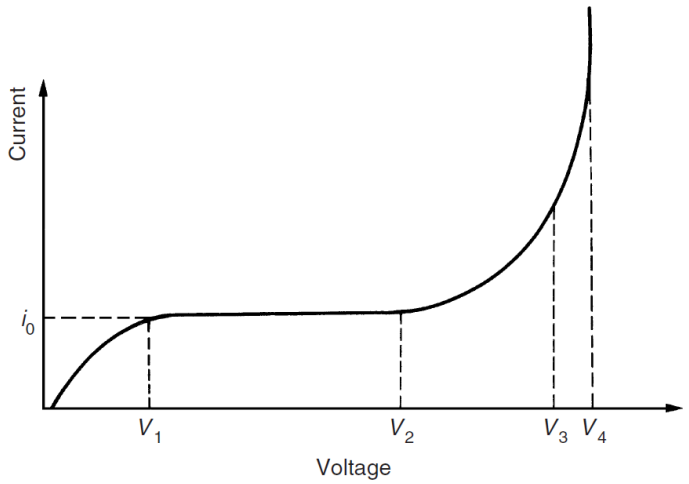

Figure 2.2. Current-voltage relation in a breakdown region [14].

In a low field region, the background current (i_0) or the photoelectric current have an almost linear relation with the voltage. In an intermediate field, in voltage up to a certain point, the current remains constant at i_0. In a high field region, exponential growth occurs due to high field effects, beginning with ionization processes. These include α and γ processes.

Where the α process refers to a collision of energetic electrons to release new electrons and the γ process refers to ionization due to processes near electrode surface, the current growth during breakdown process can be expressed as a function of α and γ processes as follow:

$$I = \frac{I_0 e^{\alpha d}}{1-\gamma(e^{\alpha d}-1)} \tag{2.15}$$

where d is the distance between the two electrodes.

The air breakdown also depends on other parameters such as temperature, pressure, humidity and the electrode geometry [14].

2.2 Diplexer Design Methods

As a key component in numerous communication systems, diplexers are frequency-selective components used to separate or combine two signals that work in various frequencies. There

are several methods available for designing a diplexer, all of which involve filters and a common junction. Diplexers allow two transmitters on different frequencies to use a common antenna at the same time. One of the main applications of transmit/receive diplexers is in the base station of mobile telephone systems. Figure 2.3 shows a simplified block diagram of the front end in base stations.

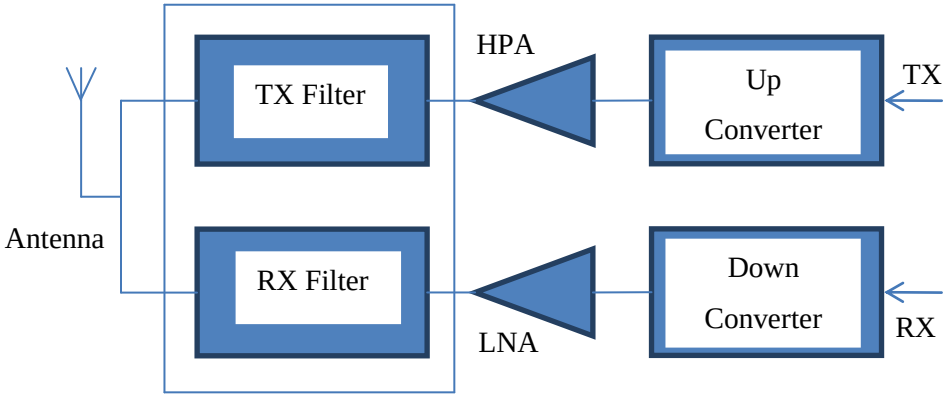

Figure 2.3. A simplified block diagram of the front end in a base station [13].

A receive filter delivers the signal in a receive frequency band to low noise amplifier and down converter, while the transmit filter is used not only to reject the out-of-band signals generated by the transmit part but also to deliver high power to the antenna. Consequently, it should have a high power-handling capability.

There are different methods available for designing a diplexer. A simple form of a diplexer consists of two 90-degree hybrids and two identical filters, which are designed to operate within the receive band with enough isolation to reject the transmit band [13]. Another approach is to design two separate filters, one for transmit and the other for receive channels, and to connect the two filters using a T-junction. The junction in this type has to be adjusted to achieve a desirable response. Another design method for a diplexer is to use a fast switch to switch the antenna between transmit and receive filters in the applications, which serves to transmit and receive signals that are not present at the same time, such as radar systems.

Generally, in conventional diplexers, an energy distribution network is used to connect the two filters working at different frequencies. Guglielmi [15] applied a waveguide manifold to connect the two filters, dividing the design task into four parts and fine-tuning a number of parameters in each part. Bastioli et al. used an innovative Y-junction to design rectangular waveguide diplexers [16], Yao et al. [17] utilized a T-junction to design a wide-band diplexer, and Saavedra [18] used a circulator for diplexer design. Utilizing a circulator instead of a manifold makes it possible to tune or exchange the filters without having to adjust the manifold. The most common approach for designing a filter is to first design the channels filters separately and then apply numerical optimization to the whole diplexer structure. In large and complex diplexer structures, this method is usually very time-consuming and requires a good starting point to converge after a few number of iterations. Atia et al. [19] proposed an optimization method for a general model of the coupled resonator filters, which was later used for diplexer optimization.

Research into this area has been extensive, and some of the highlights are as follows. Wu et al. [20] used immune clonal selection algorithm for diplexer design using optimization, while Omar et al. [21] offered a general circuit model for designing a coupled coaxial resonator diplexer. Zhang et al. [22] proposed a method for finding a very good initial point for applying a full-wave optimization method to a waveguide diplexer. Jong used two filters designed with randomly defined impedance technique to design a diplexer, and Wu et al. [23] proposed a direct synthesis for general chebyshev filters terminated by a complex load by normalizing the polynomials associated with it by the assumed impedance. Macchiarella et al. [24] used polynomials including the junction that connected the filters to synthesize the diplexer. This method was validated by a case that utilized only a slight separation between the two filters. Shin et al. [25] used an EM cosimulation technique, which is an accurate technique to reduce the design time. Skaik et al. [26] proposed novel topologies without any external junctions using any type of resonator; instead, they applied the optimization of coupling matrices for these topologies.

Chapter 3
High Power Analysis of Filters

As RF filters are widely used in communication systems, those used as transmitters should be capable of handling high power. This chapter focuses on the power handling of filters by investigating a method for predicting air breakdown via a single resonator. This method gives a good estimation of breakdown with a much lower process time as opposed to designing and soft-tuning the complete filter structure.

The method, as outlined above, is briefly explained in this chapter, and the results are shown and compared to the literature. Then, the method is applied to a two-pole coaxial filter using both capacitive disk and tap coupling. In the last part of this chapter, the method is used to find a new configuration of the coaxial resonator capable of handling higher power.

3.1 Methodology used for calculating breakdown values

Among all of the methods studied in the literature, the method based on a normalized filter prototype was chosen. The power-handling capability of the filter can be calculated by knowing that the stored energy is proportional to the maximum electric field square.

In order to ascertain the maximum stored energy in each resonator, a normalized filter prototype should be used in a circuit model. Such a model has already been investigated by Wang et al. [9]. The general two-port n-loop band-pass filter network with source and load impedances R1 and R2, shown in Figure 3.1, was used for this purpose. The circuit has N series resonators with resonant frequency $w_i, i = 1,2, \dots, N$. M_{ij} is a normalized frequency independent coupling which exists between the resonators i and j.

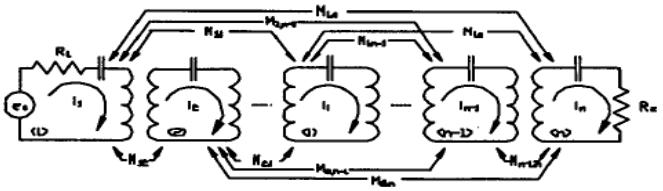

Figure 3.1. General two-port band-pass filter [9].

Assume the line impedance of each resonator to be normalized to unity using:

$$Z_0 = \sqrt{\frac{L_i}{C_i}} = 1, L_i = C_i = \frac{1}{\omega_i}, \omega_i^2 = \frac{1}{L_i C_i} \quad (3.1)$$

The loop equations can thus be expressed as: $ZI = V$

$$[R + S + jM][i_1, i_2, \dots, i_N]^t = [e_1, 0,0, \dots, 0]^t \quad (3.2)$$

$$S = \frac{j}{\omega'}\left(\frac{\omega}{\omega_0} - \frac{\omega_0}{\omega}\right), \omega' = \frac{BW}{f_0} \quad (3.3)$$

And the total energy stored in each resonator can be found from:

$$W_i = \frac{1}{4} L_i i_i^2 + \frac{1}{4} C_i V_{ci}^2 = \frac{1}{2} L_i i_i^2 = \frac{i_i^2}{2\omega_0} \quad (3.4)$$

The output power of a practical filter can then be determined as:

$$P_0 = \frac{1}{2} R_2 \omega' i_N^2 \quad (3.5)$$

At this point, and knowing that the stored energy in each resonator is proportional to the peak electric field square of the resonator ($W \propto E_0^2$), the maximum power-handling capacity of the filter can be determined. In previous work by [9], the power was calculated using an analytical approach for each specific geometry. However, in this research, the proportional relationship is used to calculate the geometries, which makes the process much easier.

This method includes three steps, as follows:

3.1.1 Step 1

The maximum stored energy and the maximum field of the single resonator are found using the eigen mode solution in HFSS. The field calculator in HFSS is used to determine the maximum stored energy (W_0) in the cavity. The following equation is used to find the stored energy:

$$E = \frac{1}{2} \varepsilon \int |E|^2 dv \quad (3.6)$$

This equation can be found in the field calculation cookbook [27]. There is also the possibility of writing this equation in the form of a function and easily load it to the calculator instead of writing the equation each time.

The maximum electric field (E_0) can be found by the field calculator as well. Another method of finding E_0 is to simply draw the complex magnitude of E in the structure. In

coaxial resonators an important point is to draw a plane in the center of the cavity and find the complex magnitude of E in the plane in order to obtain more accurate results [12].

3.1.2 Step 2

The circuit model of the filter is implemented in ADS. Each loop in the circuit model represents a resonator, and the current of the loop corresponds to that of the resonator. The input voltage source is adjusted in such a way that the input power becomes 1 Watt, which is the same input power as the High Frequency Structural Simulator (HFSS) default. Using Equation (3.4), the stored energy in all resonators is calculated and the maximum energy is derived (W_{0max}). The maximum stored energy usually occurs in the second resonator [13].

3.1.3 Step 3

From E_0, W_0, W_{0max} , the maximum electric field of the filter can be calculated (E_{0max}) using Equation (3.9).

$$W_{0max} \propto E_{0max}^2 \tag{3.7}$$

where:

W_{0max}=maximum stored energy obtained from the filter circuit model (ADS)

E_{0max}=maximum electric field obtained from the filter circuit model (ADS)

$$W_0 \propto E_0^2 \tag{3.8}$$

W_0=maximum stored energy in a single resonator at f_0 (HFSS)

E_0=maximum electric field of a single resonator at f_0 (HFSS)

From Equations (3.7) and (3.8)

$$\frac{E_{0max}^2}{E_0^2} = \frac{W_{0max}}{W_0} \rightarrow E_{0max}^2 = \frac{W_{0max}}{W_0} \times E_0^2 \rightarrow E_{0max} = \sqrt{\frac{W_{0max}}{W_0} \times E_0^2} \tag{3.9}$$

The electric breakdown strength of air is $3 \times 10^6 V/m$ [28], so E_{0max} should be below this value in order to avoid any breakdown.

3.2 Applying the power prediction method to a waveguide filter

The method is validated by implementing a 5-pole waveguide filter presented in [9] with the same parameters as below. The results show a good agreement with that of [9].

Center frequency (f_0) = 12.026 GHz, Bandwidth = 470 MHz

$R_1 = R_2 = 1.178, M_{12} = M_{45} = 0.928, M_{23} = M_{34} = 0.662$

3.2.1 Step 1

A WR75 waveguide with 0.6489in cavity length which resonates at the filter's center frequency is simulated in HFSS eigen mode in order to find E_0, W_0.

E_0 is calculated using both plotting the complex magnitude of E in the resonator (Figure 3.2) and the field calculator (Figure 3.3).

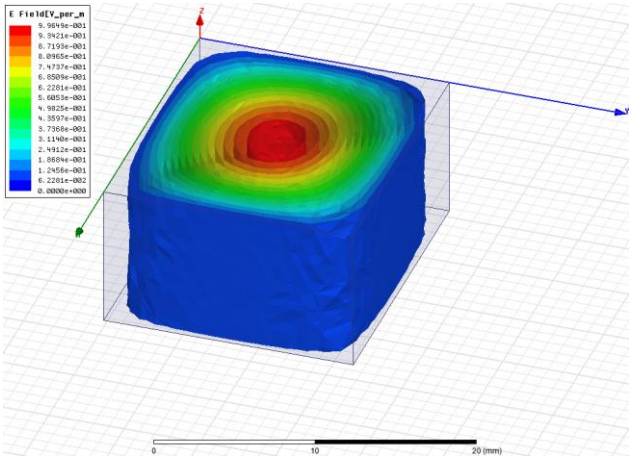

Figure 3.2. Complex magnitude of E in the waveguide resonator.

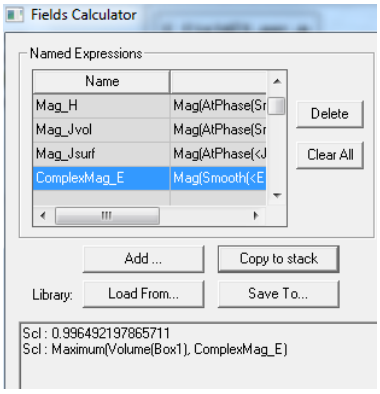

Figure 3.3. Field calculator results.

According to both of the methods, the maximum electric field is equal to 9.9649×10^{-1}V/m.

The maximum stored energy in the resonator (W_0) is also determined using the field calculator (Figure 3.4) :

```
Scl : 3.273101901238l8E-018
Scl : *(Integrate(Volume(Box1), Real(Dot(<Ex,Ey,Ez>, Conj(<Ex,Ey,Ez>)))), 4.421E-012)
```

Figure 3.4. Field calculator results for stored energy.

$$Stored\ energy\ in\ resonator(W_0) = \frac{1}{2}\varepsilon \int |E|^2\, dv = 3.273101 \times 10^{-18}\ \ J$$

3.2.2 Step 2

The circuit model of the filter is simulated in Advanced Design System (ADS) using the coupling matrix elements of the filter (Figure 3.5) and the S-parameters response of the filter are plotted (Figure 3.6).

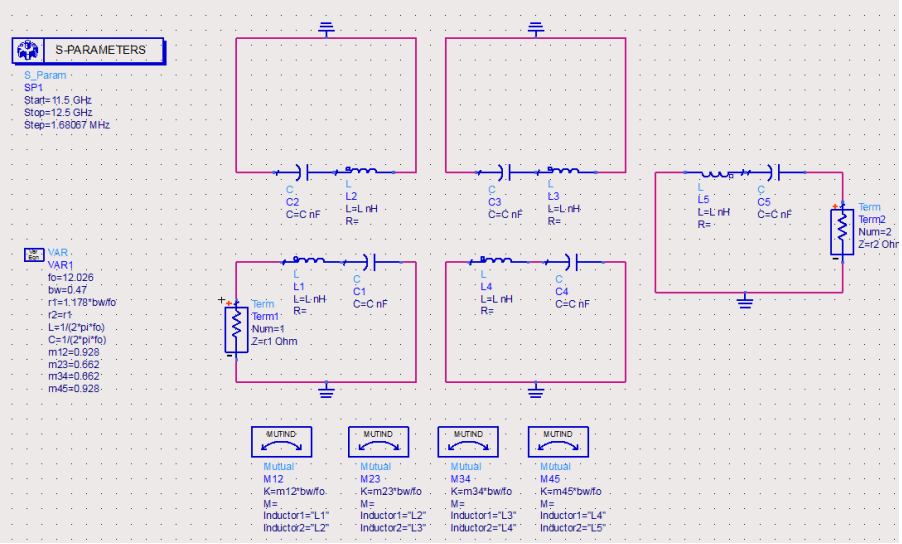

Figure 3.5. 5-pole filter circuit model.

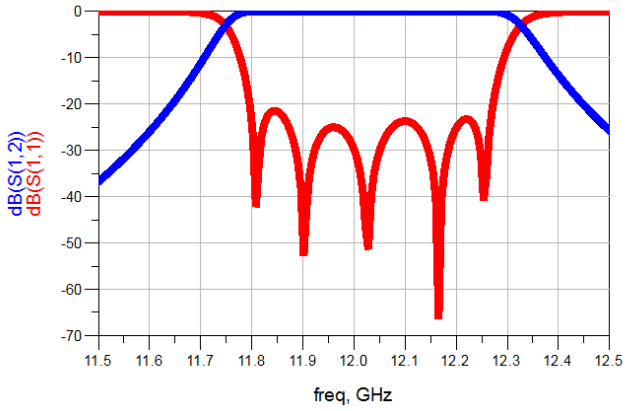

Figure 3.6. 5-pole filter response.

In order to find the maximum stored energy in the filter (W_{0max}), AC simulation should be done in ADS. As each loop represents a resonator, the current in each resonator can be measured by adding an I_Probe to each loop (Figure 3.7). At this point, the input power should be adjusted to 1 Watt by changing the magnitude of the input voltage source.

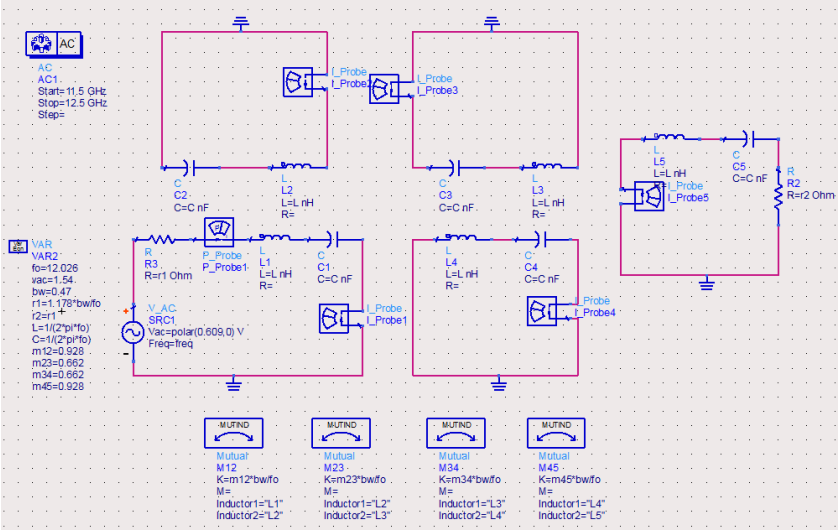

Figure 3.7. AC simulation of the filter.

Finally, Equation (3.4) is used for calculating the stored energy in the resonators. The current distribution of all five resonators can be found in Figure 3.8. As can be seen, the maximum current occurs in the lower frequency band edge of the second resonator.

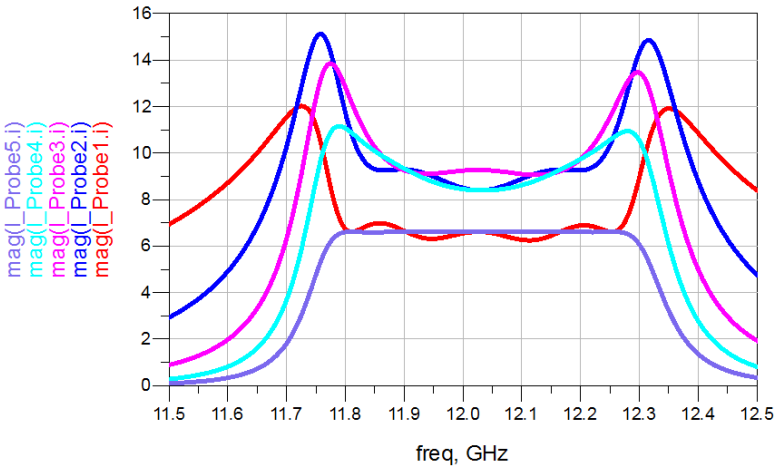

Figure 3.8. Current distribution in all resonators.

The maximum stored energy of 1.514×10^{-9} *J*, which occurs in the second resonator at 11.76 GHz, is shown in Figure 3.9.

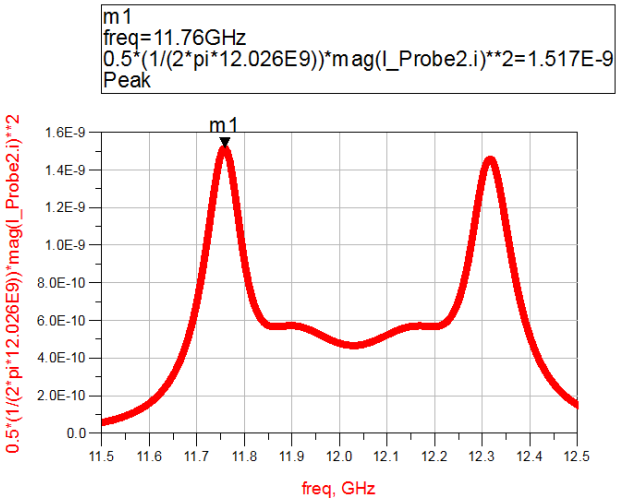

Figure 3.9. Maximum stored energy in the second resonator.

3.2.3 Step 3

From the above calculations, the breakdown voltage can be predicted as follows:

It should be noted that air breakdown voltage was considered 2.6×10^{6}V/mm, which was used in [9] in order to compare the results.

$$E_{max}=\sqrt{(E_0)^2\times\frac{W_{0max}}{W_0}}=\sqrt{(9.9649\times10^{-1})^2\times\frac{1.517\times10^{-9}}{3.273101\times10^{-18}}}=2.1453\times10^{4}v/m$$

$$\frac{E_{airBD}}{E_{1W}}=\frac{2.6\times10^{6}}{2.1453\times10^{4}}=121.1952$$

$$P_{airBD}\propto E_{airBD}^2 \tag{3.10}$$

$$P_{1W}\propto E_{1W}^2 \tag{3.11}$$

From (3.10) and (3.11) we can have:

$$\frac{P_{airBD}}{P_{1W}}=\left(\frac{E_{airBD}}{E_{1W}}\right)^2 \tag{3.12}$$

$$P_{airBD}=1W\times\left(\frac{E_{airBD}}{E_{1W}}\right)^2=1\times121.1952^2=\ 14688W$$

where E_{airBD} is the air breakdown field strength, $E_{1W}=E_{max}$, $P_{1W}=1W$ and P_{airBD} is the maximum input power that filter can handle without breakdown.

Now the complete filter should be implemented in HFSS using the dimensions given in [9], where the maximum breakdown value is found using Finite Element Method (FEM) (Figure 3.10).

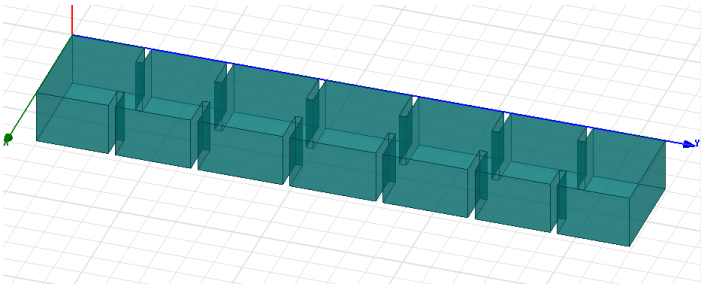

Figure 3.10. 5-pole waveguide implemented in HFSS.

An important point in this structure is assigning the ports; they should be de-embedded so that the change in the input transmission lines lengths will not affect the S-parameters (Figure 3.11).

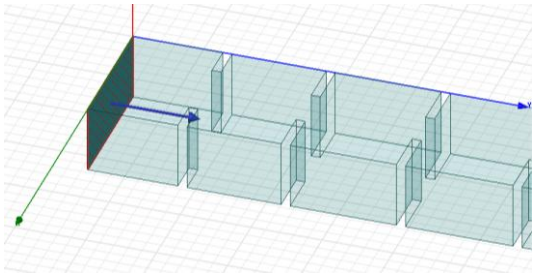

Figure 3.11. De-embedding the ports.

The maximum electric field in the structure can be found using a field calculator. The frequency should be changed to the band edge where the maximum occurs (Figure 3.12).

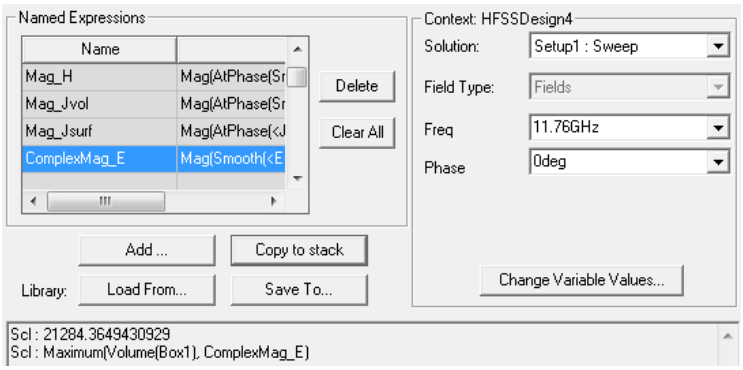

Figure 3.12. Computing the maximum electric field in the frequency band edge.

After finding the maximum electric field, the maximum power could be determined using Equation (3.12).It should be noted that the air breakdown is considered to be $2.6 \times 10^6 V/mm$ in order to compare the results with that of [9]. For all other calculations, $3 \times 10^6 V/mm$ has been used as the air breakdown value.

$$\frac{E_{airBD}}{E_{1W}} = \frac{2.6 \times 10^6}{2.1284 \times 10^4} = 122.1575$$

$$P_{airBD} \cong (122.1575)^2 = 14922\ W$$

This result can be confirmed by changing the input power in HFSS from 1 Watt to P_{airBD} (Fig 3.13).

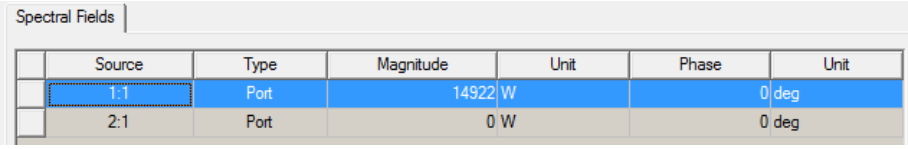

Figure 3.13. Changing the input power to P_{max}.

The field calculator is again utilized to determine the maximum electric field in the structure (Figure 3.14). The maximum electric field calculated will be equal to E_{airBD}.

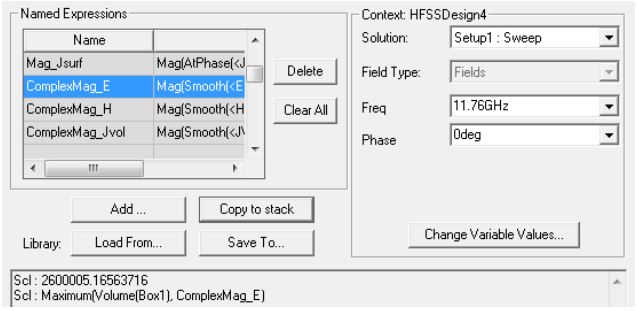

Figure 3.14. Finding the maximum electric field using a field calculator.

3.3 Applying the power prediction method to coaxial filters

As mentioned previously, this breakdown prediction method can be used for all filters, including coaxial filters. A conventional coaxial resonator is composed of an inner rod, made of metal, and an enclosure which can be either rectangular or cylindrical. These resonators are low in cost and high in tuning range but low in Q [29]. They also have a good spurious free window.

In the previous approach, the circuit model was lossless, meaning that the quality factor of the single resonator was not taken into consideration. In this attempt, by adding an impedance of $Z = jB + delta$ in the series to each loop, the effect of losses can be taken into account.

Where B represents self-inductance(M_{ii}) and delta represents the effect of the quality factor of the resonators (Q), the circuit model can be found from [13].

A 2-pole chebyshev filter with center frequency of 2.5 GHz and a bandwidth of 25.1MHz was selected as a case study. This filter was designed using two approaches for realizing the input coupling. One is to use a disk close to the resonator (capacitive coupling) and the other is to use tapping as the input coupling (inductive coupling).

The following steps describe the application of the power-handling method to the 2-pole filter.

3.3.1 Step 1

A single coaxial resonator, resonating at the center frequency of the filter (2.5GHz), is simulated in HFSS eigen mode (Figure 3.15).

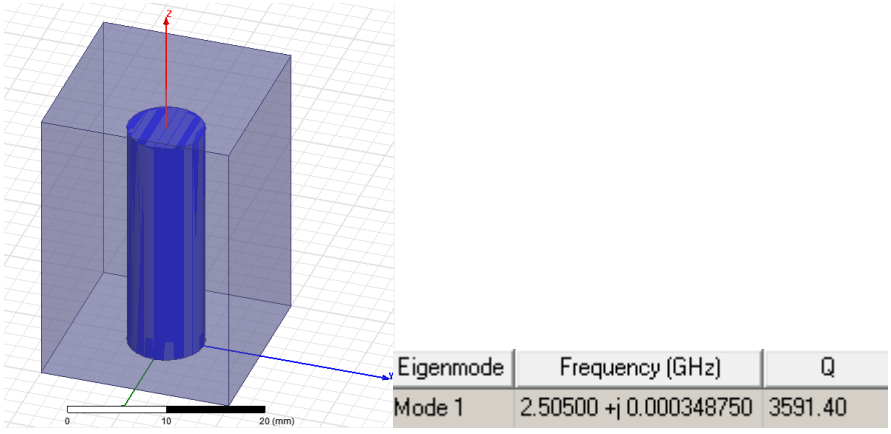

Figure 3.15.Coaxial resonator used in eigen mode.

To find the maximum E field, we have two options. The first option is to select the cavity and plot the complex magnitude of E field (Figure 3.16). The maximum electric field (E_0) using this method is equal to 0.6502 V/m**.**

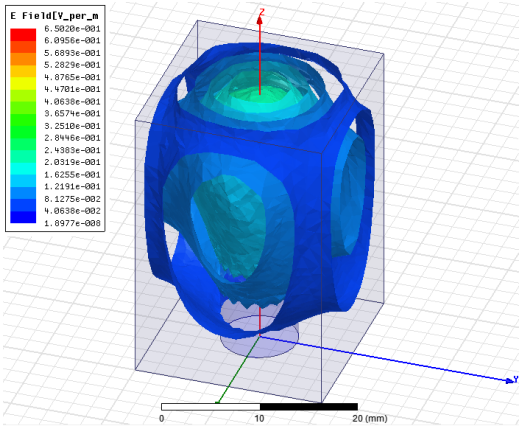

Figure 3.16. The electric field in a single cavity.

The second option is to draw a plane in the resonator and see the complex magnitude of E in that plane (Figure 3.17). This method is more accurate, and the value found using it is less than the first approach [12]. The amount of maximum electric field (E_0) utilizing the plane is equal to 0.56257 V/m. Moreover, the location where the maximum field occurs could be easily seen using the plane.

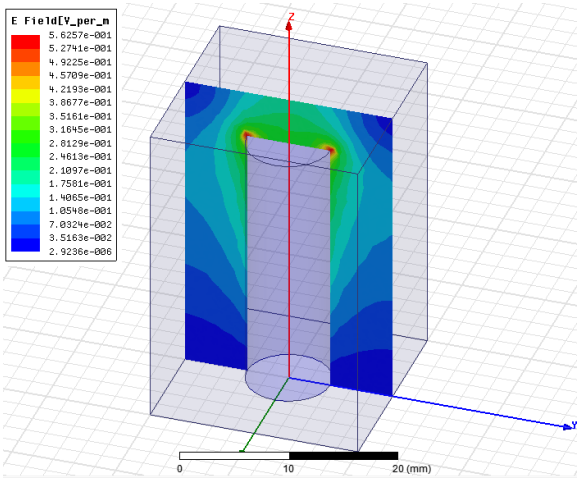

Figure 3.17. The electric field in the resonator using a plane.

The value of the stored energy(W_0) is 4.537188×10^{-19} $\boldsymbol{J}$ by implementing equation (3.4) in the field calculator (Figure 3.18).

```
Scl: 4.537193569517 37E-019
Scl: *[Integrate[Volume[Cavity], Real[Dot[<Ex,Ey,Ez>, Conj[<Ex,Ey,Ez>]]]], 4.4271E-012]
```

Figure 3.18. Field calculator results for calculating stored energy.

3.3.2 Step 2

Here, the filter circuit model in ADS is implemented to ascertain the maximum stored energy, and the Quality factor of the resonators, found from the single resonator's eigen mode, is taken into consideration (Figure 3.19). The magnitude of the input source is adjusted to ensure an input of 1 Watt. This adjustment is made in prediction of the results compared with those of the complete structure in HFSS. The coupling elements of this 2-pole chebyshev filter were found using MATLAB and used in the circuit model in ADS.

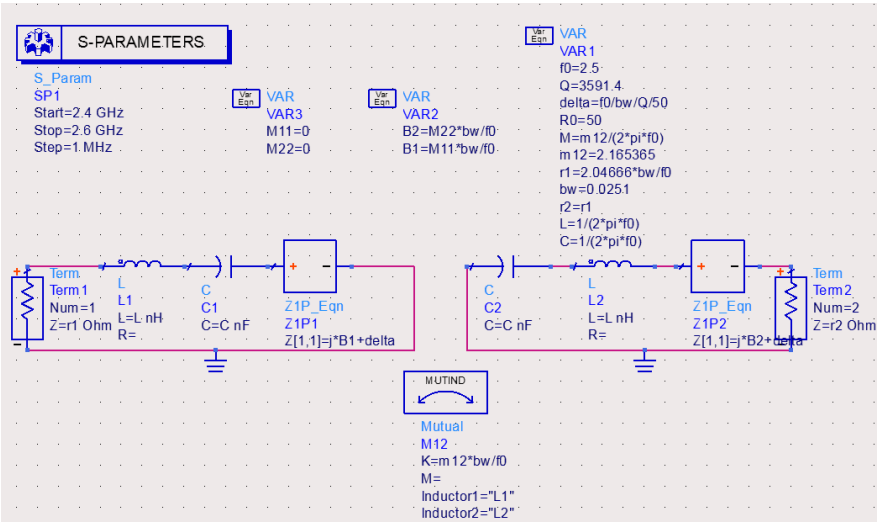

Figure 3.19. The more complete circuit model of a filter in ADS by adding the effect of self-coupling and losses.

The response of the filter circuit is shown in Figure 3.20.

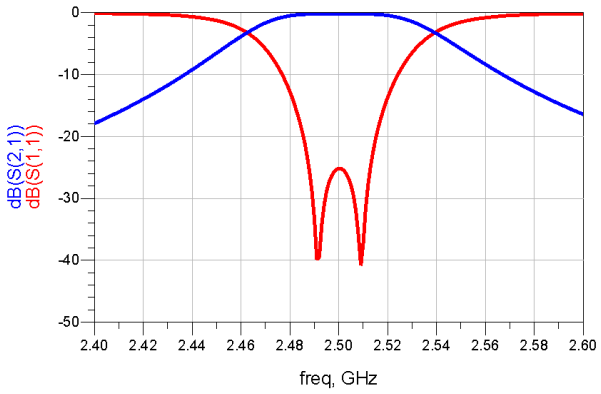

Figure 3.20. The S-parameters of the 2-pole filter.

The currents in each resonator can be found using the circuit model shown in Figure 3.21. Having found the currents, the stored energy in the resonators was determined using Equation (3.4).

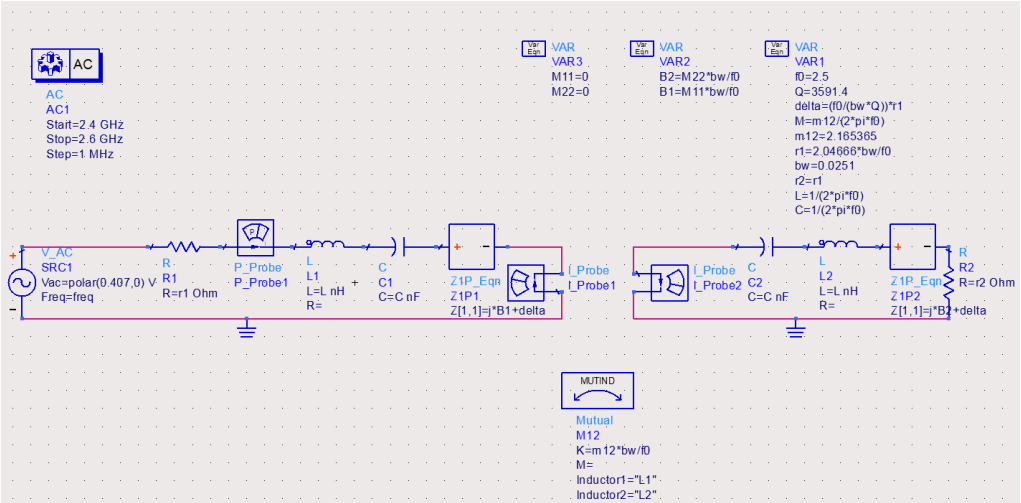

Figure 3.21.Circuit model used for finding the stored energy in the resonators.

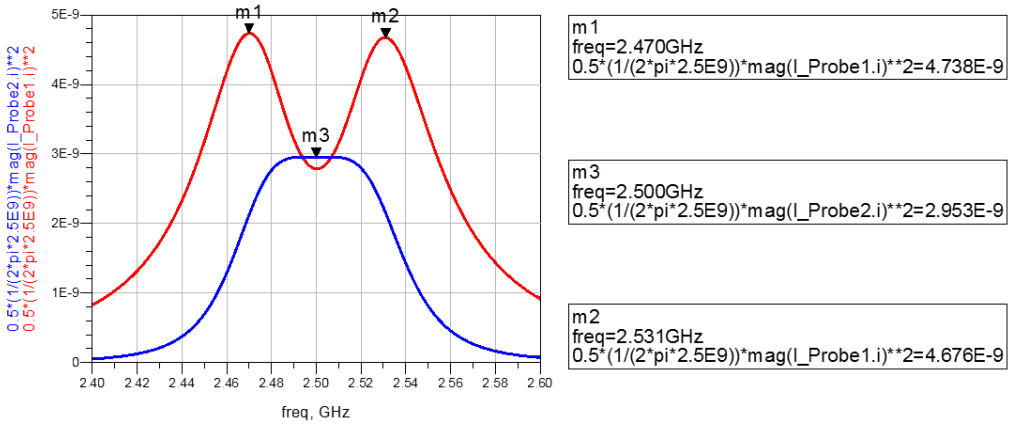

Figure 3.22. The stored energy in the resonators.

3.3.3 Step 3

At this point, the maximum electric field is calculated by looking at the maximum value in two frequencies:

1-The center frequency

2-The band edge (where the maximum breakdown happens)

The value of the maximum stored energy(W_{0max}) in the filter's center frequency (2.5GHz) is equal to 2.957×10^{-9} (J), which occurs in the second resonator.

Finding E_0, W_0 and W_{0max} , the value of E_{max} can be calculated as follows:

$$E_{max} = \sqrt{(E_0)^2 \times \frac{W_{0max}}{W_0}} = \sqrt{(5.627e-1)^2 \times \frac{2.953e-9}{4.5371884e-19}} = 4.53957 \times 10^4 \ v/m$$

Figures 3.23 and 3.24 show the realization of the filters and their responses using disk and tapping input couplings.

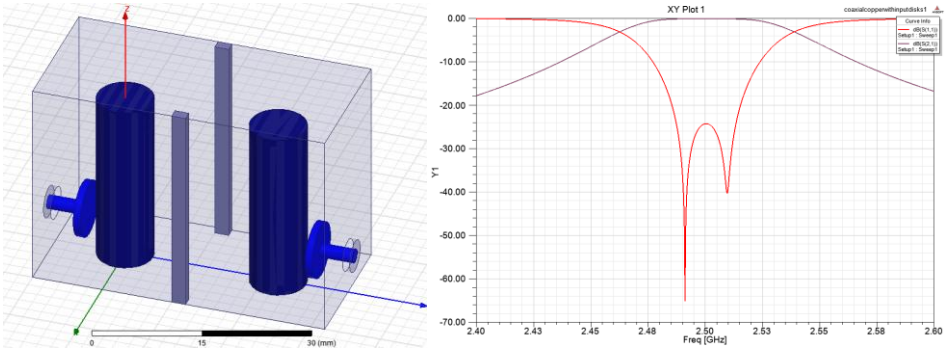

Figure 3.23. The filter structure and filter response using disks for input coupling.

The two tapping methods are compared in order to see their effect on the amount of the predicted breakdown value in the resonators.

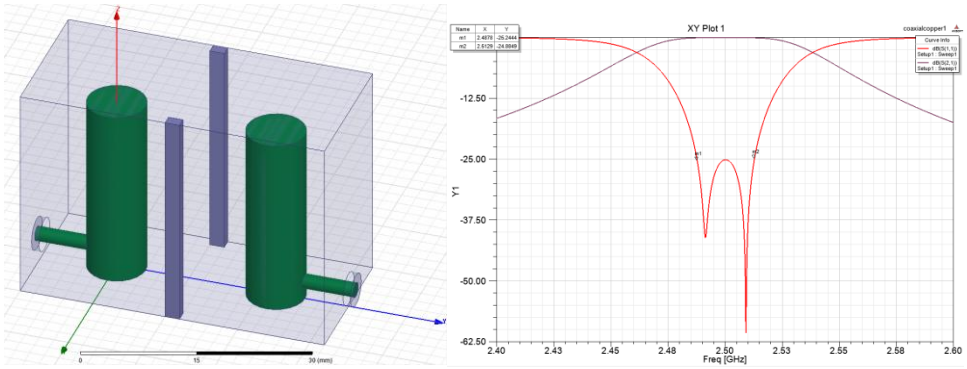

Figure 3.24.The filter structure and filter response using tapping for input coupling.

Knowing, from the circuit model, that the maximum electric field occurs in the second resonator at the center frequency, a plane is drawn in the second resonator of each filter and the maximum electric field E_{max} is found by plotting the complex magnitude of E in that

plane. As can be seen, the planes are placed in such way that the effect of tapping is excluded. The plots are shown Figures 3.25 and 3.26.

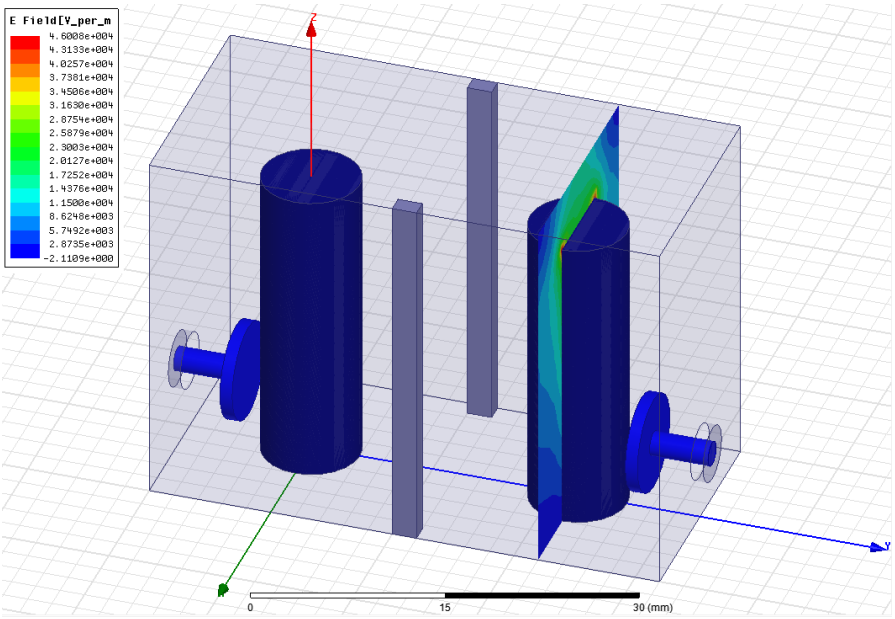

Figure 3.25.Maximum electric field in the center frequency happening in the second resonator of the filter with disks.

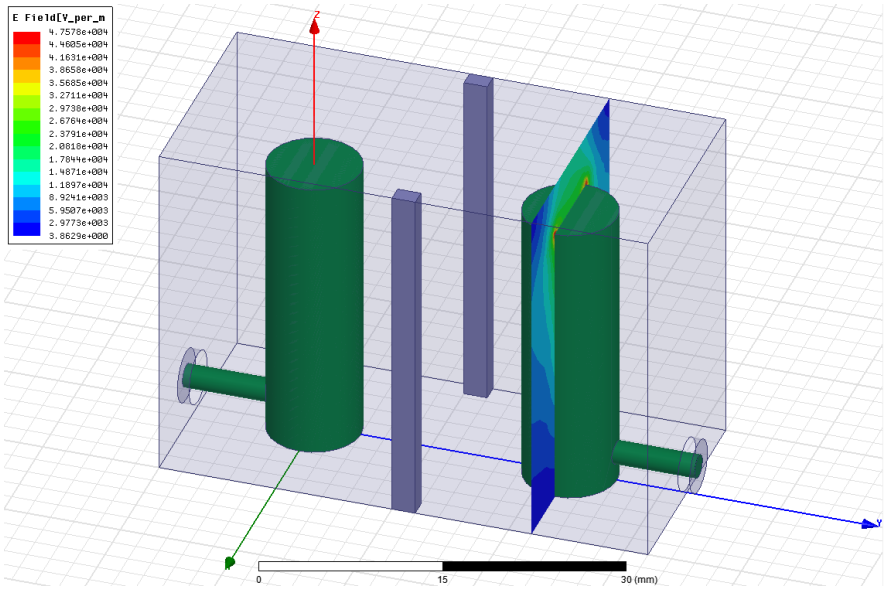

Figure 3.26. Maximum electric field in the center frequency happening in the second resonator of the filter with tapping.

The maximum input power that the filter can handle is calculated using Equation (3.12):

$$\frac{P_{airBD}}{P_{1W}} = \left(\frac{E_{airBD}}{E_{1W}}\right)^2, P_{1W} = 1W$$

$$\frac{E_{airBD}}{E_{1W}} = \frac{3 \times 10^6}{4.54264 \times 10^4} = 66.0408925$$

$$P_{airBD} = 1W \times \left(\frac{E_{airBD}}{E_{1W}}\right)^2 = 1 \times 66.0408925^2 = 4361.39W$$

In order to confirm the above findings, the input power is changed from 1 W to 4361.39 W. It results in E_{max} of 3.0384×10^6 (V/mm), which is equal to the air breakdown (Figure 3.27).

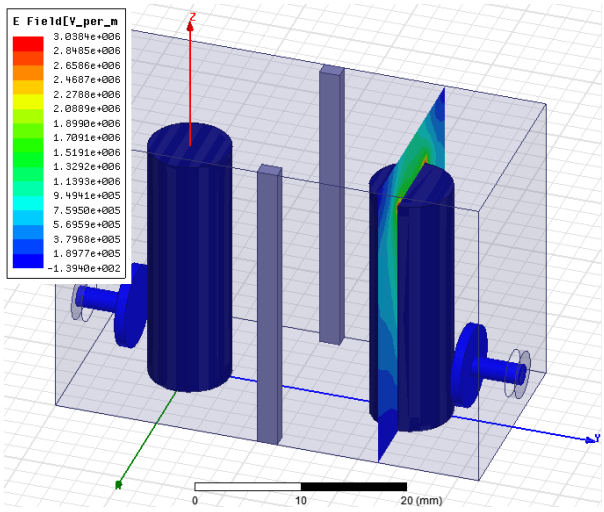

Figure 3.27. Maximum electric field after changing the input power to P_{airBD}.

To predict the stored energy in the band edge, the value of W_{0max} should be replaced by the maximum stored energy found in Figure 23, which occurs in the first resonator and is equal to 4.738×10^{-9} $\boldsymbol{J}$ at 2.47GHz (Equation 3.13).

$$E_{max} = \sqrt{(E_0)^2 \times \frac{W_{0max}}{W_0}} = \sqrt{(5.627 \times 10^{-1})^2 \times \frac{4.738 \times 10^{-9}}{4.5371884 \times 10^{-19}}} = 5.75017466 \times 10^4\ v/m$$

(3.13)

The results of plotting the complex magnitude of E in the first resonators at 2.47 GHz for both of the filters can be found in Figures 3.28 and 3.29.

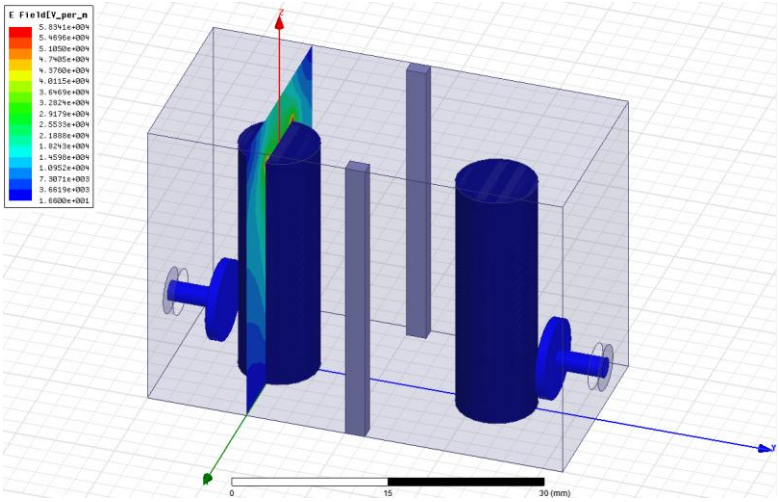

Figure 3.28. Complex magnitude of E in the band edge.

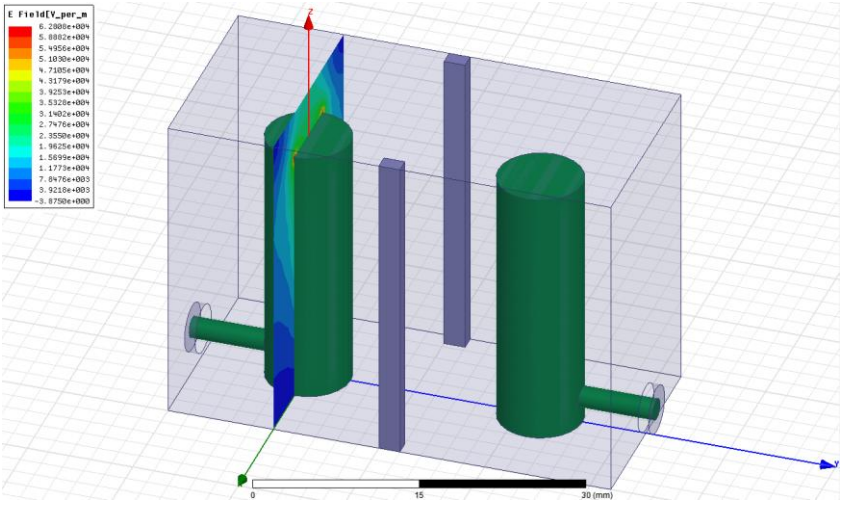

Figure 3.29. Complex magnitude of E in the band edge.

The maximum input power in this case was calculated equal to 2719.655 W, and the corresponding electric field plot in the first resonator was drawn which is shown in Figure 3.30.

$$\frac{E_{airBD}}{E_{1W}} = \frac{3 \times 10^6}{5.752601 \times 10^4} = 52.15319$$

$$P_{airBD} = 1W \times \left(\frac{E_{airBD}}{E_{1W}}\right)^2 = 1 \times 52.15319^2 = 2719.655W$$

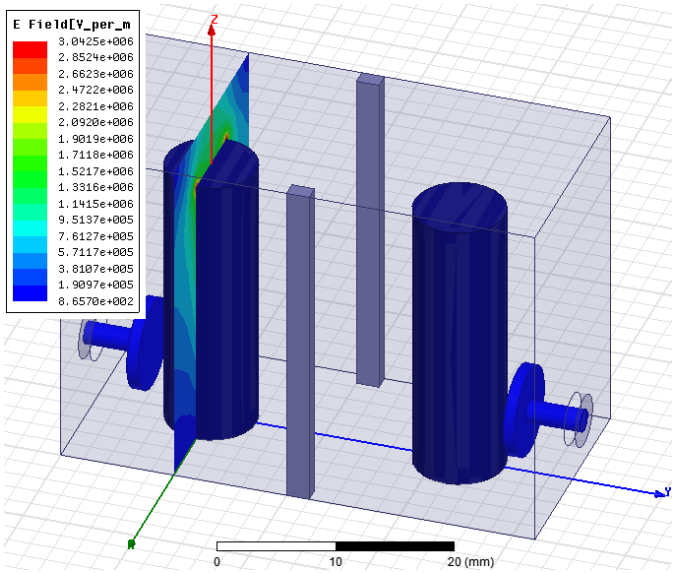

Figure 3.30. Complex magnitude of E after changing the input power to P_{airBD}.

All of the results are summarized in Table 3.1.

Table 3.1. Comparison of disk and taping filters in terms of breakdown.

		Predicted	***Complete structure(HFSS)***
Using disk	*At Center frequency*	4.53957×10^4 V/m	4.6008×10^4 V/m
	Maximum	5.75017×10^4 V/m	5.8341×10^4 V/m
Using tapping	*At Center frequency*	4.539575×10^4 V/m	4.7578×10^4 V/m
	Maximum	5.75017×10^4 V/m	6.2808×10^4 V/m

A good agreement is found between the predicted values and the values found from the complete model in HFSS. However, using the disk shows more accurate results in the band edge, since adjusting the input coupling is completely independent of the resonator's height.

It can be noted that this method provides information for individual resonators only and is not able to provide information about the electric field in other parts of the structure. In order to compare the realization of input couplings, the complex magnitude of E was plotted for both designs, with the measurement planes crossing the input probes (Figures 3.31 & 3.32).

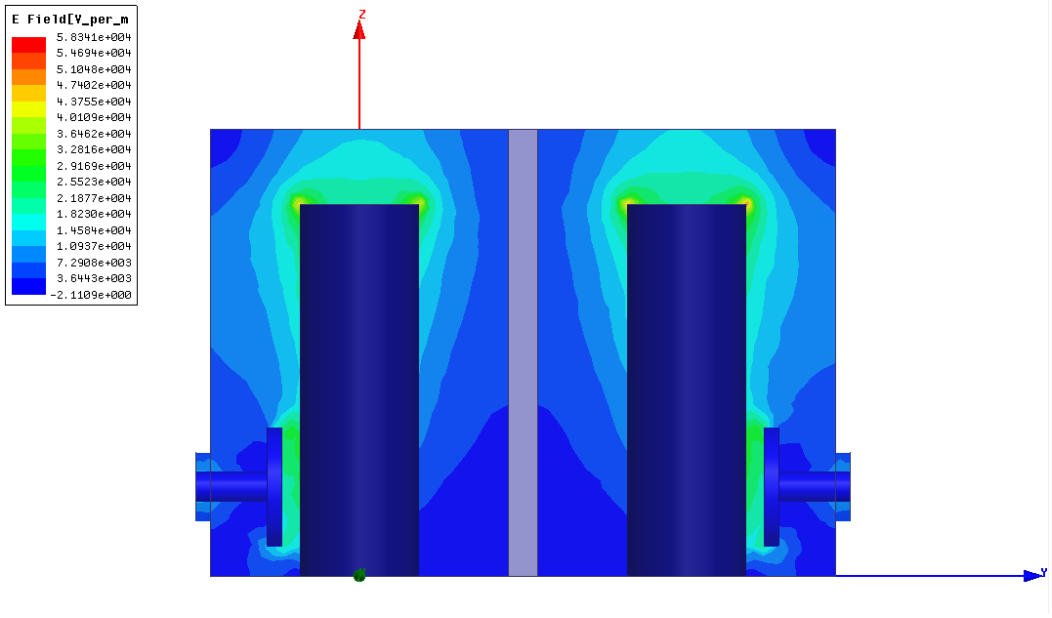

Figure 3.31. Field distribution in the filter with capacitive input coupling.

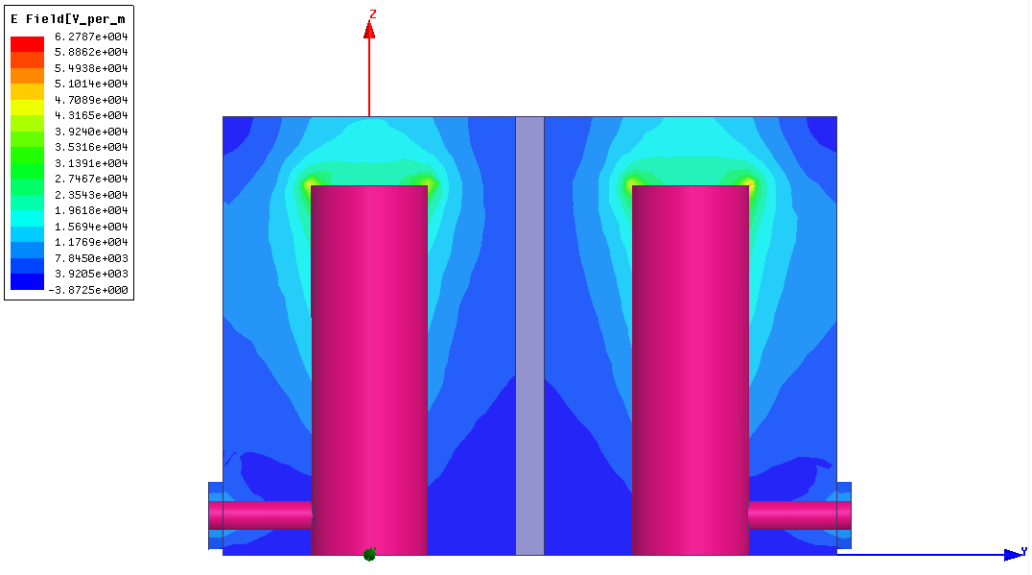

Figure 3.32. Field distribution for the filter with inductive input coupling.

Although more accurate results come from using a disk to realize the input coupling, the electric field between the disk and the resonator will be much higher than the tapping case. Thus, tapping enables better power-handling. Moreover, the practical implementation of a disk involves more difficulties compared to tapping.

The reason that the maximum electric field is lower when using disks is that the height of the resonators is lower. As well, frequency adjustments have been done by changing the disks size and the gap between the resonator and the disk.

3.4 Using the power-handling prediction method to find a resonator with better power-handling

In previous sections, the power-handling prediction method was used to determine the maximum electric field, and hence maximum power, in a band-pass filter. In this section, the method is implemented to find the power handling of the existing coaxial structures and to come up with a new structure with enhanced power-handling capability. The goal is also to keep the frequency, quality factor and size of the resonator the same. After finding such a resonator, a filter with better power-handling performance can be designed.

First of all, in order to achieve better power handling, the electric field should be uniform, which is why shapes such as spheres or half-spheres are good choices.

The quality factor arising from eigen mode is actually the unloaded Q, which could be calculated using Equation 3.14:

$$Q_u = \omega_0 \frac{W_T}{P_{loss}} \tag{3.14}$$

where $W_T = W_e + W_m$ and P_{loss} is the power dissipated in the resonator. The amount of Q depends on both the size of the structure and the field distribution. The bigger the structure, the higher the quality factor will be. The cavity size is assumed to be $20mm \times 20mm \times 30mm$ and the cylinder diameter is 8mm. Furthermore, the resonance frequency of all the resonators is adjusted to 2.5GHz, and all of the resonators are made of copper.

Step 1 of the method is done for all structures, and the values of E_0, W_0 are found for each resonator. Each resonator's shape, field distribution and stored energy can be found in Figures 3.33 to 3.37.

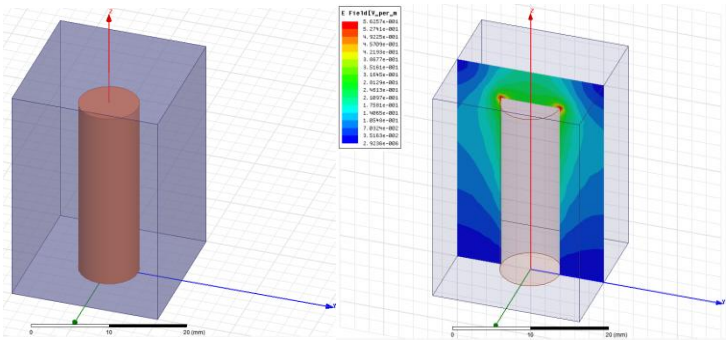

Figure 3.33. Conventional coaxial resonator.

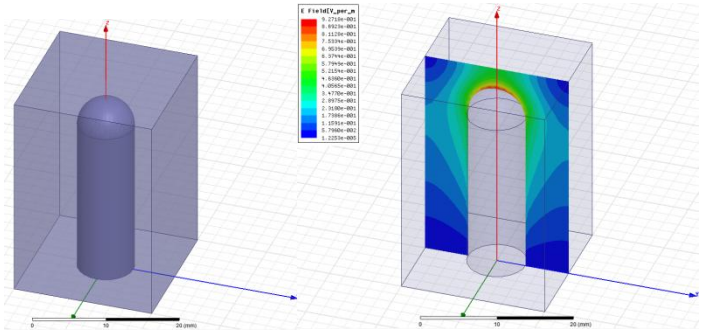

Figure 3.34. Adding a small half-sphere to the top of the resonator.

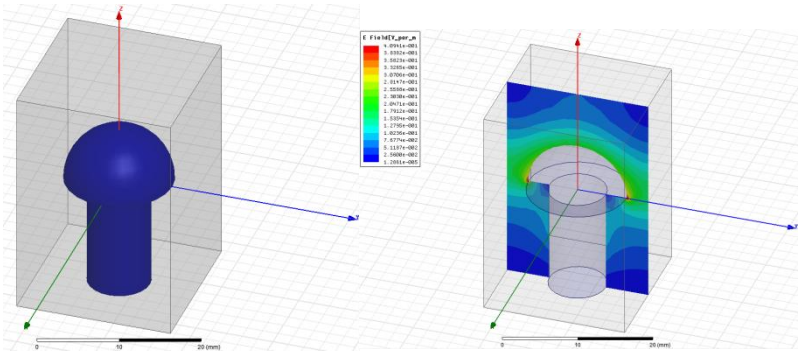

Figure 3.35. Reducing the height of the resonator and adding a half-sphere to the top.

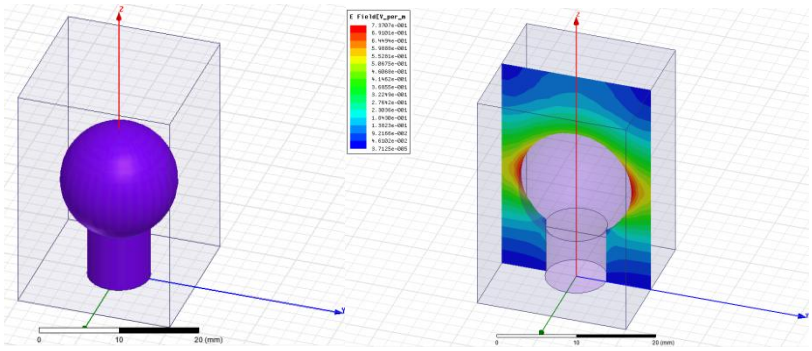

Figure 3.36. Reducing the height of the resonator and adding a sphere to the top.

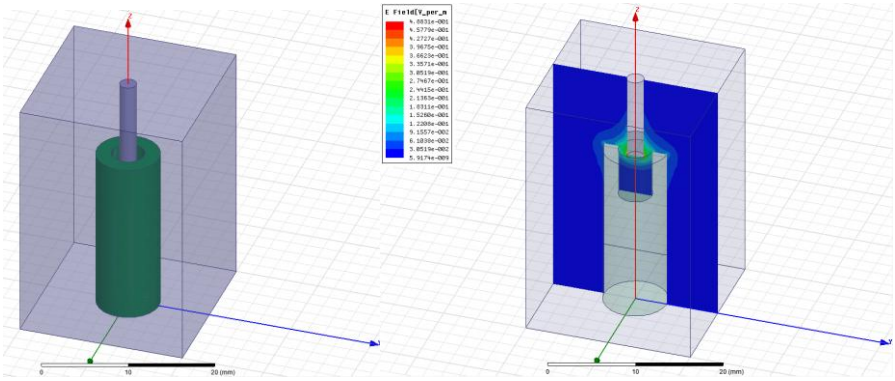

Figure 3.37. Adding a screw to the resonator.

Step 2, which is finding the maximum stored energy using the circuit model in ADS, was already performed in the previous section. Since these resonators will be used to produce the same filters as in that section (center frequency=2.5GHz, BW=25.1MHz), the previously determined value of W_{0max} equal to 4.738×10^{-9} at 2.47 GHz (Figure 23) can be used. An important point here is that, if the Q value is not the same for all resonators, it will not be possible to use a single circuit model for them.

Step 3 is done in order to predict E_{max} , using the following equation:

$$E_{max} = \sqrt{(E_0)^2 \times \frac{W_{0max}}{W_0}}$$

The results of Steps 1 to 3 can be found in Table 3.2.

Table 3.2. The results of Steps 1 to 3 of the power-handling analysis method on different resonators.

Shape	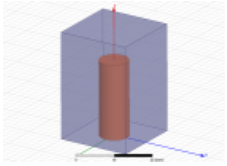	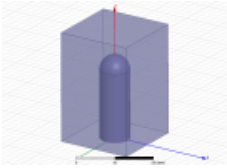	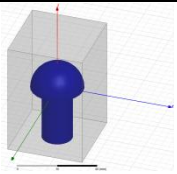	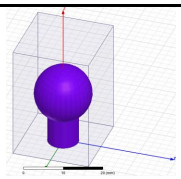	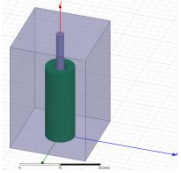
$\boldsymbol{Q}$	3591.4	3615.72	3237.22	2972.99	3445.73
$\boldsymbol{E_0}$	0.56257 V/m	0.92718 V/m	0.40941 V/m	0.73707 V/m	0.48831 V/m
$\boldsymbol{W_0}$	4.5371 $\times 10^{-19}$ J	1.3943 $\times 10^{-18}$ J	3.0693× 10^{-19} J	2.273 $\times 10^{-18}$ J	1.1166 $\times 10^{-20}$ J
$\boldsymbol{E_{max}}$	5.7489 $\times 10^{4}$ V/m	5.4048 $\times 10^{4}$ V/m	5.086 $\times 10^{4}$ V/m	3.364 $\times 10^{4}$ V/m	3.180 $\times 10^{5}$ V/m

From the above table, it can be seen that resonator 4 (with a sphere on top) has the best power handling capability, but that its quality factor is the lowest among all of the resonators listed. Another drawback associated with resonator 4 is the difficulty in producing such a shape.

It should be noted that the resonators are compared in terms of E_{max}, where a lower maximum electric field means better power-handling performance.

The resonator with the second-best power-handling and a quality factor that is almost equal to the conventional coaxial resonator, is resonator 3, which includes a half-sphere connected to the rod. (This resonator will be called the mushroom-shaped resonator from this point onwards). The mushroom-shaped resonator was selected as the best type among the studied structures and was used to design a 4-pole filter.

It also can be noted that, since W_{0max} is the same for all of the resonators, only by calculating $\sqrt{\frac{(E_0)^2}{W_0}}$ can the resonators be compared easily and the one with the better power-handling determined.

In order to improve the quality factor of a combine resonator shown in Figure 3.38, the ratio of D/d should be equal to 3.59 [30].

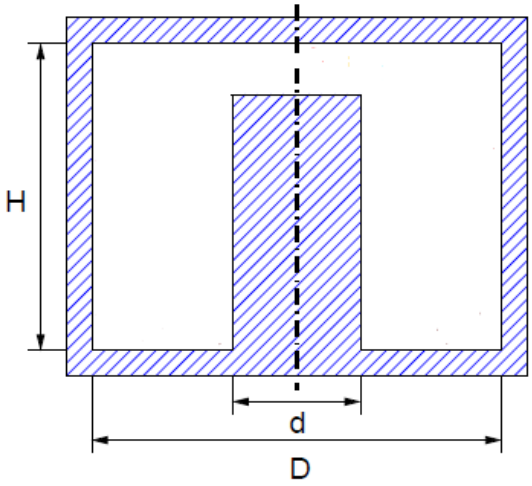

Figure 3.38. Conventional coaxial resonator [30].

Another way of improving the quality factor of coaxial resonators is to change the material of the inner rod from metal to dielectric [26]. However, the only problem with this approach is that the spurious window will become smaller and the price higher.

3.5 Four-pole mushroom-shaped filter design

Applying the power handling analysis method for this resonator, the maximum E field, E_{max}, can be predicted as follows:

Step 1: $E_0 = 0.47882\ V/m$ and $W_0 = 5.086898 \times 10^{-19}$ from eigen mode analysis in HFSS.

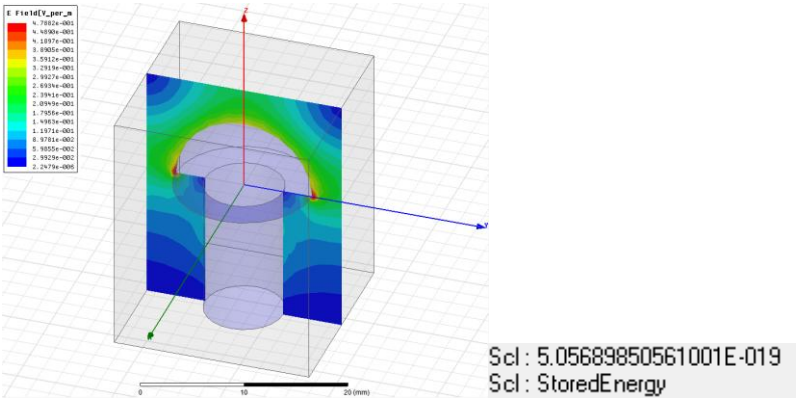

Figure 3.39. Maximum electric field and stored energy in HFSS.

Step 2: From the circuit model of the filter with a center frequency=2.5GHz and BW=14MHz, the maximum stored energy was equal to $W_{omax} = 3.335 \times 10^{-8}$ at 2.491 GHz (Fig 33).

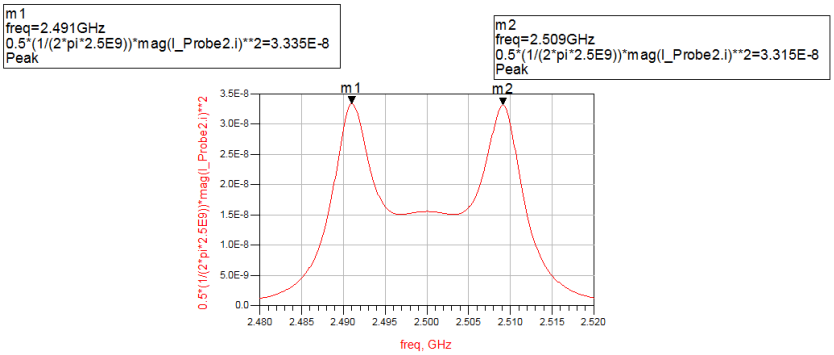

Figure 3.40. Stored energy distribution in the second resonator.

Step 3: $E_{max} = \sqrt{(E_0)^2 \times \frac{W_{0max}}{W_0}} = \sqrt{0.47888^2 \times \frac{3.335 \times 10^{-8}}{5.056898 \times 10^{-19}}} = 1.2260 \times 10^5\ V/m$

This resonator was used to design and implement a 4-pole chebyshev filter. Figure 3.41 shows the HFSS simulation of the filter and its response. The filter was designed from aluminum to make the machining process easier.

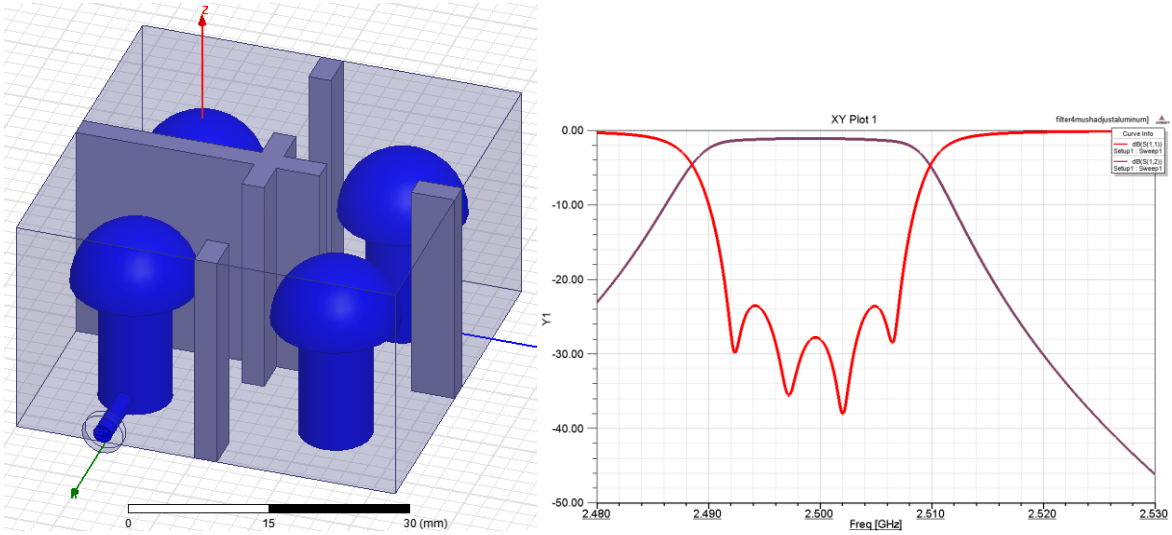

Figure 3.41. The complete filter structure and filter response in EM simulator (HFSS).

As can be seen in Figure 3.42, the maximum electric field occurs in the second resonator, which is equal to 1.4552×10^5 V/m at 2.491 GHz. This result also matches the predicted value.

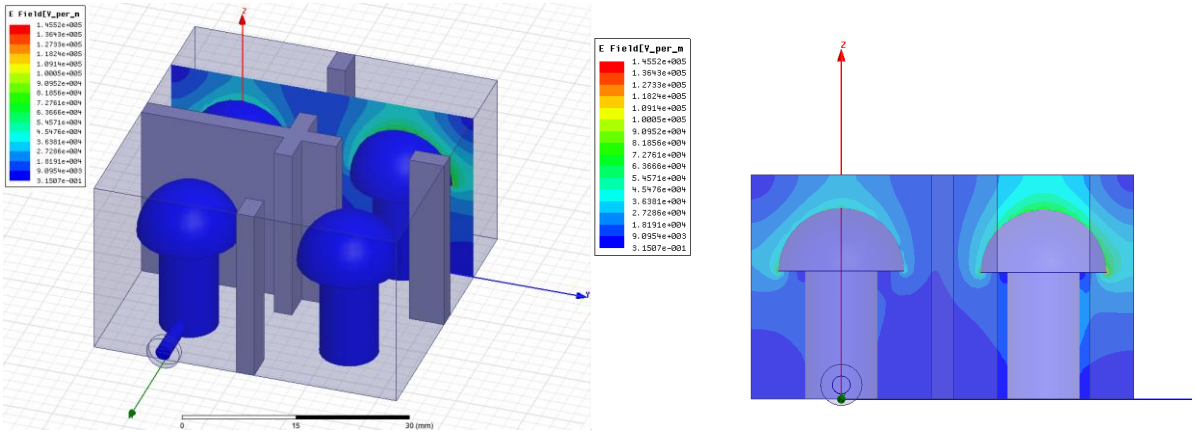

Figure 3.42. Field distribution in the complete filter structure.

Figure 3.43 shows the final complete design of the filter including. All of the details were exported to the Solid Works® CAD program to be used by the machine shop.

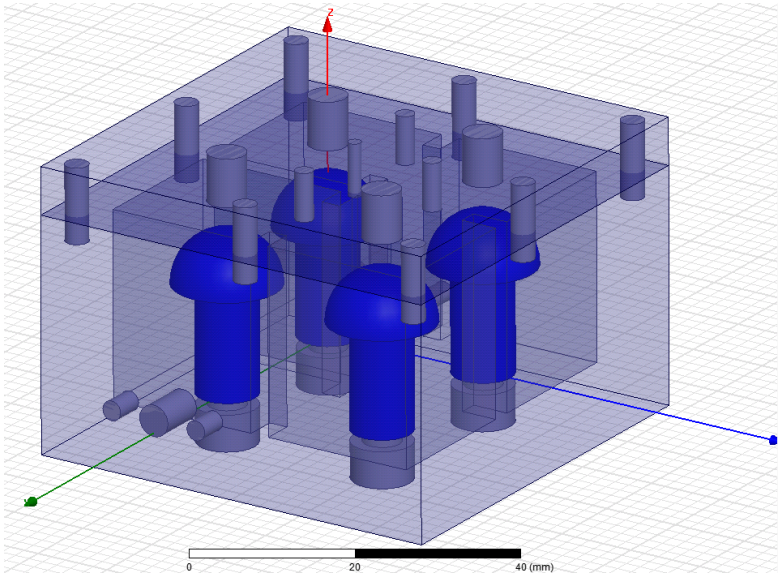

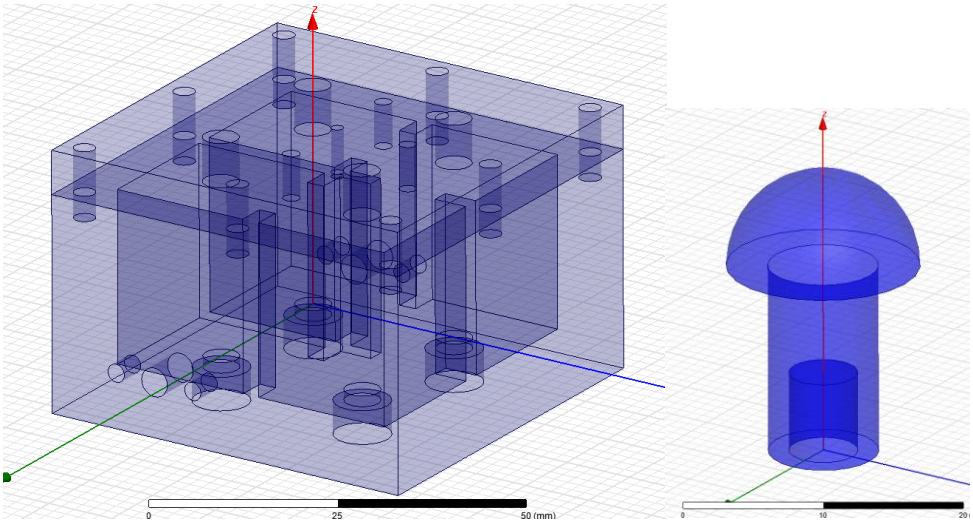

Figure 3.43. The complete design of 4-pole filter.

Figures 3.44 and 3.45 illustrate the filter.

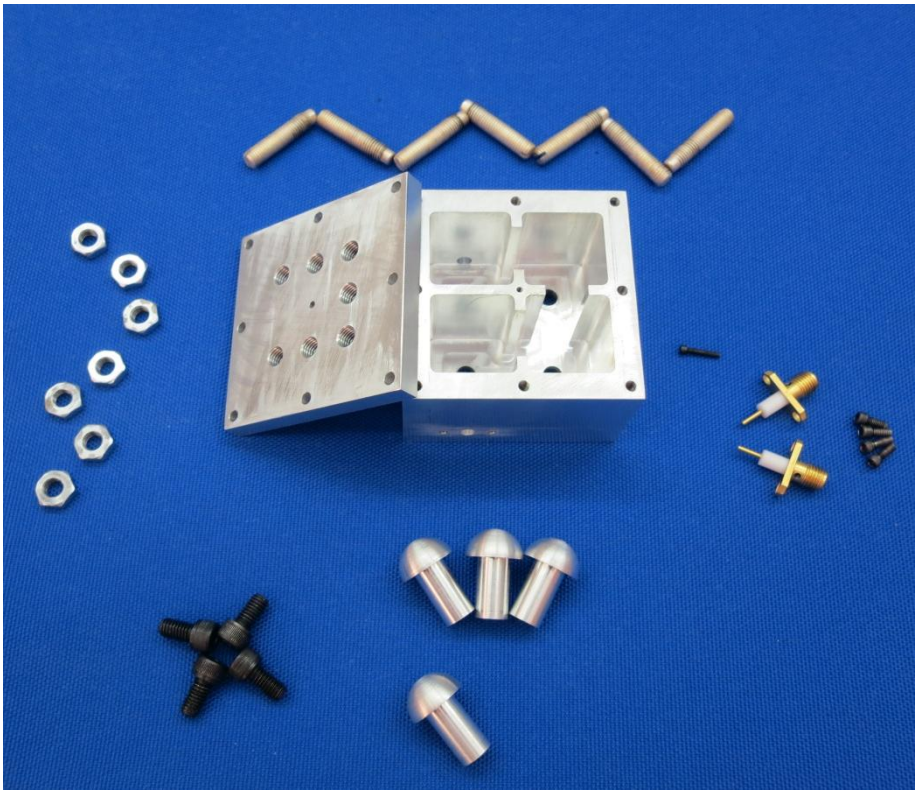

Figure 3.44. Pieces used in the filter.

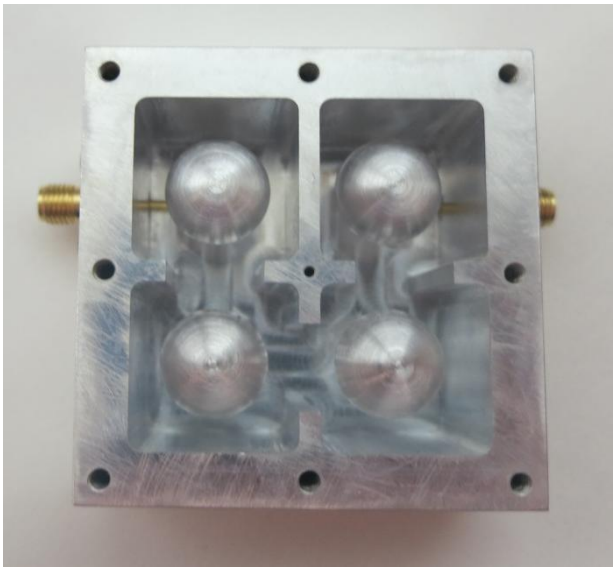

Figure 3.45. Inside the filter.

3.5.1 Measurement results

The S-parameters of the filter were measured in the CIRFE lab using both Power Network Analyzer (PNA) and Voltage Network Analyzer (VNA). The results were saved in S2p file format to enable them to be imported to ADS (Figure 3.46).

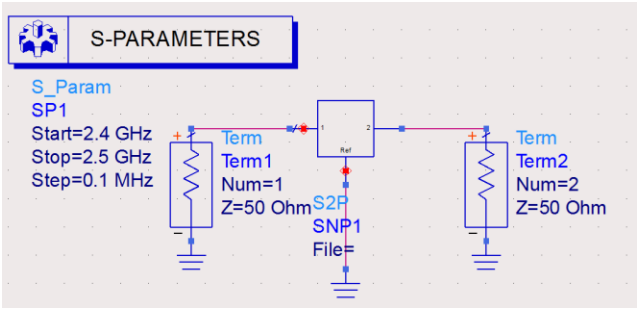

Figure 3.46. Simple circuit for reading S2p files in ADS.

Figure 3.47 shows the measurement results before tuning. Nearly all of the filters required tuning after being made. This may be due to errors in machining or small differences such as sharp edges in the design model. Nevertheless, even by using tuning screws, the resonator will have better power-handling capability than conventional coaxial resonators, since in both cases tuning screws might be used (hence, the effects of the tuning screws will be the same). The measurement results after tuning can be found in Figure 3. 48.

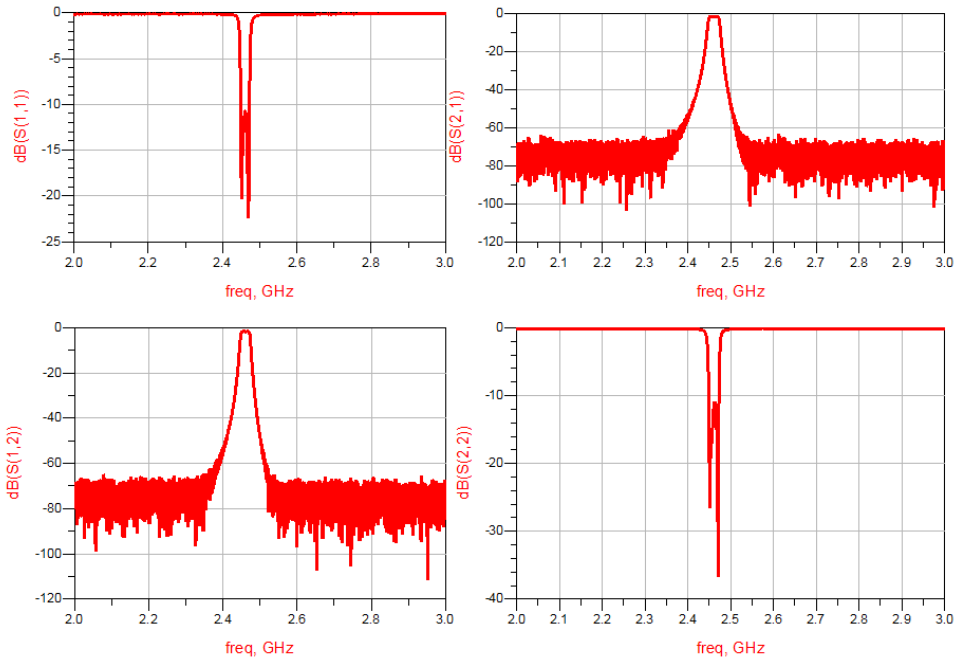

Figure 3.47. Measurement results before tuning.

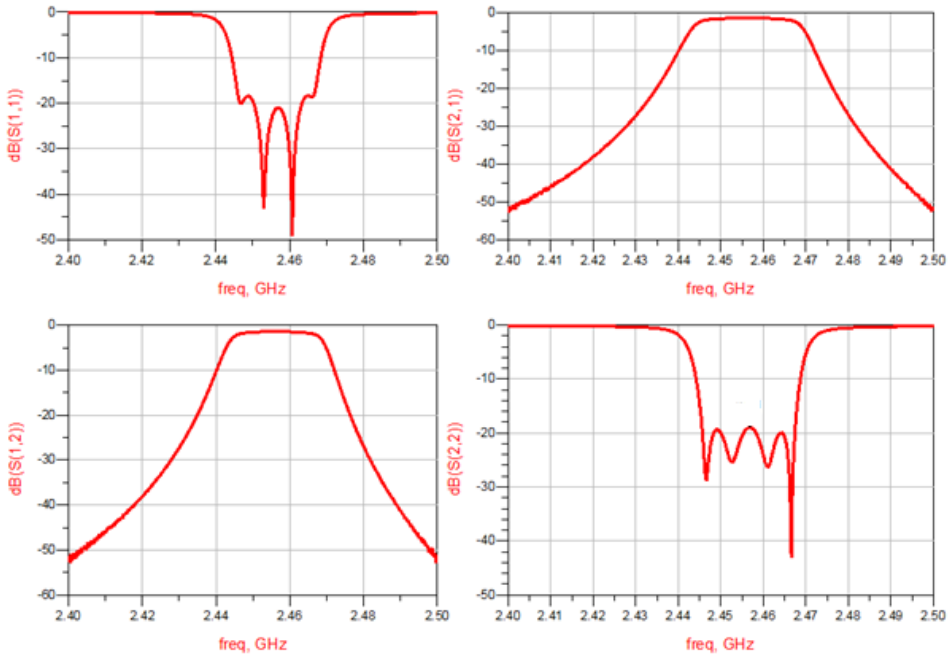

Figure 3.48. . Measurement results using PNA (after tuning).

The measurement results using VNA can be found in Figure 3.49.

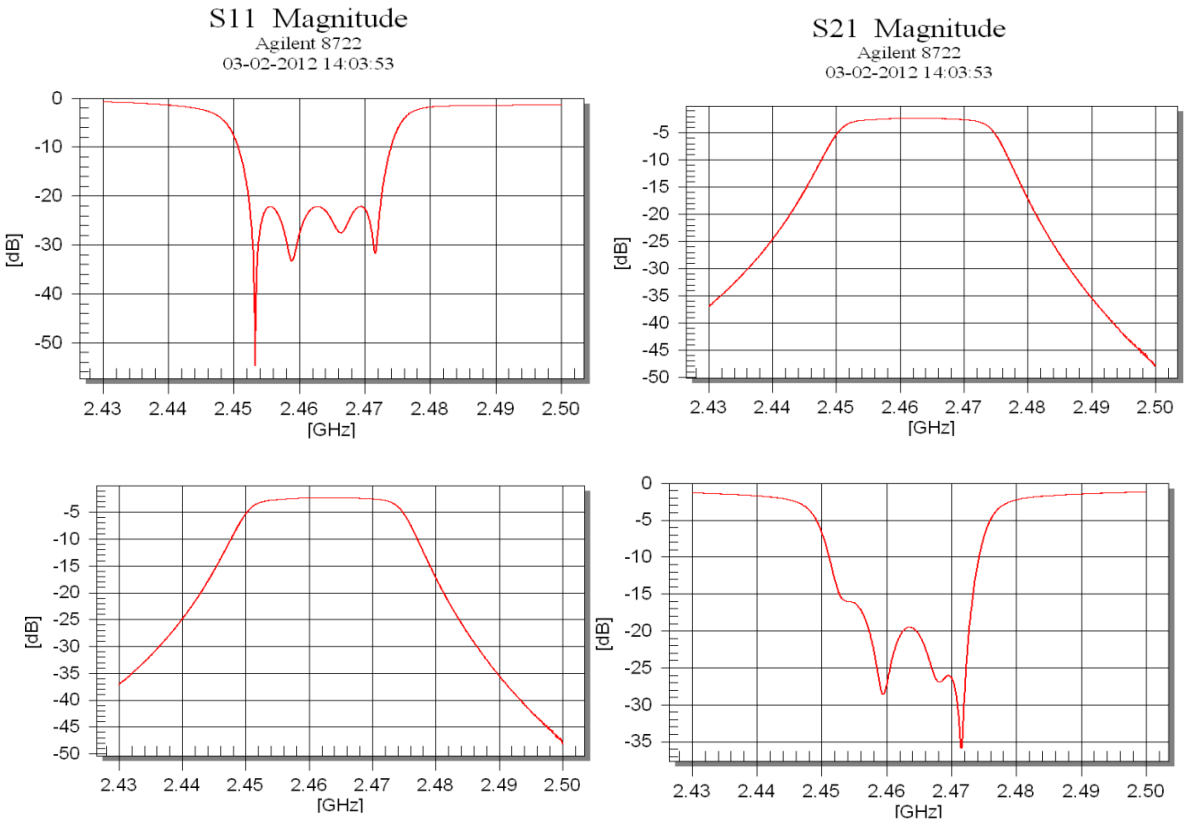

Figure 3.49. Measurement results using VNA.

In light of the measured results given in Figure 3.48, the filter undergoes a frequency shift. Specifically, the filter is designed for a center frequency of 2.5GHz, and a shift of 45 MHz is observed. The main reason for this shift is that the resonators were attached to the cavity using screws, meaning that the resonators might not be placed exactly at the center. A suggested solution could be attaching the resonators to the lid of the filter (in one piece).

Chapter 4
Design and Analysis of High Power Diplexers

Diplexers have become an important component in wireless communications. However, as the spectrum becomes more crowded, diplexers allow simultaneous transmission and reception of signals from a single antenna. In order to have a high-dynamic range transceiver, a diplexer with high isolation and low insertion loss is needed [31].

In conventional diplexers, two doubly-terminated filters are connected to each other using a form of energy distribution network which could be a manifold, a T-junction, a Y-junction, or a circulator. There are numerous approaches for designing a diplexer, some of which are explained in [32]. The most common approach is to design two separate ideal filters and connect them using a common junction. The desired diplexer response can then be achieved by optimizing the junction and the filters.

4.1 Diplexer Design using two ideal filters

In this approach, two ideal filters are designed and then connected using a junction. The junction should be optimized in order to obtain an ideal response for the diplexer.

The desired bands for the diplexer are as follows:

Band 1= 1920MHz-1980MHz (Tx)

Band 2=2110MHz-2170MHz (Rx)

First, two separate (chebyshev) filters were designed in HFSS using the step-by-step method from the filter book. After the first design is ready, it is possible to use either the space mapping method [13] or the manual optimization method to achieve the ideal response.

The optimization was carried out using coupling matrix parameter extraction, after which the parameters were changed manually. The two filters and their responses are shown in Figure 4.1 & 4.2.

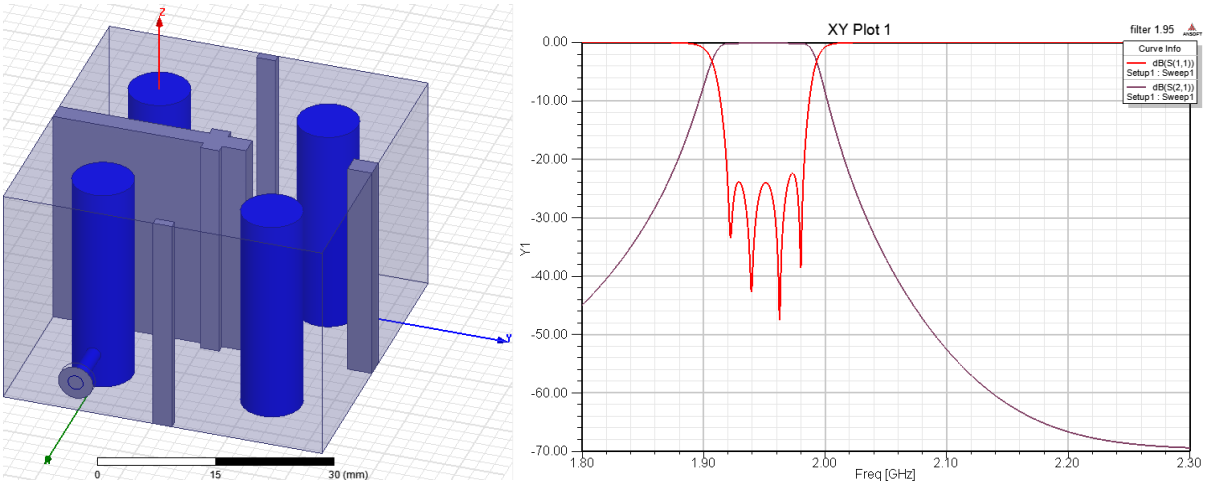

Figure 4.1. Filter 1- Centre frequency=1.95GHz, BW=60MHz.

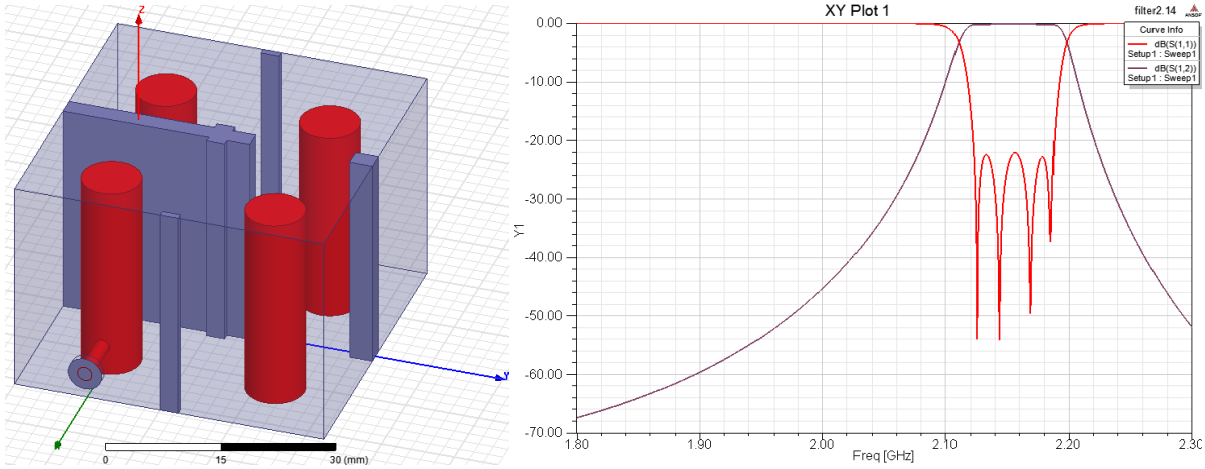

Figure 4.2. Filter 2-Centre frequency=2.14GHz, BW=60MHz.

A coaxial manifold made of two bends, a T-junction, and four pieces of coaxial transmission lines was used. The circuit model of the diplexer is shown in Figure 4.5a, where the T-junction, bend and filters where imported from HFSS as SNP files. The bends (Figure 4.3) and the T-junction (Figure 4.4) were designed in HFSS and their S-parameters were exported to ADS.

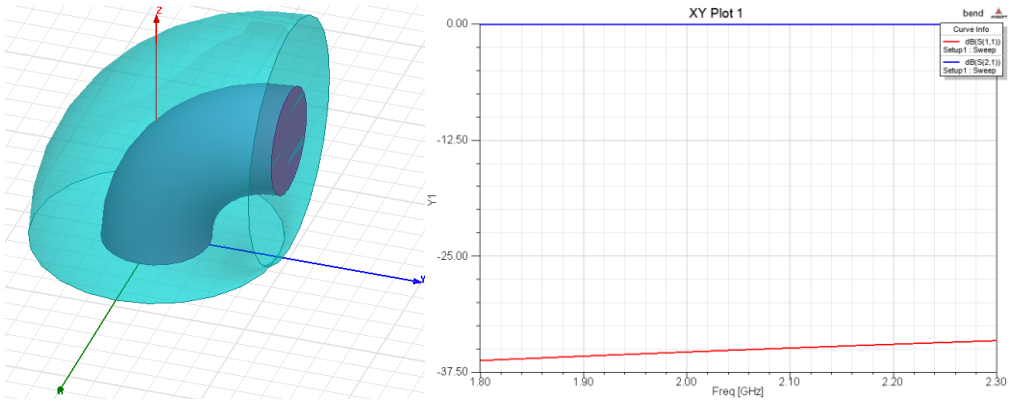

Figure 4.3. Bend.

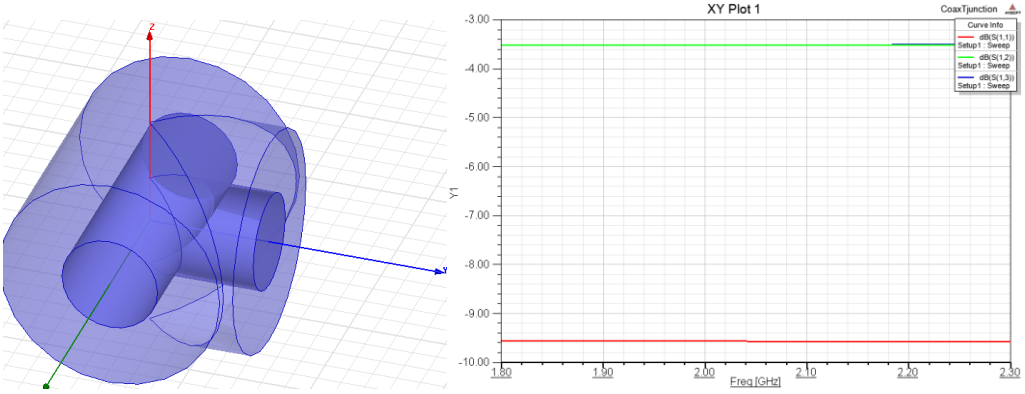

Figure 4.4.T-junction.

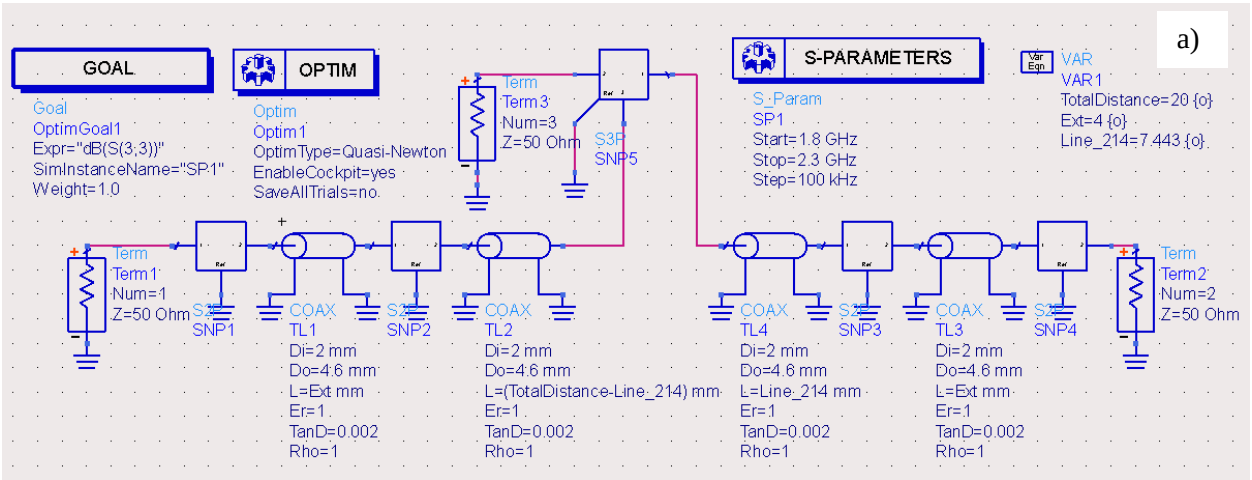

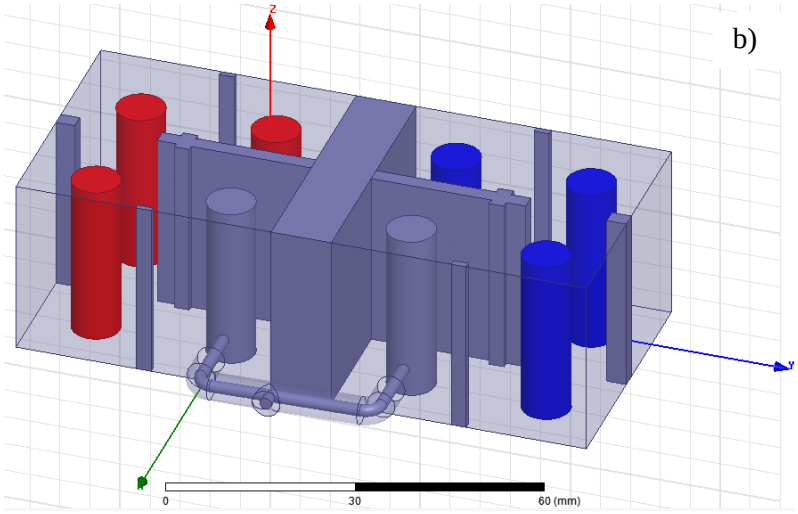

Figure 4.5. a) ADS Circuit Model; b) Complete diplexer structure in HFSS.

In the realization of the diplexer in HFSS, two filters are placed side by side, separated by a wall. The thickness of the wall, along with the filter dimensions and the location of the ports dictate the length of the junction required to connect the two filters (Figure 4.5 b). This length is assumed to be a constant value at the beginning of the design by adjusting the wall thickness. Knowing the total length of the junction, the lengths of the coaxial lines can then be adjusted (using optimization in ADS) to achieve an ideal diplexer response. After finding the ideal lengths for the coaxial lines, they can be updated in HFSS. The response of the circuit after adjustments is shown in Figure 4.6.

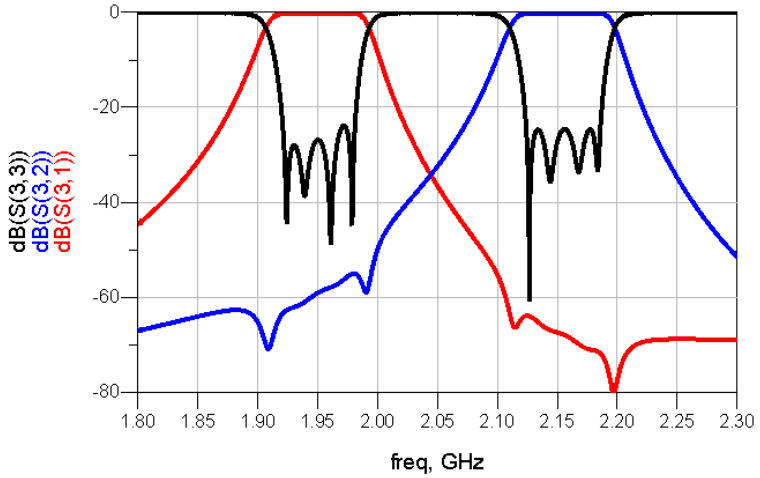

Figure 4.6. Final result of the diplexer after optimization.

The response of the diplexer in HFSS can be found in Figure 4.7.

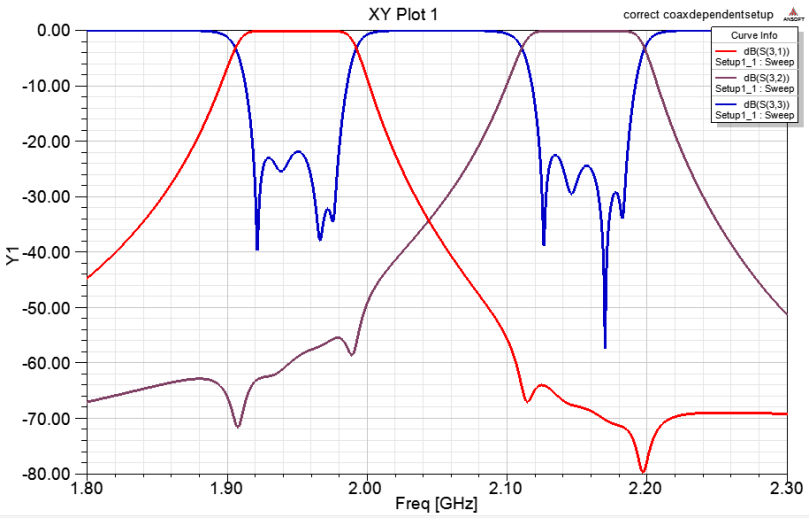

Figure 4.7. EM results of diplexer.

The difference between the results from ADS and HFSS may be due to the possibility that the filter in HFSS does not match the ADS results.

Next, the power-handling analysis is applied to the diplexer (The air breakdown in the resonators was presented in Chapter 3). Since the filter, which is dedicated to the transmission, needs to be studied in terms of power handling, the circuit model of the transmit filter and its response are drawn in Figures 4.8, 4.9 and 4.10.

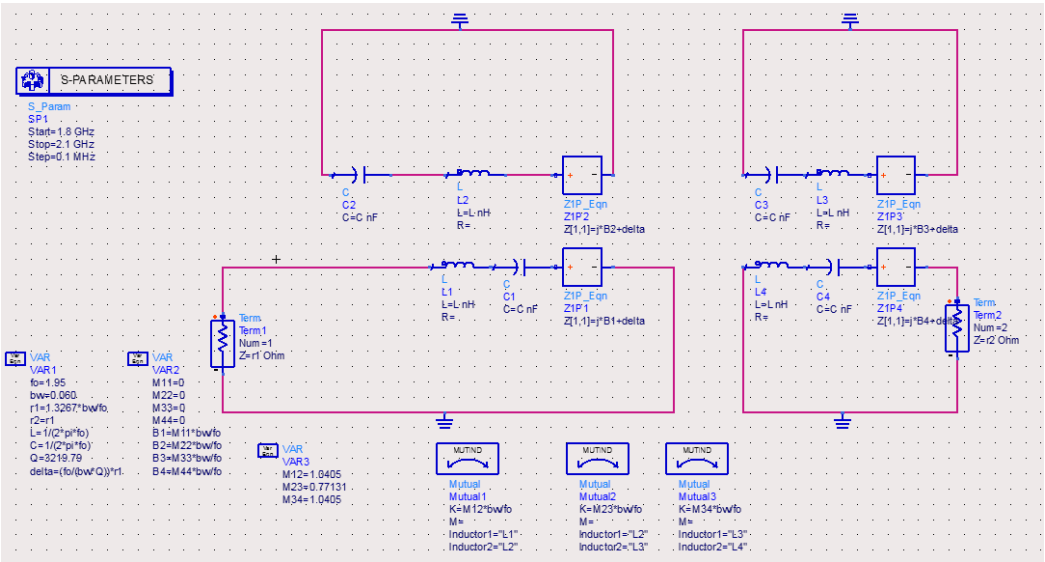

Figure 4.8. Four-pole filter band-pass filter prototype circuit model.

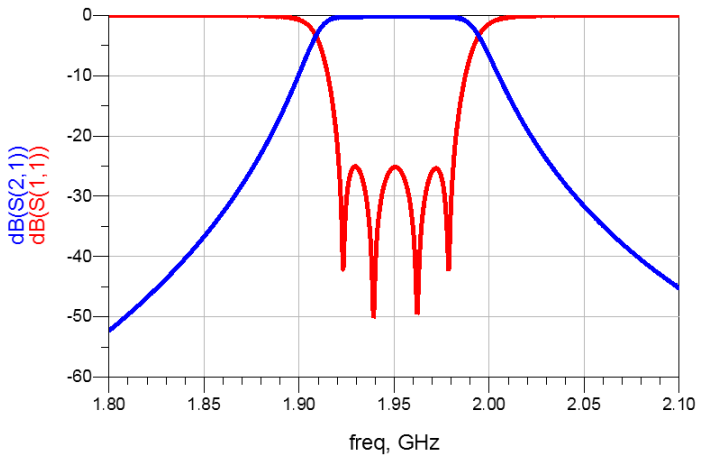

Figure 4.9. 4-pole filter response.

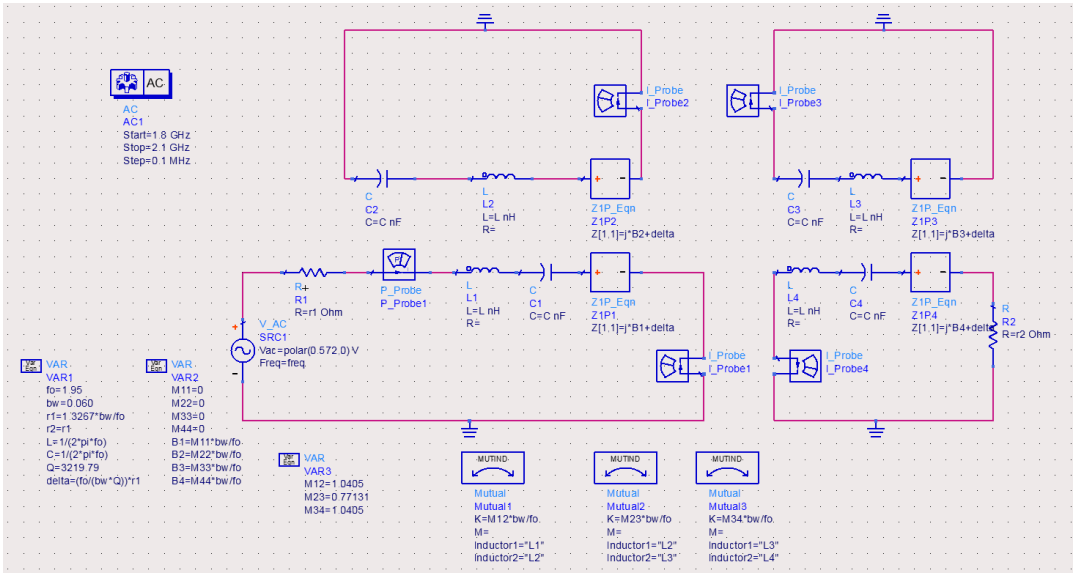

Figure 4.10. Complete circuit model of the Tx filter in ADS.

The input source is changed until the input power becomes 1 Watt. This adjustment must be done in order to match the input power of the circuit model with the default input power in HFSS, which is 1 Watt.

The stored energy in all resonators is calculated by measuring the currents in each resonator and using the following equation:

$$Stored\ energy = \frac{i_i^2}{2\omega_0}$$

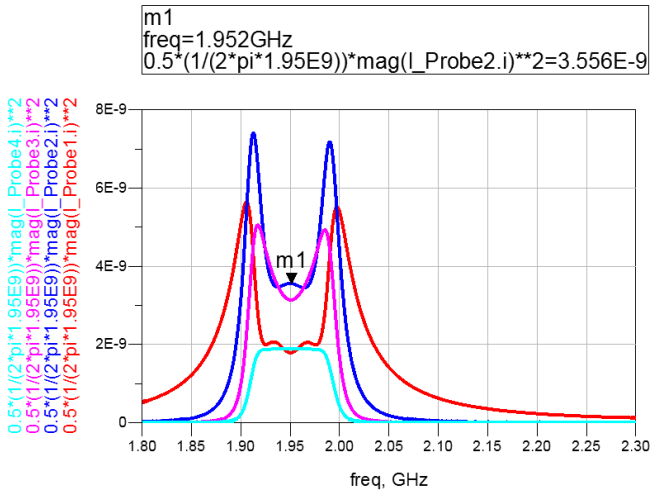

Figure 4.11. Stored energy in all resonators.

The maximum stored energy in the center frequency, which occurs in the second resonator, is equal to $3.3556 \times 10^{-9}(W_{omax} = 3.55 \times 10^{-9}J)$ (Figure 4.11).

On the other hand, using the eigen mode of a single cavity, the maximum electric field was found to be equal to 0.5111 V/m, and the maximum stored energy was $1.5683 \times 10^{-9}1$.J (Figure 4.12). ($Maximum\ stored\ energy = \frac{1}{2}\varepsilon \int |E|^2 dv$)

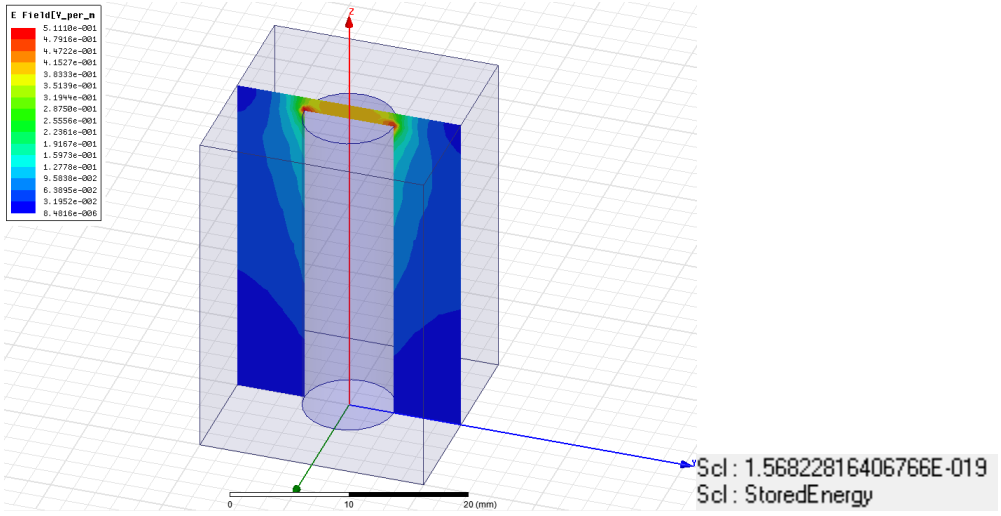

Figure 4.12. Maximum electric field and stored energy in a single resonator

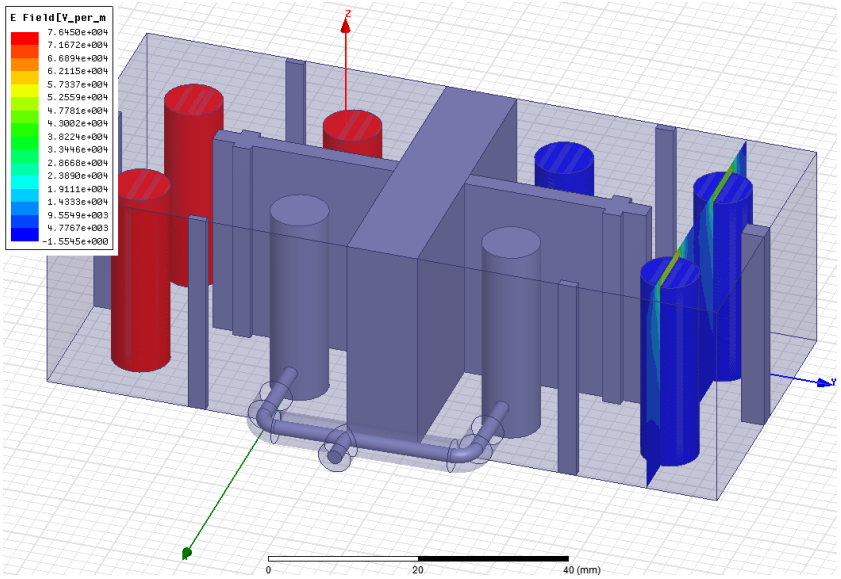

Figure 4.13. The maximum electric field in the complete diplexer.

Therefore, E_{max} can be calculated as follows:

$$E_{max} = \sqrt{(E_0)^2 \times \frac{W_{0max}}{W_0}} = \sqrt{(5.1110 \times 10^{-1})^2 \times \frac{3.556 \times 10^{-9}}{1.56822816 \times 10^{-19}}} = 7.6963 \times 10^4 \; v/m$$

The results can be compared to what is obtained from simulating the complete diplexer in HFSS (Figure 4.13). Table 4.1 shows the maximum electric field at the center frequency (1.95GHz) for both cases.

Table 4.1. The maximum electric field at the center frequency (1.95GHz).

Predicted	$\mathbf{7.6963 \times 10^4}$ V/m
Complete structure(HFSS)	7.6450×10^4 V/m

Very good agreement is found between the predicted value and the value from the complete structure (HFSS).

At the next stage, the maximum electric field where the maximum stored energy happens (on the band edge) is predicted and compared with the complete structure.

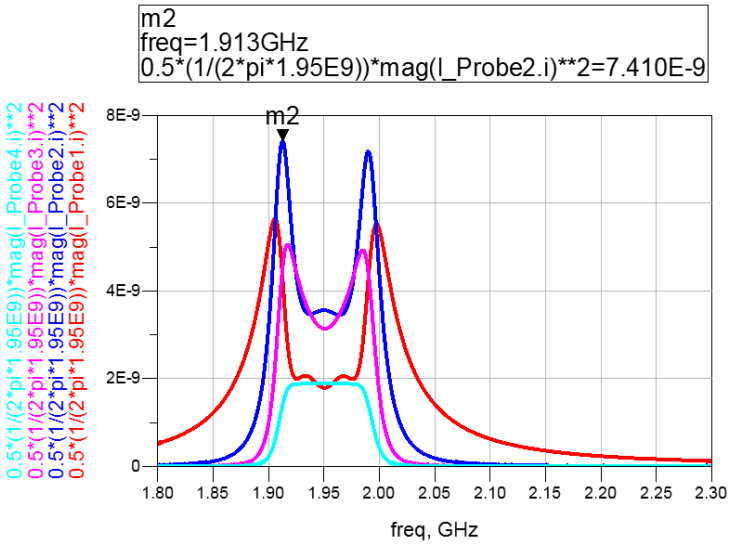

Figure 4.14. Stored energy in all resonators.

The predicted maximum field was calculated as follows:

$$E_{max} = \sqrt{(E_0)^2 \times \frac{W_{0max}}{W_0}} = \sqrt{(5.1110 \times 10^{-1})^2 \times \frac{7.410 \times 10^{-1}}{1.56822816 \times 10^{-19}}} = 1.111 \times 10^5 \; v/m$$

The maximum E field was also measured in an HFSS model, as shown in Figure 4.15.

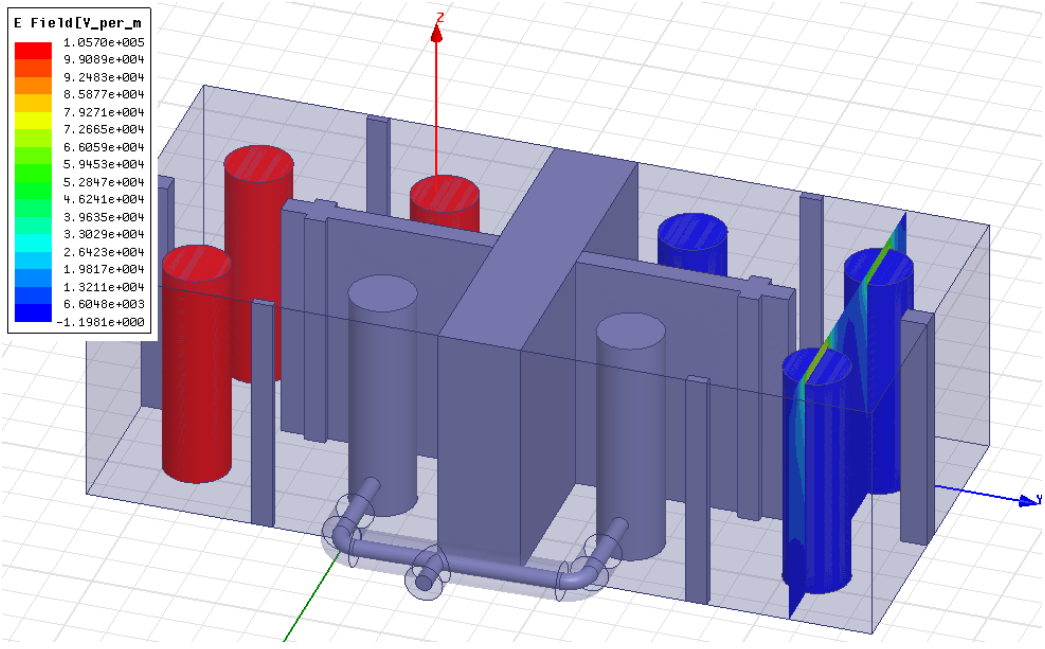

Figure 4.15. . Maximum electric filed in the complete HFSS structure happening in the band edge.

The results can be compared in Table 4.2:

Table 4.2. The maximum electric field at the band edge (1.1913GHz).

Predicted	$\mathbf{1.0570 \times 10^5}$ V/m
Complete structure(HFSS)	1.111×10^5 V/m

4.2 Wired connected diplexer design using a coaxial manifold diplexer circuit model

In the previous section, a diplexer was designed using two ideal filters connected by a coaxial manifold. Based on this design, it is possible to develop a circuit model of the ideal diplexer and use this model to design a conventional diplexer that employs wire to connect the two filters.

The proposed method transforms the coaxial manifold to a wire connection by using the same length of wire and then trying to match the group delay of the two models.

This method can be used to find a good starting point for designing a diplexer without having to solve complicated numerical methods. However, using the group delay method to match the two circuits is not the best approach, as the wall between the two filters has to be opened slightly to connect the resonators by wire. The existence of even this slight gap distorts the electric field in the resonators.

The following actions were taken in order to realize the above-mentioned method:

All of the resonators were detuned (except for the first two, which were connected to the common port). The group delay seen from the common port was derived for both connection types (wire and coax) and were matched by adjusting the corresponding parameters of wire connected to the diplexer. These parameters include the height of the resonators, tapping positions, and wire length.

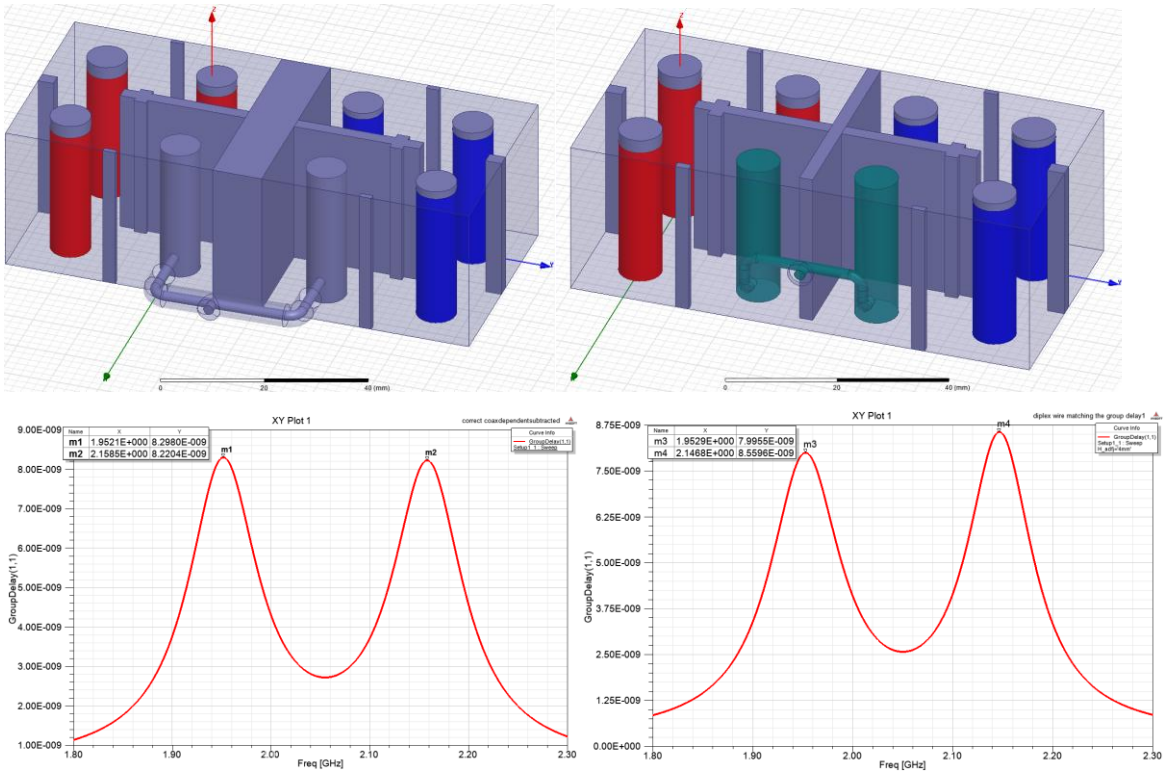

Figure 4.16. Group delay of the two structures after adjustments.

The response of the diplexer using the above method is shown in Figure 4.17. Overall, it shows a good starting point for the optimization.

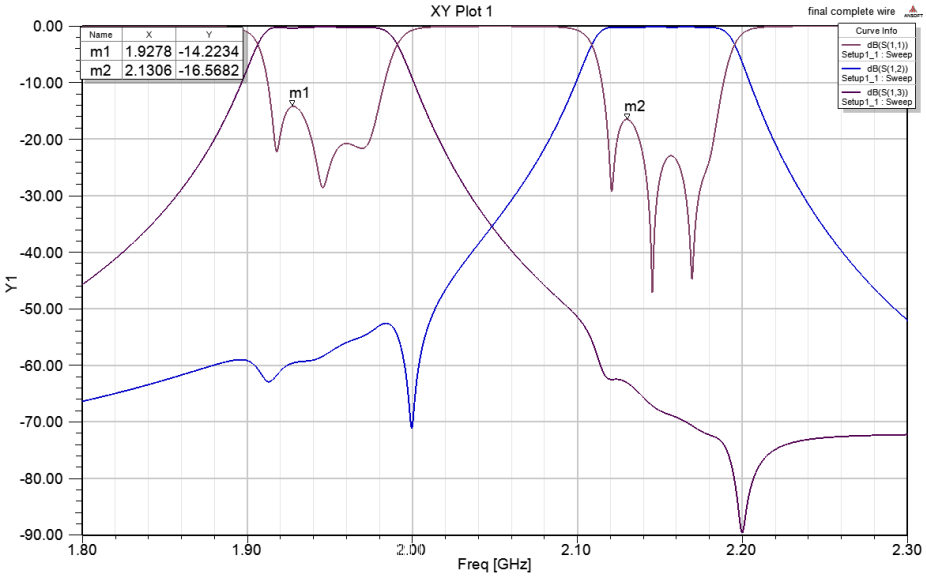

Figure 4.17. The response of the filter after the group delay adjustment.

4.2.1 Applying the power-handling method to a wire-connected diplexer

The maximum field in the wire-connected diplexer was predicted using the method described above. The results are in good agreement with the E field measured using the FEM model (Figure 4.18), as shown in Table 4.3. The miniscule difference may be due to changes in the length of the resonators during the adjustments.

Table 4.3. The maximum electric field in the wire connected diplexer at the center frequency.

Predicted	$\mathbf{7.6963 \times 10^4}$ V/m
Measured complete structure(HFSS)	7.1645×10^4 V/m

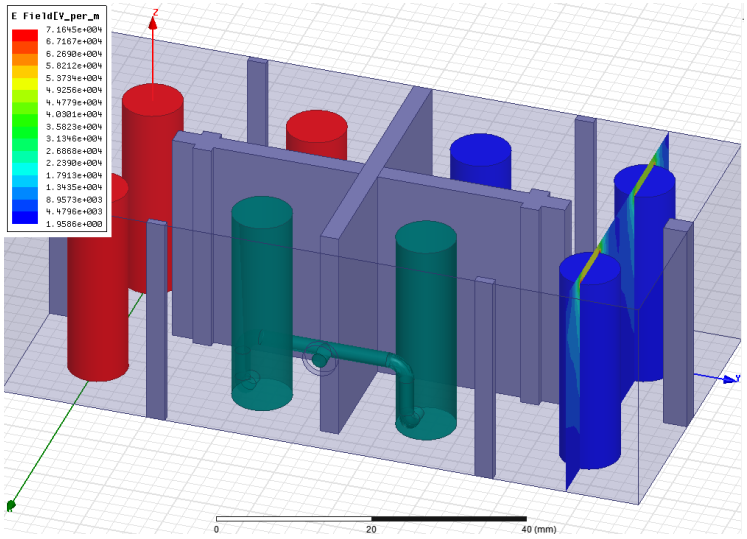

Figure 4.18. The maximum electric field in the complete HFSS structure.

4.3 Designing a diplexer using the group delay method and space mapping

There are several different approaches that may be adopted in designing a diplexer. One approach, which was tackled in the previous section, is to design two separate filters, optimize each of them, and then try to find the junction that provides the desired response. A second approach is to simulate the diplexer using the ideal coupling matrix of each filter as well as the S-parameters of the junction exported from HFSS to ADS (SNP file). In this

approach, the coupling matrix elements (especially those closest to the common port) along with the T-junction position should be optimized to obtain the ideal response.

After optimization, a new coupling matrix for each filter can be found. By knowing the coupling matrices of the filters, it is possible to design them in HFSS using either EM-based synthesis or the group delay method (coaxial manifold in HFSS is matched to the ADS manifold).

4.3.1 Forming a circuit model to obtain an ideal diplexer response

In the proposed method, we first design the junction in HFSS, after which the S-parameters of the junction are exported to ADS in an SNP file. Here, the coupling matrix model of the filters is used to represent each filter. From this, a diplexer model will be simulated in ADS and optimized to achieve the ideal response.

Figure 4.19 shows the first circuit response by connecting the two ideal filters and imported junction. The circuit model in ADS is shown in Figure 4.20.

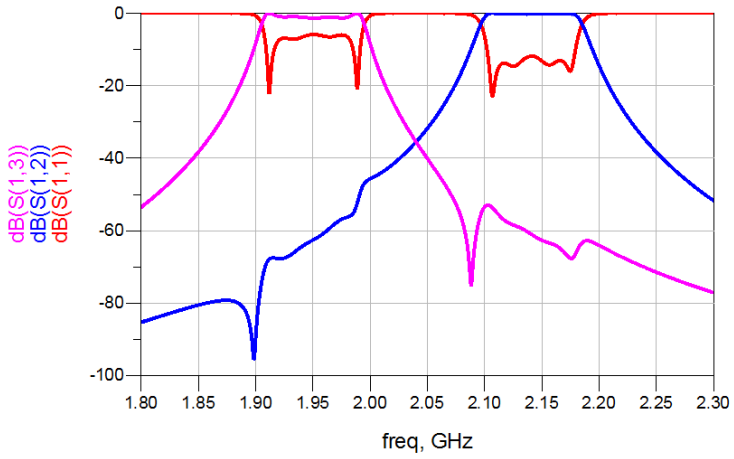

Figure 4.19. The circuit model before optimization.

The response was optimized by changing the first few elements of the coupling matrix, with various optimization algorithms used to achieve the ideal response. After applying random optimization, a Quasi Newton optimization algorithm was employed. The optimization variables were R_S, M11, M22, M12 for Filter1, and R_S2, M112, M222, M122 for Filter2.

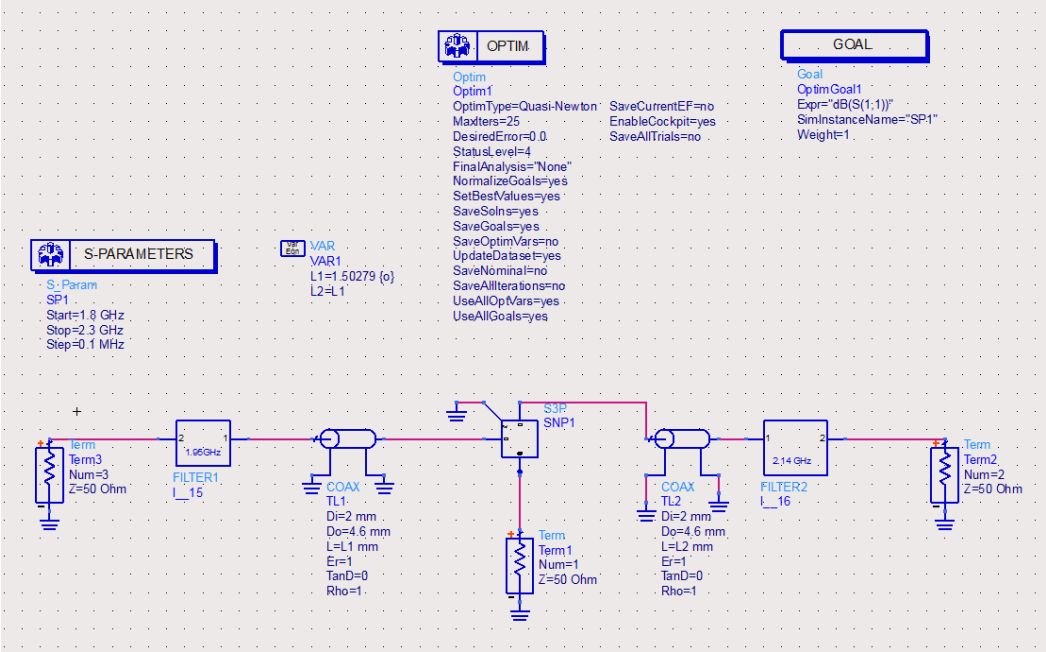

Figure 4.20. Circuit model of the diplexer in ADS.

The optimization goal used can be found in Figure 4.21.

Limit lines

	Name	Type	Min	Max	Weight	freq min	freq max
1	limit1	<		-25	1	1.92e+09	1.98e+09
2	limit2	<		-25	1	2.11e+09	2.17e+09

Figure 4.21. Optimization goal in ADS.

The final response of the diplexer after optimization is shown in Figures 4.22 and 4.23.

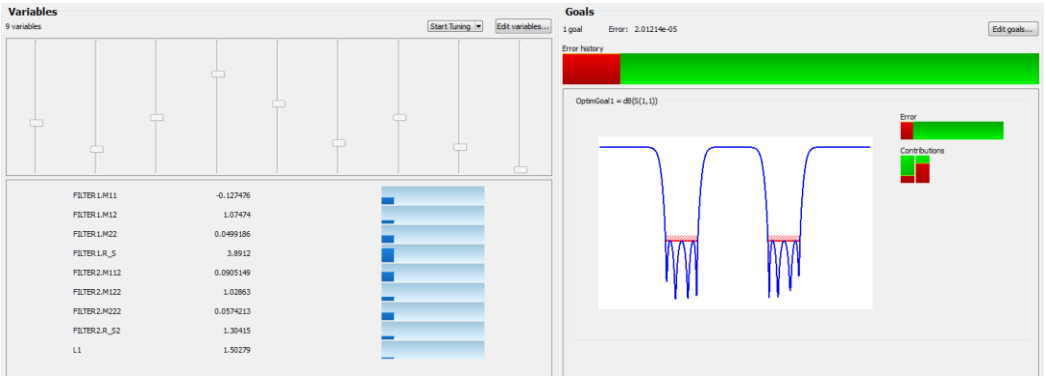

Figure 4.22. The optimization cockpit in ADS.

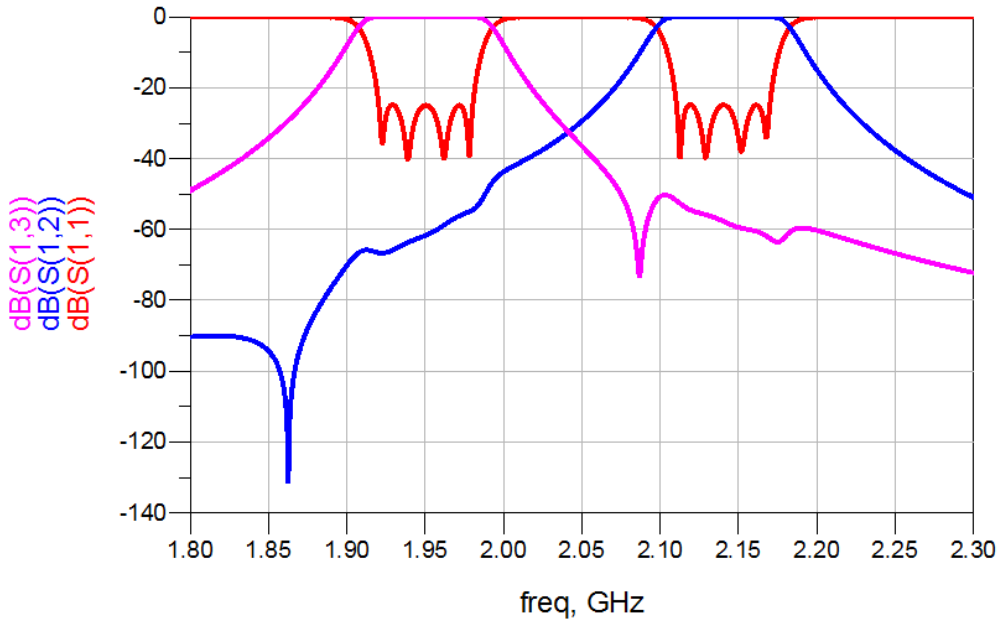

Figure 4.23. Final response of the diplexer.

At this point, we are faced with the choice either to design the two filters using their new coupling matrices, or to use the group delay method in order to design the complete diplexer structure all at once. Using the group delay method for optimization is better than optimizing the complete structure at once, since only a few elements are tuned at each step. Hence, the second option was chosen. By looking at the common port, the group delay of the filter was found and matched to the ideal filter's group delay. In this method, both of the filters are designed at once.

In this approach, the coupling matrix of each filter will change. The new filters and the new M values can be found in Figures 4.24 and 4.25.

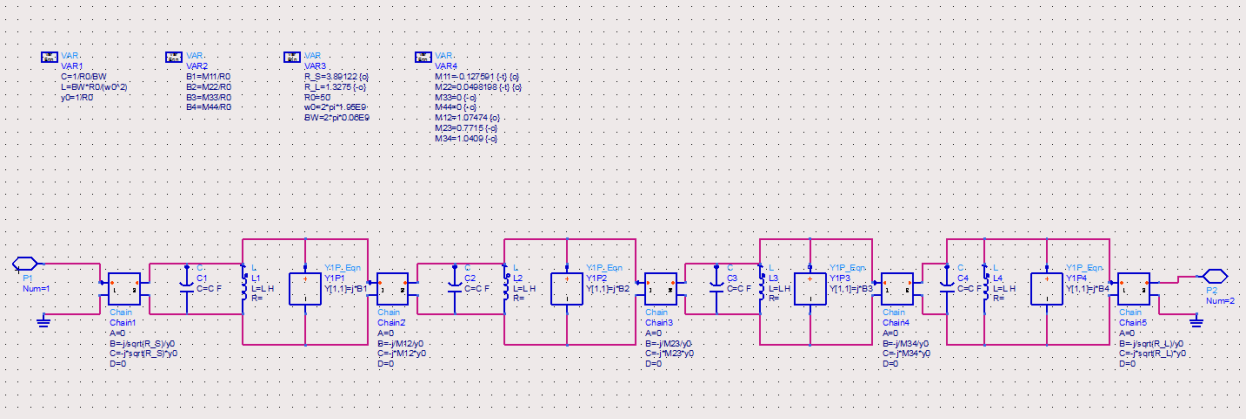

Figure 4.24. Filter1 after optimization.

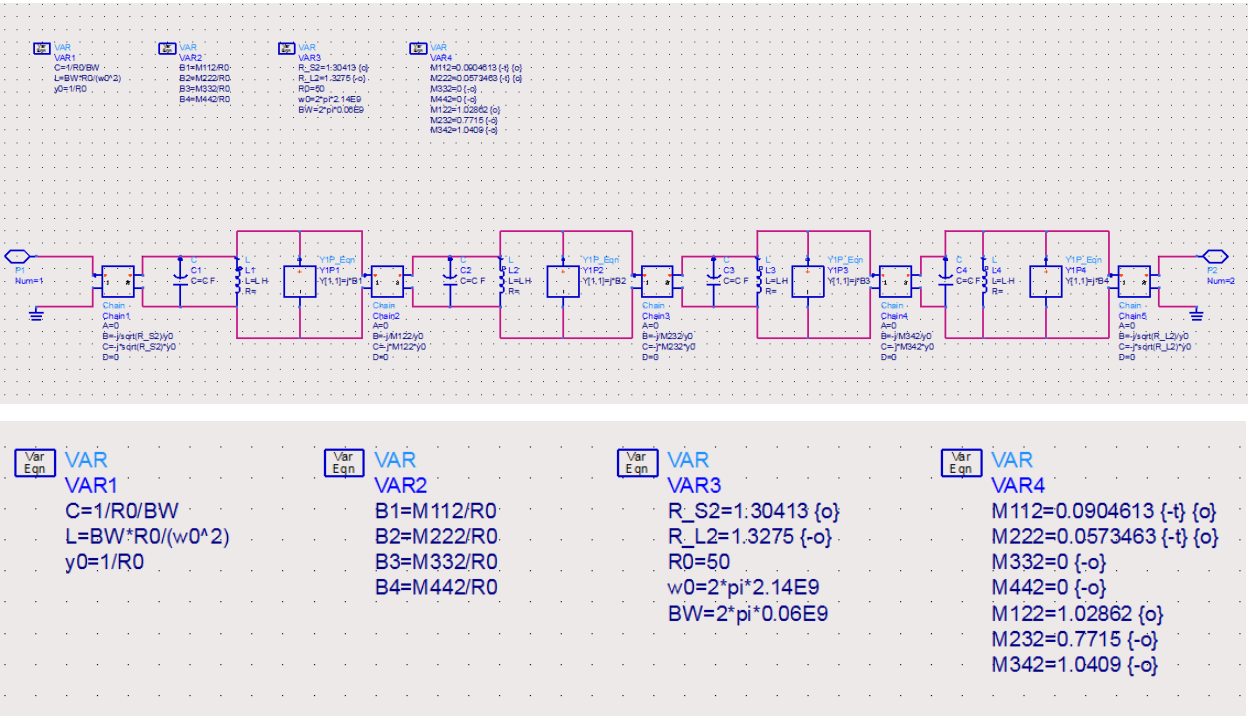

Figure 4.25. Filter2 after optimization.

The circuit model used to determine the ideal group delay of the filters is shown in Figure 4.26.

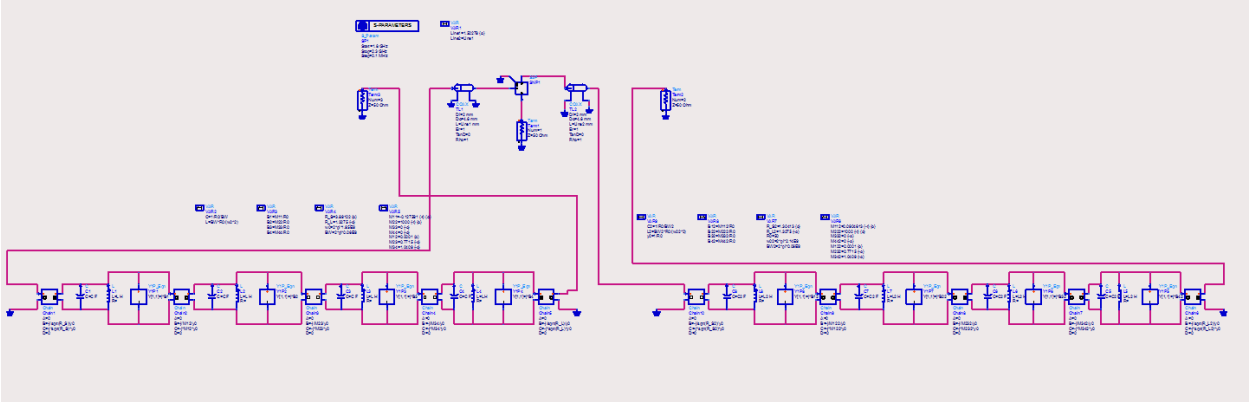

Figure 4.26. Circuit model using J inverters.

These coupling matrices are the base materials to design a diplexer in HFSS in a step-by-step fashion.

4.3.2 Method description

As the next stage in the design process, a complete structure of the diplexer should be implemented in HFSS. The size of the cavities and the diameter of the resonator should be selected in such a way that the maximum adjacent coupling, available in the circuit model, is realizable. The junction was designed previously to be used in the circuit model and therefore does not require any modification. The height of the resonators, size of the walls, and the position of the probes can be preset randomly.

Now, having an ideal circuit model in ADS and a physical structure in HFSS, the group delay matching method can be applied to achieve physical dimensions, resulting in an ideal diplexer in HFSS. These steps are as follows.

First, all of the resonators must be detuned (except for the first two, which are connected to the junction in both the circuit and HFSS models). Then, the group delay, as seen from the common port in HFFS, should be matched to that of the circuit model in ADS by changing the height of the resonators and the position of the probes. The procedure for matching and adjusting the new dimensions is explained in the next section.

At this point in the process, one resonator from each filter will be tuned, and thus the next steps involve tuning the other resonators. In this case, resonators 3 and 4 in each filter are detuned. Again, the group delay as seen from the common port of the two models should be matched to achieve the tuned height of the second resonators along with the size of the wall between resonators 1 and 2 in each filter. The steps should proceed in the same way, so that the third resonator and the corresponding walls in each filter can be adjusted to match the group delay found in HFSS with that of the circuit model in ADS.

At the final step, instead of looking at the common port, the group delays at two of the other ports must be seen. At the same time, resonators 1 and 2 from each filter should be detuned to adjust the height of the fourth resonators as well as the walls between 3 and 4 and the position of the filter probes.

It should be noted that the resonators should be detuned by being shortened instead of being removed to get more accurate results. Also, in the ADS circuit model, the resonators can be detuned by setting the self-coupling to a high value (for example, 1000).

Filter's box was assumed $42.5mm \times 90mm \times 30mm$ and the barrier between the two boxes was $42.5mm \times 5mm \times 30mm$. All of the resonators were placed in the structure in order to short them (Figure 4.27).

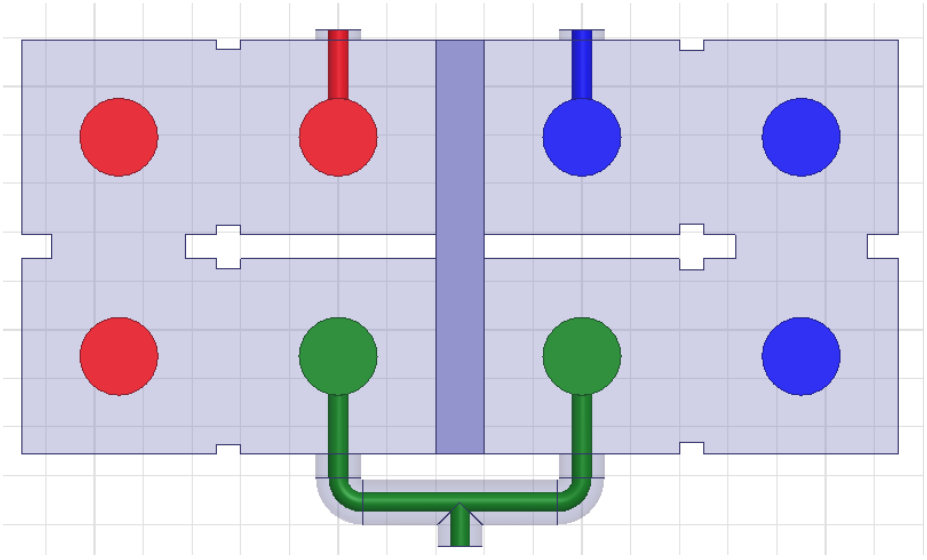

Figure 4.27. Top view of the diplexer in HFSS.

A block diagram of the above-described method is shown in Figure 4.28.

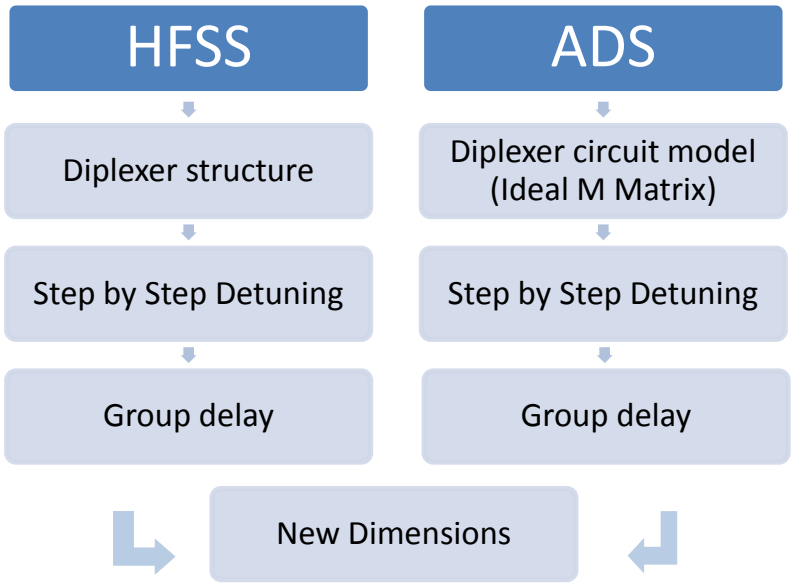

Figure 4.28. The method steps using HFSS and ADS.

4.3.3 Updating the new dimensions by matching the group delay found from the circuit model with that of HFSS using space mapping

The group delay results from HFSS are imported in ADS. Then, using ADS optimization, the corresponding coupling values from the group delay are extracted, and the resulting M values are used to find new dimension. This can be done by calculating the difference between the ideal M value and the extracted M values. However, there must be a relation between the variation of each M value and the variation of physical dimensions to relate differences in M values to changes in the physical dimension. It is assumed that there is a dominant linear relation between one coupling matrix value and one physical dimension, which implies that the effect of that M value on other physical parameters is ignored. For example, M_{ii}corresponds to the height of the i^{th} resonator.

Hence, a space-mapping code was developed in MATLAB that takes the ideal M matrix vector, the physical dimension vector (from HFSS), its corresponding extracted M matrix vector, and an M matrix-physical dimension relationship vector as input and calculates new dimensions as the output.

The above process is then repeated in an iterative fashion until the group delay response of the HFSS matches the ideal group delay.

The following shows how the relation between M values and physical dimension is established:

In order to find the relation between M_{ii} and the resonator's height in HFSS eigen mode, the variation in the height of the resonator is plotted versus variations of M_{ii}, using $\Delta Mii = \frac{-(f-f_0)}{BW} \times 2$, as illustrated in Figure 4.29.

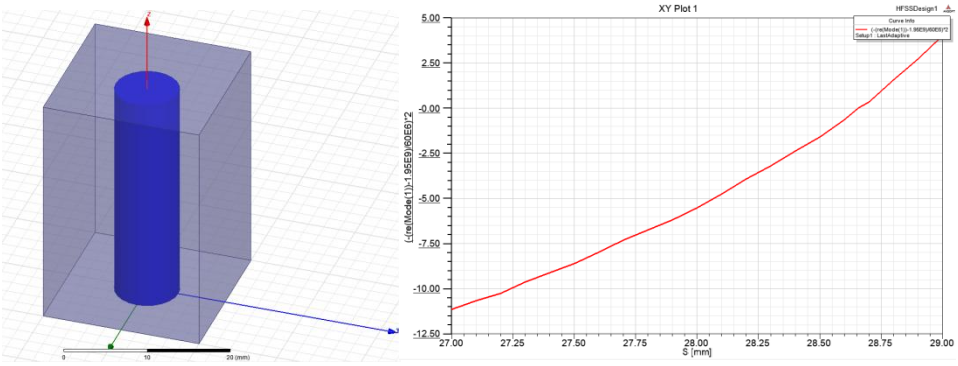

Figure 4.29. Height of the resonator versus M_{ii} .

Likewise, the relation between the size of the wall and M_{ij}, can be determined using the following relationship, as shown in Figure 4.30.

$$\Delta Mij = \frac{f_0}{BW} \times \frac{(f_e^2 - f_m^2)}{(f_e^2 + f_m^2)}$$

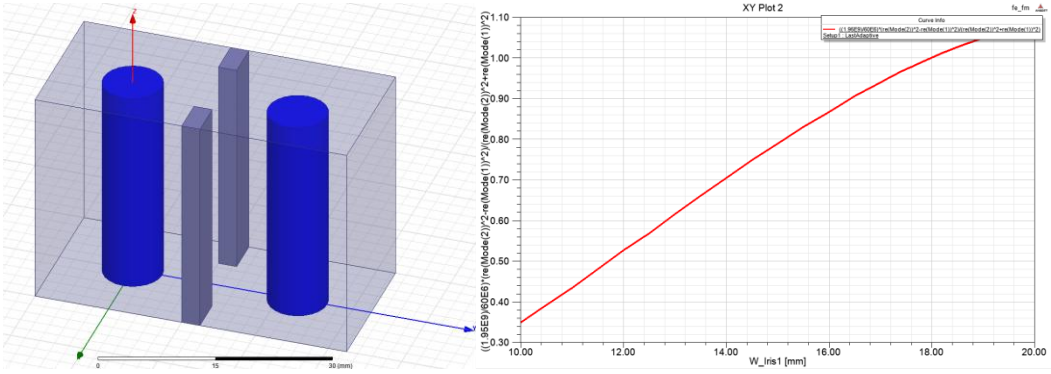

Figure 4.30. Size of the wall versus M_{ij}.

Figure 4.31 also shows the relationship between the height of the probe and the input coupling. The input coupling is calculated using the following:

$$R = \frac{4}{(\omega_2 - \omega_1)} \times \frac{1}{\tau(\omega)}$$

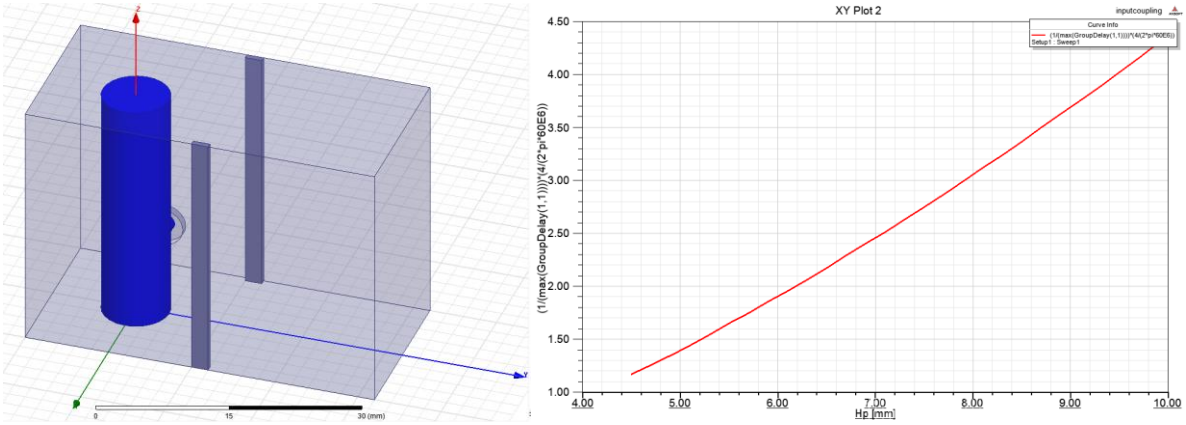

Figure 4.31. Height of the probe versus the input coupling (which is represented by R in the coupling matrix).

The above method is applied to design the diplexer, as presented in the following section.

4.3.3.1 Tuning the first resonators looking at the common port

The physical structure in HFSS is shown in Figure 4.32, where all of the resonators except the first ones are detuned.

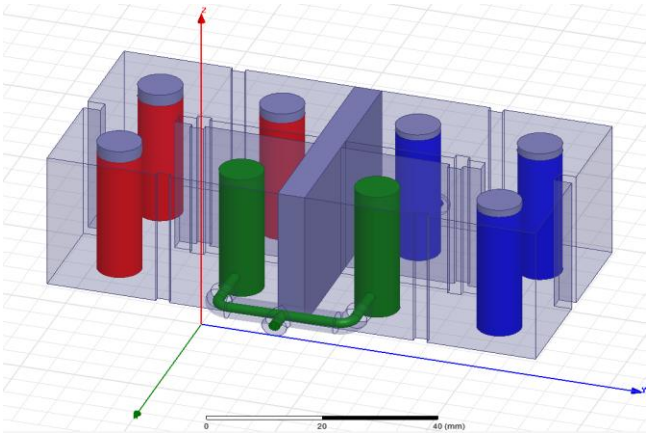

Figure 4.32. The structure used in HFSS for adjusting the first resonator from each filter.

As was explained in the Methodology section, the new dimensions of the first two resonators are updated using several iterations of group delay matching, using space mapping. Figure 4.33 shows the group delay results of both the circuit model and the HFSS structure after adjustments.

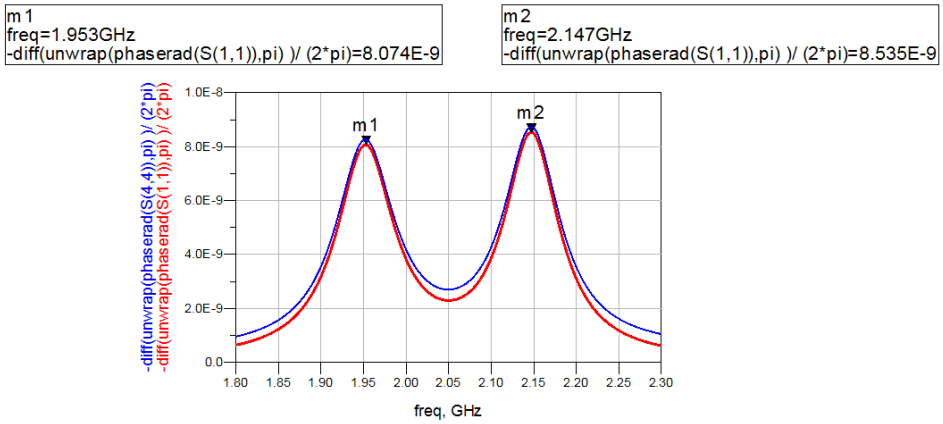

Figure 4.33. Matched group delays of the HFSS (blue) model and the ideal circuit model (red).

4.3.4 Tuning the first two resonators

In Figure 4.34, a structure is shown where all of the resonators (except the first two from each filter) are detuned.

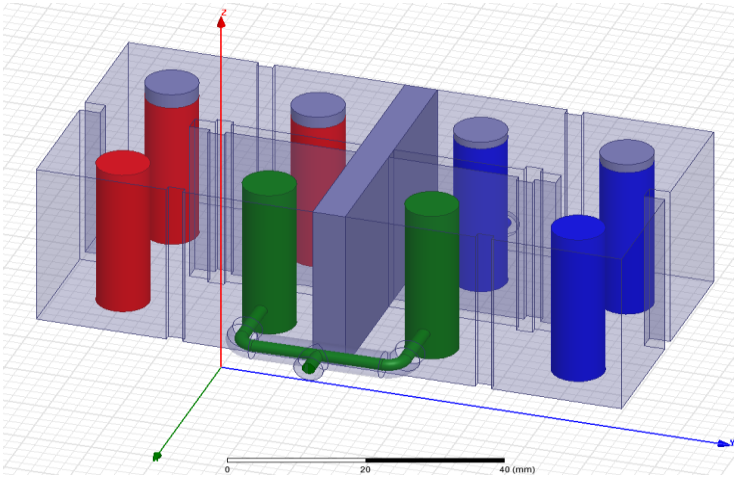

Figure 4.34. The structure used in HFSS for adjusting the first two resonators of each filter and the walls between them.

In Figure 4.35, the group delays from HFSS (the red plot) and ADS (the blue plot) is shown after applying space mapping.

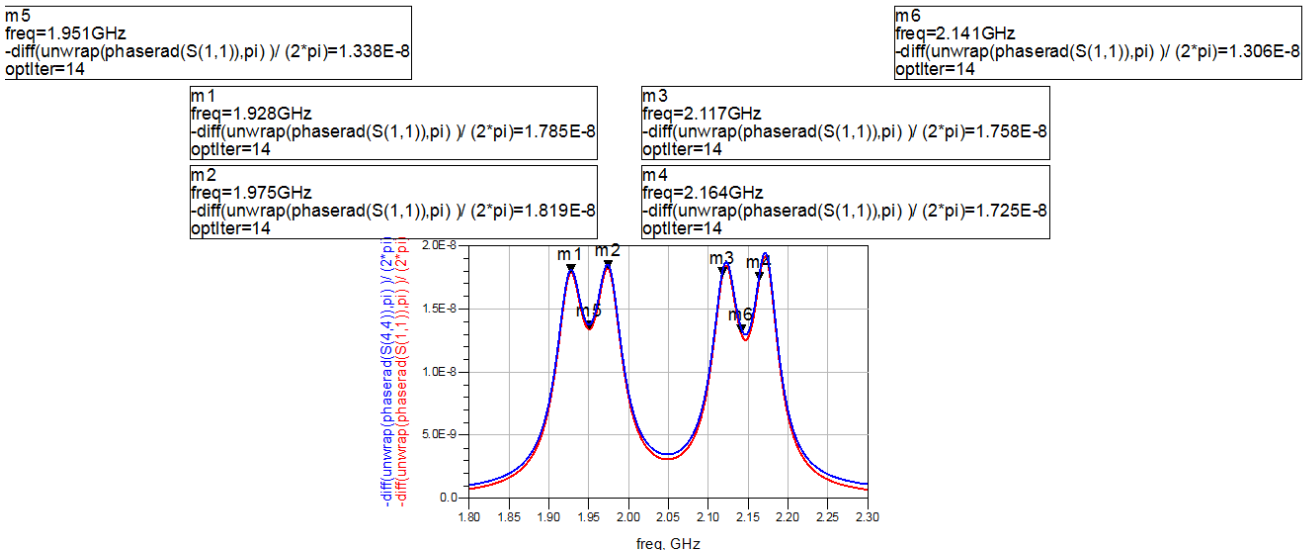

Figure 4.35. Group delays after being matched using space mapping.

4.3.5 Three first resonators from each side

The structure used in this part is shown in Figure 4.36. As can be seen, the extraction was performed twice. The first extraction was done using seven variables (Figure 4.37). However, after applying space mapping to obtain the new dimensions, the group delays did not match perfectly (Figure 4.38).

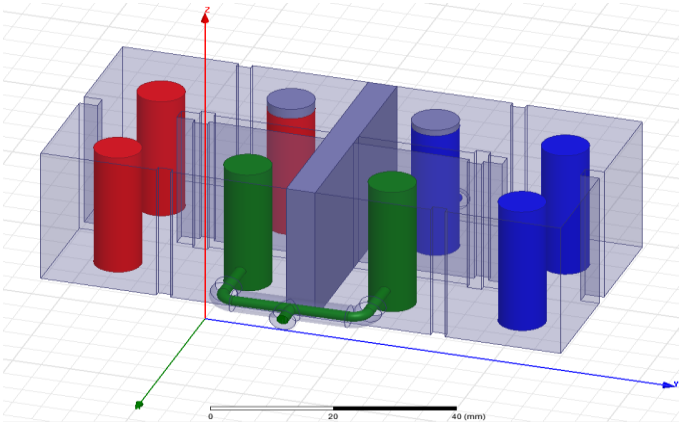

Figure 4.36. The structure used for matching the first three resonators of the filters and the walls between them.

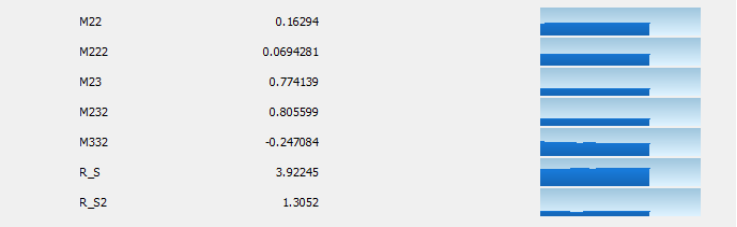

Figure 4.37. Parameter extraction using seven variables.

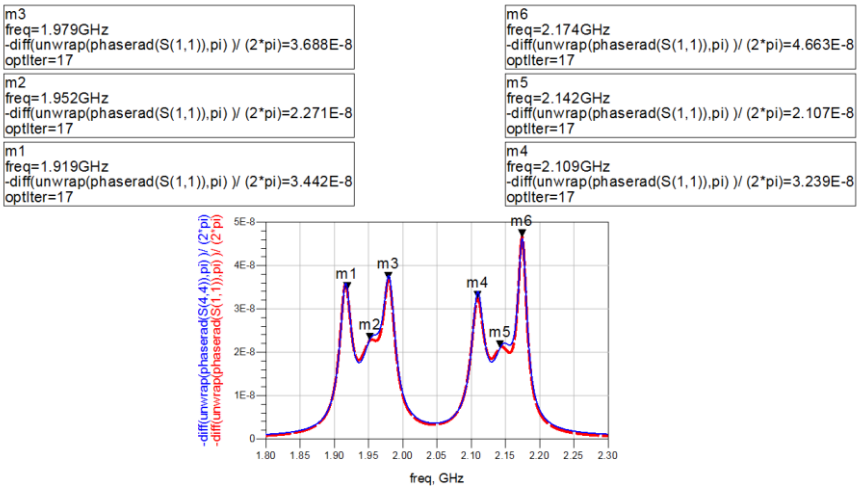

Figure 4.38. The group delay of the circuit model and HFSS structure did not match perfectly.

Extraction using seven variables could not proceed any further, so the number of variables was increased to 11 (Figure 4.39). After two more iterations, the two plots, representing the group delays of the ideal circuit model and the HFSS structure, matched perfectly (Figure 4.40).

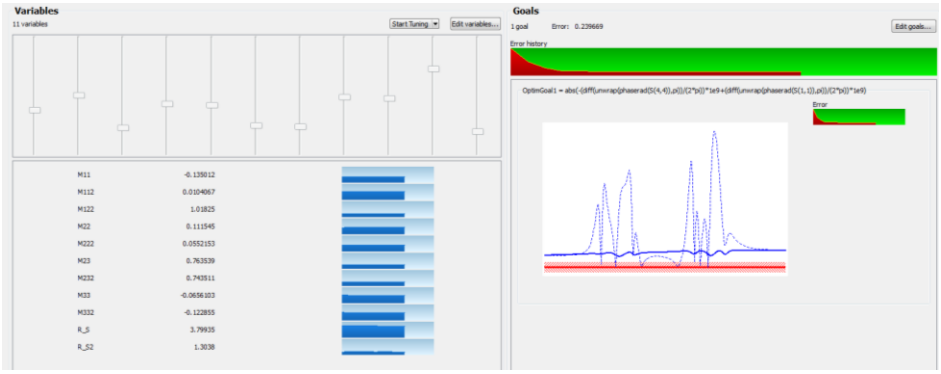

Figure 4.39. Parameter extraction using eleven variables.

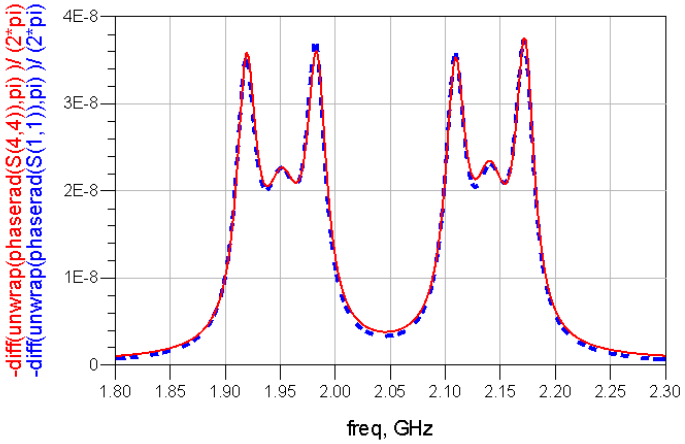

Figure 4.40. The ideal group delay response and the group delay from HFSS.

4.3.6 Tuning resonators 3 and 4 of each filter looking at other ports

Having tuned the first three resonators of each filter looking at the common port, the first two resonators, looking from the other ports, should also be tuned (Figure 4.41).

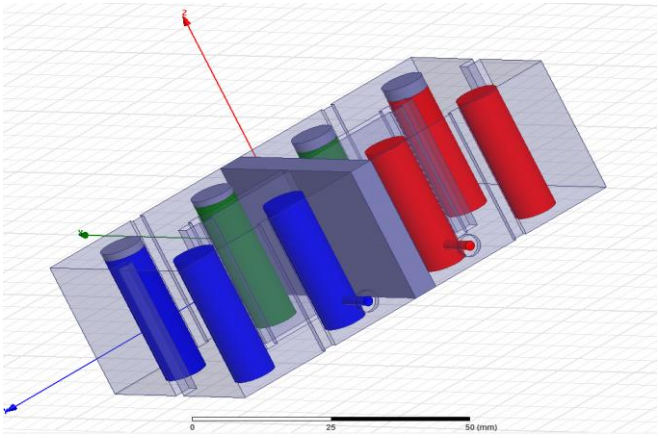

Figure 4.41. HFSS structure for tuning resonators 3 and 4 of each filter and the walls between them.

The group delay method is applied and the new dimensions are found. As we can see, the group delays of the circuit model and the HFSS structure matched after a number of iterations (Figure 4.42). Moreover, as the lower band group delays were matched after manually changing the dimensions, there was no need to apply space mapping.

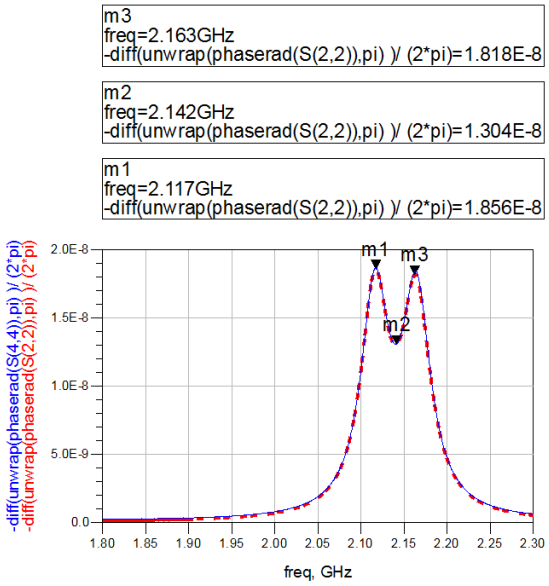

Figure 4.42. The group delays of the upper bond filter.

The complete response of the diplexer after applying the proposed method can be found in Figure 4.43.

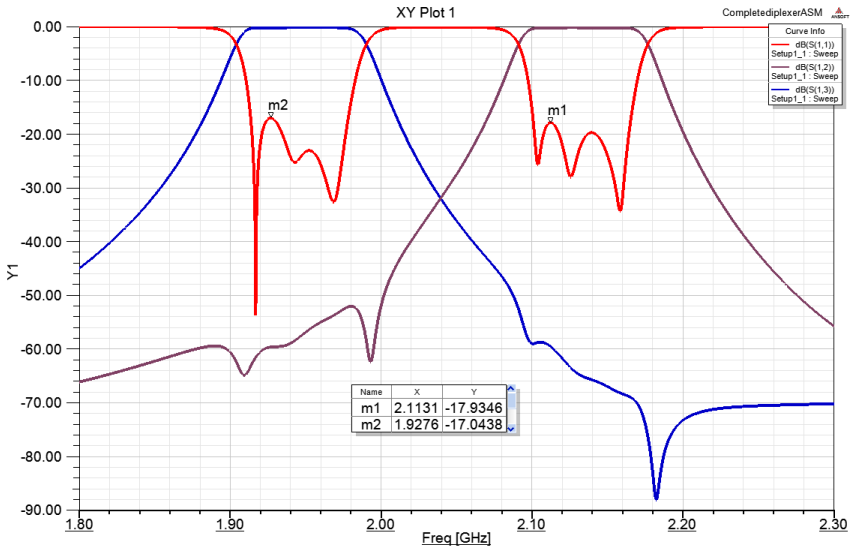

Figure 4.43. The response of the diplexer after completing the method.

The last step of the method could potentially be replaced by adjusting only one resonator from each filter. The diplexer response in changing the last step is shown in Figure 4.44.

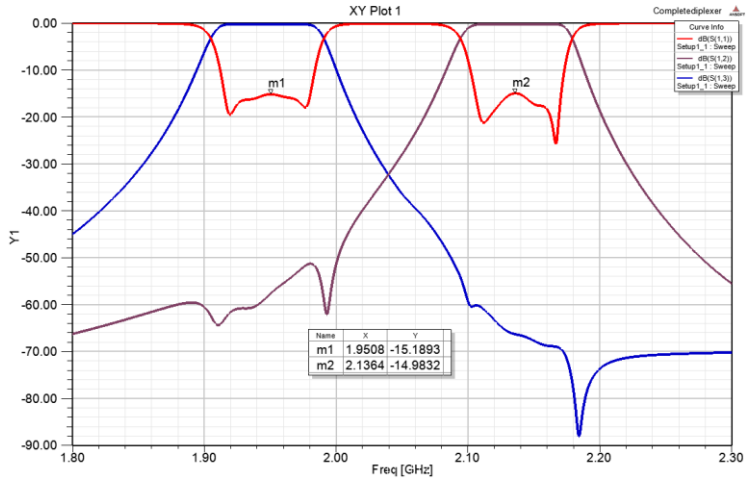

Figure 4.44. The response of the filter in changing the last step.

The return loss of the two responses is compared with the ideal return loss (Figures 4.45 & 4.46). Both of these methods appear to work fine.

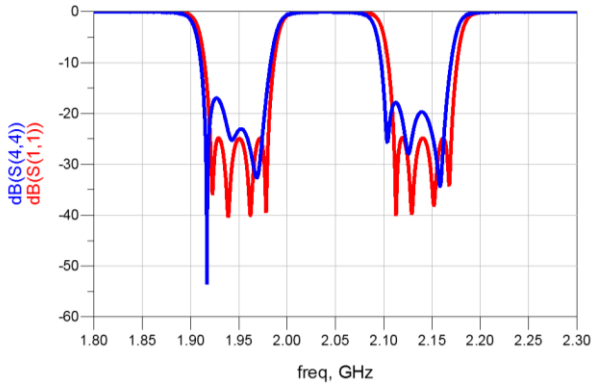

Figure 4.45. Comparing the ideal return loss with the method's return loss.

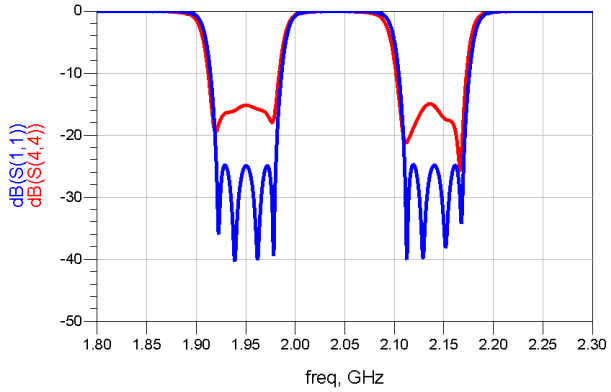

Figure 4.46. Comparing the ideal return loss with the method's return loss by changing the last step.

4.4 Diplexer with wire connection

For a diplexer with wire connections, the exact same procedure was followed. The only difference was that the structure was matched with the ideal circuit model in two steps.

4.4.1 Step 1

This step involves detuning the last resonator in each filter while looking at the common port and adjusting the first three resonators and their inter resonator coupling at once. Figures 4.48, 4.49 and 4.50 show the results of the three extraction steps.

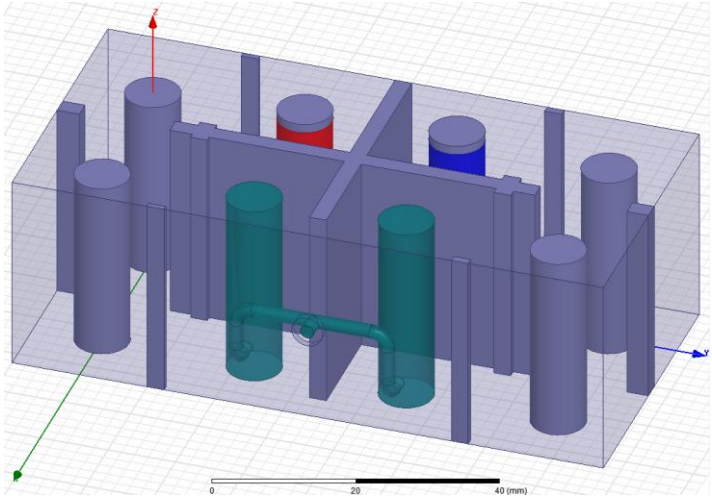

Figure 4.47. Detuning the last resonator of each filter.

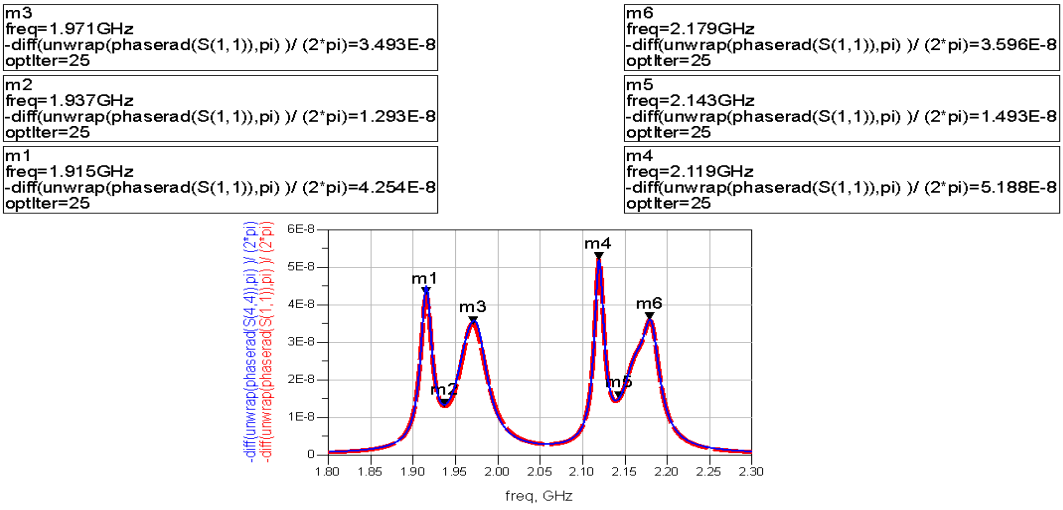

Figure 4.48. Extraction 1.

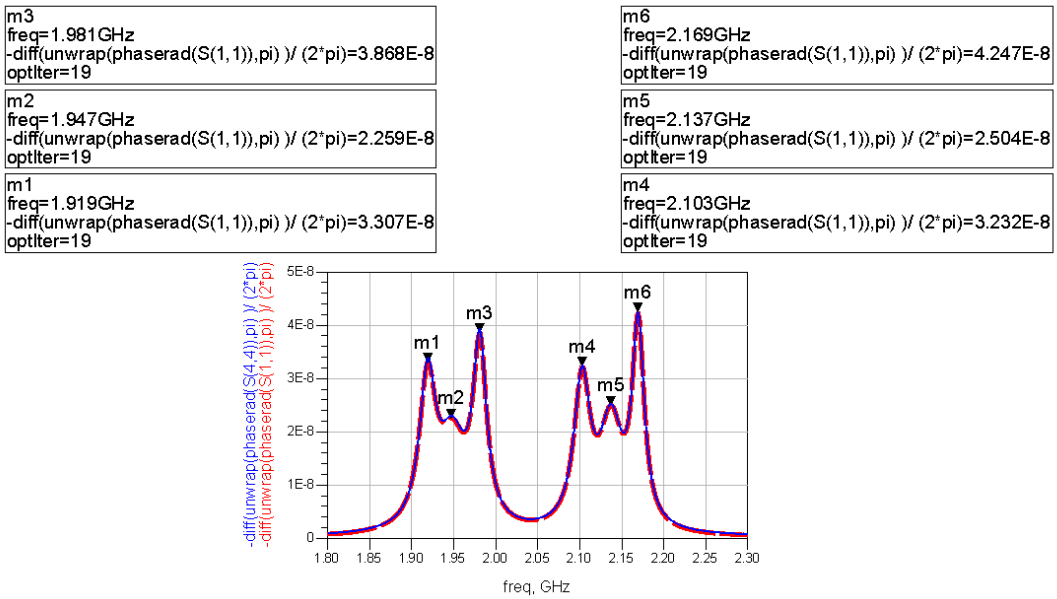

Figure 4.49. Extraction 2.

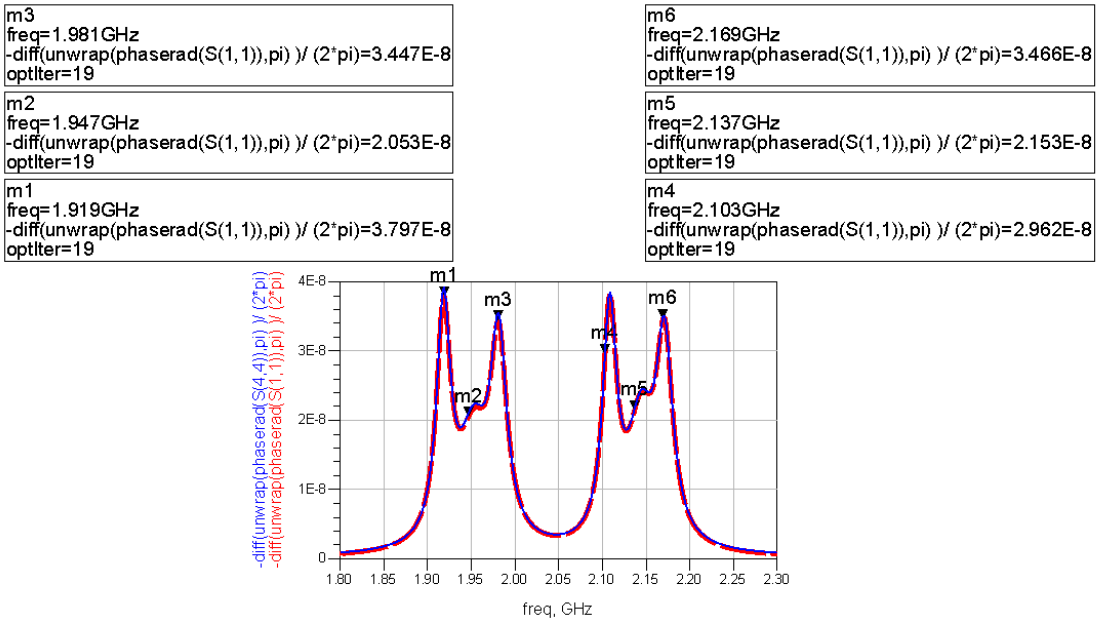

Figure 4.50. Extraction 3.

4.4.2 Step 2

Adjusting the two resonators from the other side was achieved by following this method. The adjusted group delay results can be viewed in Figure 4.51.

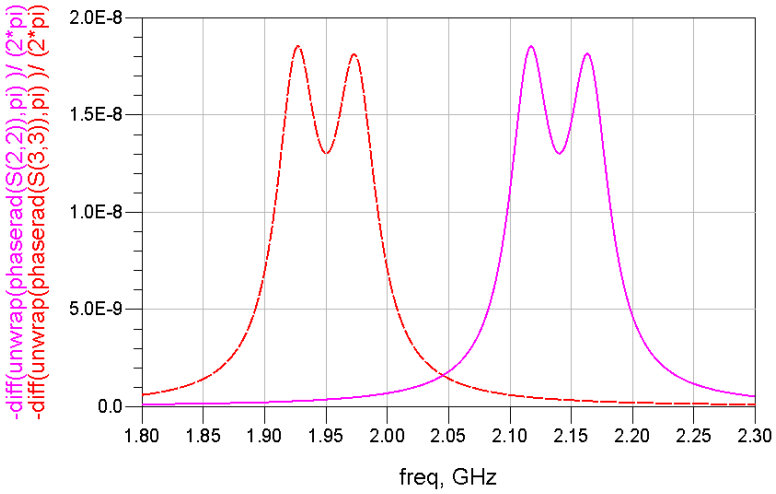

Figure 4.51. Adjusted group delay results looking at the other two ports.

The response of the complete diplexer is illustrated in Figure 4.52. If the second step is changed to looking at only one resonator, the response will change to Figure 53.

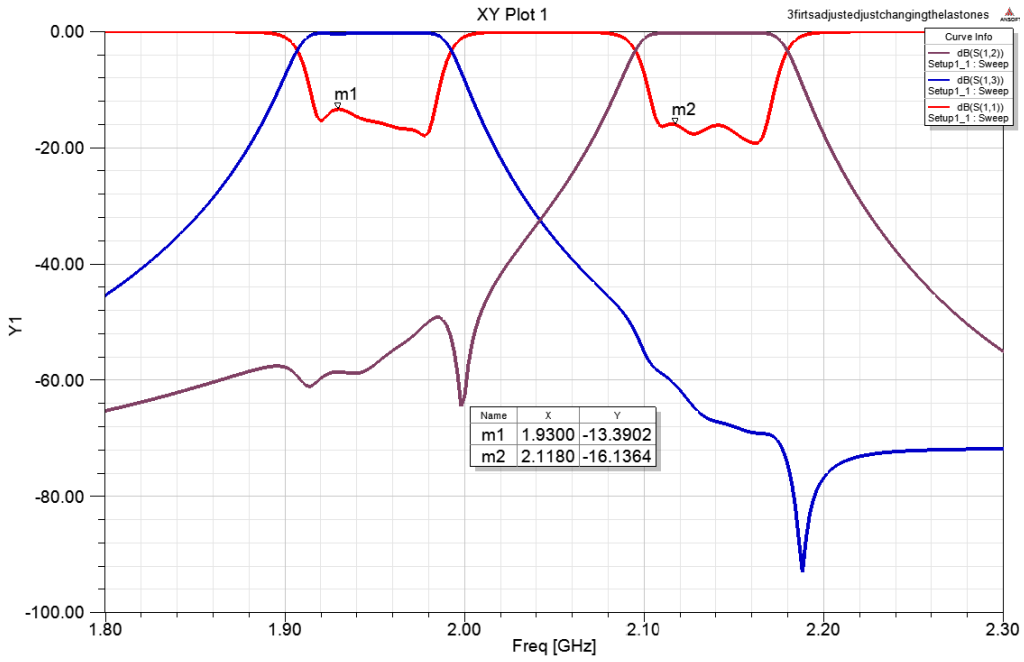

Figure 4.52. The diplexer response using the method.

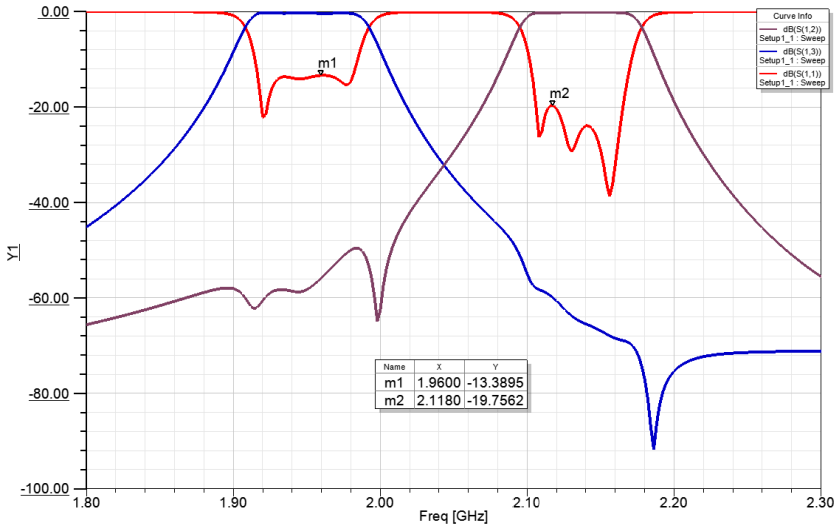

Figure 4.53. The diplexer response by changing only the last resonators and the last irises.

The return loss of the two responses was compared with the ideal return loss (Figures 4.54 & 4.55). Both of these methods appear to work fine.

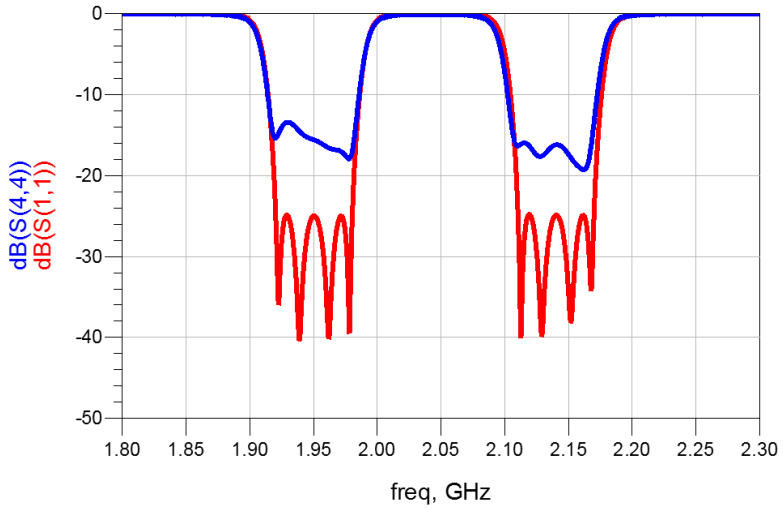

Figure 4.54. Comparing the return loss of the ideal and designed diplexers.

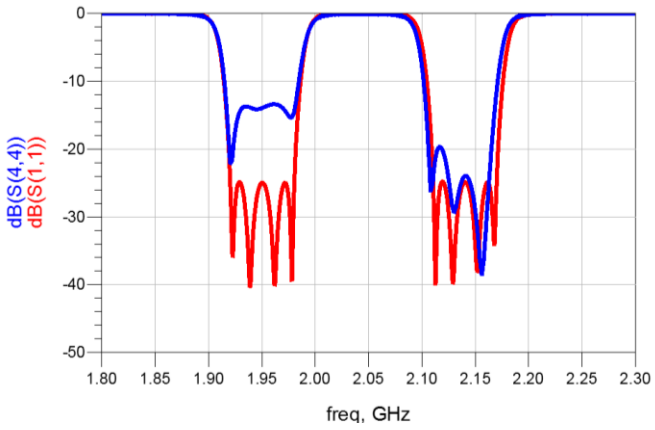

Figure 4.55. Comparing the results of ideal and designed diplexer by changing only the last resonator heights and irises in step 2 of the method.

Using this method, without having to design two ideal filters, provides a very good starting point for the diplexer design. An optimization method can then be applied to fine-tune the response. Obtaining a circuit model of the diplexer by initially utilizing optimization in ADS, and knowing the type of resonators that can be used, we can easily predict the maximum power-handling capability of the diplexer.

Chapter 5
Conclusion

After studying the methods available for predicting the power-handling capability of filters in the first part of this work, the best available method was selected and modified to be used as the prediction method. The selected method was applied to a waveguide resonator with a previously known power-handling capability from the literature, and the results were perfectly matched. The method was used to design a 2-pole filter using both inductive and capacitive input couplings, and the estimated results were compared to the results found from EM simulations. The results showed a good agreement with those of EM simulation, and the process time was considerably reduced. The method was used to devise a new coaxial resonator configuration that can handle more power compared to the conventional coaxial resonator within the same cavity size. A variety of configurations were considered and analyzed using the method, and the best one was selected. The new resonator was used to design and implement a 4-pole chebyshev filter. Simulation results showed higher power-handling performance using the abovementioned resonators, and the fabricated filter response was measured in the CIRFE Lab.

In another part of the thesis, the design method of coaxial diplexers was investigated to find an efficient and systematic design. A coaxial diplexer was first simulated by connecting two ideal filters using a coaxial manifold T-junction. An optimum dimension of the junction was determined, resulting in an ideal diplexer response by importing the EM simulation of each block as a SNP file to ADS and adjusting the dimension in ADS. Although this approach quickly results in an ideal response diplexer, its design is not desirable due to the use of a coaxial manifold. This was replaced with a wire junction, which was found to be more practical. Hence, the group delay seen from the common port of this diplexer was used to match and replace the manifold junction with an internally connected wire junction, while all of the resonators (except the first two) were detuned. The power handling of both diplexers was then determined using both the prediction method and EM simulation, showing a close agreement.

A new approach for designing diplexers was also proposed. The method involves simulating an EM simulation imported junction and ideal coupling matrices of two filters as a diplexer model in ADS, after which coupling matrices were adjusted to achieve an ideal diplexer response through optimization. Having obtained an ideal circuit model in ADS and a physical structure in HFSS, a group delay matching method was then applied to achieve physical dimensions, resulting in an ideal diplexer in HFSS.

In this method, each physical dimension was related to a coupling matrix element by matching the group delay of a circuit model and an HFSS model using parameter extraction and space mapping. Each matching include importing the HFSS results into the circuit model, extracting corresponding coupling elements, finding new dimensions using a space-mapping algorithm, and updating new dimensions in HFSS. The process was repeated until the group delay of HFSS matched that of the circuit model. The matching was done in a step-by-step fashion, starting from the common port and ending with two other ports of the diplexer, while all resonators were detuned except for the first two at the beginning; one resonator from each side was added to be tuned in each step until all of the resonators were tuned. As the final steps, the input coupling of each port was adjusted by matching the group delay, and all of the resonators, except the two corresponding ones, were detuned.

Bibliography

[1] S. B. Cohn, "Design Considerations for High-Power Microwave Filters," *Microwave Theory and Techniques, IRE Transactions on,* vol. 7, pp. 149-153, 1959.

[2] L. Young, "Peak Internal Fields in Direct-Coupled-Cavity Filters," *Microwave Theory and Techniques, IRE Transactions on,* vol. 8, pp. 612-616, 1960.

[3] C. Ernst and V. Postoyalko, "Comparison of the stored energy distributions in a QC-type and a TC-type prototype with the same power transfer function," in *Microwave Symposium Digest, 1999 IEEE MTT-S International,* vol.3, pp. 1339-1342, 1999.

[4] C. Ernst, V. Postoyalko and N. G. Khan, "Relationship between group delay and stored energy in microwave filters," *Microwave Theory and Techniques, IEEE Transactions on,* vol. 49, pp. 192-196, 2001.

[5] T. Nishikawa, K. Wakino, K. Tsunoda and Y. Ishikawa, "Dielectric high-power bandpass filter using quarter-cut TE/sub 01delta/ image resonator for cellular base stations," in *Microwave Symposium Digest, 1987 IEEE MTT-S International,* 1987, pp. 133-136.

[6] T. Olsson, D. Andersson, J. Jordan, M. Lisak, V. Semenov and M. Ahlander, "Microwave breakdown in air-filled resonators," in *Microwave Symposium Digest, 1999 IEEE MTT-S International,* 1999, pp. 915-918 vol.3.

[7] A. R. Harish and R. J. Cameron, "Peak voltage analysis in high power microwave filters," in *Microwave Filters and Multiplexers (Ref. no. 2000/117), IEE Colloquium on,* 2000, pp. 10/1-10/5.

[8] A. Sivadas, Ming Yu and R. Cameron, "A simplified analysis for high power microwave bandpass filter structures," in *Microwave Symposium Digest. 2000 IEEE MTT-S International,* vol.3, pp. 1771-1774, 2000.

[9] Chi Wang and K. A. Zaki, "Analysis of power handling capacity of band pass filters," in *Microwave Symposium Digest, 2001 IEEE MTT-S International,* 2001, pp. 1611-1614 vol.3.

[10] C. Ernst and V. Postoyalko, "Prediction of peak internal fields in direct-coupled-cavity filters," *Microwave Theory and Techniques, IEEE Transactions on,* vol. 51, pp. 64-73, 2003.

[11] Ming Yu, "Power-handling capability for RF filters," *Microwave Magazine, IEEE,* vol. 8, pp. 88-97, 2007.

[12] Morten Hagensen, "Simplified Power Handling Analysis of Microwave Filters," *Microwave Journal,* Vol.55, No.9, pp. 132-140, 2012.

[13] R. J. Cameron, C. M. Kudsia and R. R. Mansour, *Microwave filters for communication systems: fundamentals, design, and applications,* Wiley-Interscience, 2007.

[14] E. Kuffel, W. S. Zaengl and J. Kuffel , *High Voltage Engineering Fundamentals,* 2nd ed, Elsevier Newnes, 2000.

[15] M. Guglielmi, "Optimum CAD procedure for manifold diplexers," in *Microwave Symposium Digest, 1993., IEEE MTT-S International,* 1993, pp. 1081-1084 vol.2.

[16] S. Bastioli, L. Marcaccioli and R. Sorrentino, "An original resonant Y-junction for compact waveguide diplexers," in *Microwave Symposium Digest, 2009. MTT '09. IEEE MTT-S International,* 2009, pp. 1233-1236.

[17] Hui-Wen Yao, A. E. Abdelmonem, Ji-Fuh Liang, Xiao-Peng Liang, K. A. Zaki and A. Martin, "Wide-band waveguide and ridge waveguide T-junctions for diplexer applications," *Microwave Theory and Techniques, IEEE Transactions on,* vol. 41, pp. 2166-2173, 1993.

[18] C. E. Saavedra, "Diplexer using a circulator and interchangeable filters," in *Devices, Circuits and Systems, 2008. ICCDCS 2008. 7th International Caribbean Conference on,* 2008, pp. 1-5.

[19] W. A. Atia, K. A. Zaki and A. E. Atia, "Synthesis of general topology multiple coupled resonator filters by optimization," in *Microwave Symposium Digest, 1998 IEEE MTT-S International,* 1998, pp. 821-824 vol.2.

[20] K. -. Wu and W. Meng, "A Direct Synthesis Approach for Microwave Filters With a Complex Load and Its Application to Direct Diplexer Design," *Microwave Theory and Techniques, IEEE Transactions on,* vol. 55, pp. 1010-1017, 2007.

[21] A. A. Omar, S. Safavi-Naeini and S. K. Chaudhuri, "Design and synthesis of microwave coupled resonator diplexers for cellular base stations," in *Electrotechnical Conference, 2002. MELECON 2002. 11th Mediterranean,* 2002, pp. 305-307.

[22] Duanwei Zhang, Yongjiu Zhao, Wei Liu, Wei Zhao and Quan Sun, "A fast synthesis approach for diplexer with E-plane T-junction design," in *Information Science and Engineering (ISISE), 2010 International Symposium on,* 2010, pp. 133-136.

[23] Qiuyi Wu, Licheng Jiao and Yangyang Li, "Design RF diplexer by directional immune clonal selection algorithm," in *Systems, Man and Cybernetics, 2009. SMC 2009. IEEE International Conference on,* 2009, pp. 4214-4217.

[24] G. Macchiarella and S. Tamiazzo, "Novel Approach to the Synthesis of Microwave Diplexers," *Microwave Theory and Techniques, IEEE Transactions on,* vol. 54, pp. 4281-4290, 2006.

[25] Sanghoon Shin and Sridhar Kanamaluru, "Diplexer design using EM and circuit simulation techniques," *Microwave Magazine, IEEE,* vol. 8, pp. 77-82, 2007.

[26] T. F. Skaik, M. J. Lancaster and F. Huang, "Synthesis of multiple output coupled resonator circuits using coupling matrix optimisation," *Microwaves, Antennas & Propagation, IET,* vol. 5, pp. 1081-1088, 2011.

[27] Ansoft HFSS Field Calculator Cookbook. "A Brief Primer and Collection of Step-by-step Calculator Recipes for Use in HFSS Fields Post-processing".

[28] John S. Rigden, *Macmillan encyclopedia of physics*, New York : Simon & Schuster Macmillan, 1996.

[29] Chi Wang, K. A. Zaki, A. E. Atia and T. G. Dolan, "Dielectric combline resonators and filters," *Microwave Theory and Techniques, IEEE Transactions on*, vol. 46, pp. 2501-2506, 1998.

[30] M. Hoft and S. Burger "Q-factor improvement of combline resonators," *German Microwave Conference (GeMic)*, 2005.

[31] L. Q. Li, C. H. Liang, G. Li, and Z. SunL q Li, "The design technique for coaxial resonator cavity duplexer," *Progress In Electromagnetics Research*, Vol. 2, pp. 105–114, 2008.

[32] Skaik, Talal; Michael Lancaster,. "Coupled Resonator Diplexer without External Junctions." Journal of Electromagnetic Analysis and Applications (JEMAA). Scientific Research Publishing, Inc. 2011.